UNIVERSITY OF CALIFORNIA
RIVERSIDE

A Theoretical Development of a Multicarrier Wireless Relay System and a Practical Exploration of Full-Duplex Radio Communication

A Dissertation submitted in partial satisfaction
of the requirements for the degree of

Doctor of Philosophy

in

Electrical Engineering

by

Yiming Ma

June 2014

Dissertation Committee:

Professor Yingbo Hua, Chairperson
Professor Ilya Dumer
Professor Ertem Tuncel

The Dissertation of Yiming Ma is approved:

Committee Chairperson

University of California, Riverside

Acknowledgments

I would like to thank my committee chair, Dr. Yingbo Hua, who has guided and encouraged me during my whole PhD study.

I would like to thank my committee, Dr. Ilya Dumer and Ertem Tuncel, without whose help, I would not have been here.

I would like to thank Dr. Ping Liang, for his advise and help in the full-duplex project.

I would like to thank Dr. An Liu for his input in the relay power scheduling.

I would like to thank Dr Bob Ulman of Army Research Office for his support of our project on full duplex radio, which has made possible the completion of this Ph.D thesis.

I would like to thank Dr. Gang Chen for assistance with equipment testing.

I would like to thank Yifan Li, Qiping Zhu and Chaitanya Mauskar for their collaboration in full-duplex project.

I would like to thank my Labmates, Armen Gholian, Ali Cirik and Qian Gao for their kindly encouragement and accompany.

I would like to thank Pavle Kirilov for assistance with PCB design.

To my parents.

ABSTRACT OF THE DISSERTATION

A Theoretical Development of a Multicarrier Wireless Relay System and a Practical Exploration of Full-Duplex Radio Communication

by

Yiming Ma

Doctor of Philosophy, Graduate Program in Electrical Engineering
University of California, Riverside, June 2014
Professor Yingbo Hua, Chairperson

As the demand for mobile wireless network increases, the radio spectrum becomes an increasingly more precious resource. This dissertation explores two important problems to increase the efficiency of radio spectral usage. The first is a novel transmitting scheme for a multicarrier relay system with direct link between source and destination. This scheme dynamically distributes the power at both the source and relay nodes between two transmitting phases and among multiple carriers according to channel state information. The second is an exploration of several new methods for practical realization of full-duplex radio communication. Among them are a time-domain transmit beamforming method and an all-analog adaptive radio interference cancellation. Critical hardware issues such as phase noise, IQ imbalance and nonlinearity are handled in our exploration. This dissertation contains results of algorithmic development, computer simulation as well as hardware implementation.

Contents

List of Figures

List of Tables

Part I

A Theoretical Development of a Multicarrier Wireless Relay System

Chapter 1

Introduction

A three-node relay system as shown in Fig. 1.1 has attracted much attention in the literature. While the capacity of such a system remains an open problem, various attempts have been focused on specific relay schemes and their achievable regions. One of the most recent works is in [1] where the authors developed algorithms to maximize the relay system throughput by assuming that the relay node is non-regenerative and the powers at the source node and the relay node can be controlled over multiple subcarriers. Specifically, the relay communication in [1] is achieved in two phases. In the first phase, source node transmits signal to relay. In the second phase, relay amplifies and transmits the signal received from the first phase to the destination node. We call the first phase *source phase* and the second phase *relay phase*. In [1], there is no direct link between the source node and the destination node. As a result, the source node is always silent during the relay phase. With the presence of direct link between, the source node has an additional freedom to distribute its power among the two phases, instead of only transmitting in the

source phase. [2] presents a power allocation algorithm to minimize a general cost function for the three-node relay systems with direct link. Moreover, we allow the source to transmit in both source and relay phase. The following conten has previously published in [2].

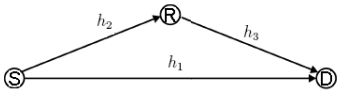

Figure 1.1: A multicarrier three-node relay system, where $k = 0, 1, \cdots, N-1$ is the index of subcarriers, and the source transmits in both phases 1 and 2. S, R and D in the figures stands for source node, relay node and destination node, respectively

The effect of the direct link has also been considered in [3, 4, 5, 6, 7, 8, 9]. But in all these works, the source node and the relay node each transmit only in one of two separate time slots[1] for each carrier. In fact, except for [9], all other works mentioned above only allow the source to transmit in the source phase. Many other prior works such as [10, 11, 12, 13] do not consider the direct link. More recent works on relays can be found in [14].

In this paper, we let the source repeat a transmission of the same information (transmitted in the source phase) to the destination in the relay phase. In other words, we split the total source power into two slots for transmitting the same information. This additional freedom makes the required power allocation algorithms differ from those published before. The achieved capacity is higher than the case where the source power is only limited to one of two time slots for each carrier, which is a special case of our relay scheme. However, this new scheme introduces several technical challenges as elaborated below.

- **More Complicated Non-convex Optimization Objective**: Since source node

[1] We use "phase" and "slot" interchangeably.

can transmits in both phases, we need to consider the joint optimization of source power allocation at both phases and relay power allocation at the relay phase. This not only increases the number of optimizatin variables but also makes the optimization objective a more complicated non-convex function.

- **More Complex Coupling between Source and Relay Power Allocation**: The source and relay power optimization is coupled in a more complex way as the destination node gets signal from both source and relay nodes during the relay phase.

From an application point of view, the three-node multicarrier relay system shown in Fig. 1.1 can be a simple abstraction of a multiuser multicarrier downlink relay system shown in Fig. 1.2 where the destination nodes can select different subcarriers in each phase. In the multiuser case, the channel gains of a link among different subcarriers are generally diverse, and hence the power allocations at both the source and relay nodes over all subcarriers are particularly important. The proposed algorithm can also be used to solve the power allocation problems in the multiuser multicarrier relay systems for given subcarrier allocation.

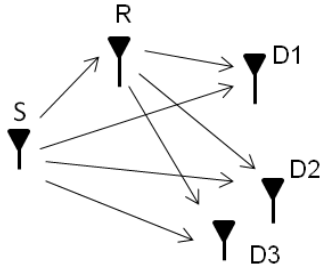

Figure 1.2: A multiuser application of the relay system shown in Fig. 1.1 where the destination nodes (users) can select different subcarriers embedded in OFDM frames in each phase.

Several of the previous works such as [3, 4, 5, 6, 7, 8] considered MIMO relay systems. The work in this paper is limited to single-antenna nodes. While our contributions do not entirely generalize the previous works on MIMO relay systems, the insight shown in this paper could help achieve that goal in the future.

In the next section, we present in detail the system model and the problem formulation. The problem formulated is a joint optimization of source power allocation over two phases and relay power allocation in the second phase. Two types of cost functions are considered. Using the alternating optimization (AO) method[12], the joint optimization problem is decomposed into two subproblems, namely the optimization of relay power allocation for given source power allocation, and the optimization of source power allocation for given relay power allocation. These two subproblems are respectively addressed in Section 3 and Section 4. Then the overall AO algorithm and the optimality analysis is given in Section 5. Although the exact solution to the joint optimization problem is not guaranteed, the AO algorithm converges to a stationary point which is asymptotically optimal for large relay transmit power or large source-relay channel gain. Simulation examples are given in Section 6 to illustrate the superior performance of the proposed AO algorithm.

Chapter 2

System Model and Problem Formulation

The relay architecture is shown in Fig. 1.1. We consider an OFDM based multi-carrier system. Each packet of information is encoded into N independent complex symbols, $\tilde{x}_k$, $k = 0, 1, \cdots, N-1$, of zero mean and unit variance. To transmit a packet of information from the source to the destination, the relay scheme has two phases.

In source phase, the source transmits $\tilde{x}_{1,k} = \sqrt{p_{1,k}}\tilde{x}_k$, $k = 0, 1, \cdots, N-1$, over N subcarriers towards the destination and the relay, the relay does not transmit but receives $\tilde{y}_{r,k}$, $k = 0, 1, \cdots, N-1$, and the destination receives $\tilde{y}_{d1,k}$, $k = 0, 1, \cdots, N-1$. The power of $\tilde{x}_{1,k}$ is $p_{1,k}$.

In relay phase, the source transmits again but it transmits $\tilde{x}_{2,k} = \sqrt{p_{2,k}}\tilde{x}_k$, $k = 0, 1, \cdots, N-1$, the relay does not receive but, concurrently with the source, transmits $\tilde{x}_{r,k} = \tilde{g}_k\tilde{y}_{r,k}$, $k = 0, 1, \cdots, N-1$, and the destination receives $\tilde{y}_{d2,k}$, $k = 0, 1, \cdots, N-1$.

The relay factor $\tilde{g}_k$ has the amplitude g_k and the phase β_k. The power of $\tilde{x}_{2,k}$ is $p_{2,k}$.

The channel coefficient of the k-th subcarrier from the source to the destination is denoted by $\tilde{h}_{1,k}$, that from the source to the relay is $\tilde{h}_{2,k}$, and that from the relay to the destination is $\tilde{h}_{3,k}$. We use $h_{l,k}$ as the amplitude of $\tilde{h}_{l,k}$, and $\alpha_{l,k}$ the phase of $\tilde{h}_{l,k}$. For clarity, we assume that all the channel coefficients are non-zero. The algorithms developed in this paper can be easily extended to solve the cases when some of the channel coefficients are zero.

The N subcarriers used in source phase for $\tilde{x}_{1,k}$ are indexed by $k = 0, 1, \cdots, N-1$. But the N subcarriers used in relay phase for $\tilde{x}_{2,k}$ (from source to destination) and $\tilde{x}_{r,k}$ (from relay to destination) are indexed by $\bar{k} = \bar{0}, \bar{1}, \cdots, \overline{N-1}$, which can be a permutation of those used in source phase. Namely, $\bar{k}$ is a function of k via a given permutation. Permuation can be used to model the subcarrier allocation in multi-user relay systems, where a user may be allocated with a different subcarrier in the relay phase.

Now, we can write that in source phase, the destination and the relay receive, respectively,

$$\tilde{y}_{d1,k} = \tilde{h}_{1,k}\tilde{x}_{1,k} + \tilde{n}_{d1,k} \tag{2.1}$$

$$\tilde{y}_{r,k} = \tilde{h}_{2,k}\tilde{x}_{1,k} + \tilde{n}_{r,k} \tag{2.2}$$

and in relay phase, the destination receives

$$\tilde{y}_{d2,k} = \tilde{h}_{3,\bar{k}}\tilde{x}_{r,k} + \tilde{h}_{1,\bar{k}}\tilde{x}_{2,k} + \tilde{n}_{d2,\bar{k}} \tag{2.3}$$

where $\bar{k}$ in $\tilde{h}_{3,\bar{k}}$ and $\tilde{h}_{1,\bar{k}}$ of (2.3) is a permuted version of k in $\tilde{h}_{1,k}$ and $\tilde{h}_{2,k}$ of (2.1) and (2.2). All the noise terms $\tilde{n}_{d1,k}$, $\tilde{n}_{r,k}$ and $\tilde{n}_{d2,k}$ are assumed to be independent of each other

and across subcarriers, and have zero mean and unit variance. Note that there is no loss of generality to assume the unit variance. If the variance of $\tilde{n}_{d1,k}$ and $\tilde{n}_{d2,k}$ is γ_d, we can divide (2.1) and (2.3) by $\sqrt{\gamma_d}$ and adjust the notations. And if the variance of $\tilde{n}_{r,k}$ is γ_r, we can divide (2.2) by $\sqrt{\gamma_r}$ and adjust the notations.

Combining all the previous equations, we can write the received signals in both phases as a vector:

$$\tilde{\mathbf{y}}_k = \tilde{\mathbf{h}}_k \tilde{x}_k + \tilde{\mathbf{n}}_k \tag{2.4}$$

with $\tilde{\mathbf{y}}_k = [\ \tilde{y}_{d1,k},\quad \tilde{y}_{d2,k}\ ]^T$ and

$$\tilde{\mathbf{h}}_k = [\ \sqrt{p_{1,k}}\tilde{h}_{1,k},\quad \sqrt{p_{1,k}}\tilde{g}_k\tilde{h}_{2,k}\tilde{h}_{3,\bar{k}} + \sqrt{p_{2,k}}\tilde{h}_{1,\bar{k}}\ ]^T \tag{2.5}$$

$$\tilde{\mathbf{n}}_k = [\ \tilde{n}_{d1,k},\quad \tilde{g}_k\tilde{h}_{3,\bar{k}}\tilde{n}_{r,k} + \tilde{n}_{d2,\bar{k}}\ ]^T \tag{2.6}$$

Since the covariance matrix of the noise vector $\tilde{\mathbf{n}}_k$ is $\mathbf{C}_k = \text{diag}\left(1, g_k^2 h_{3,\bar{k}}^2 + 1\right)$, a sufficient statistics for $\tilde{x}_k$ is

$$\hat{\tilde{x}}_k = \tilde{\mathbf{h}}_k^H \mathbf{C}_k^{-1} \tilde{\mathbf{y}}_k \tag{2.7}$$

One can then verify that the SNR of $\hat{\tilde{x}}_k$ is

$$\text{SNR}_k = p_{1,k}h_{1,k}^2 + \frac{|\sqrt{p_{1,k}}\tilde{g}_k\tilde{h}_{2,k}\tilde{h}_{3,\bar{k}} + \sqrt{p_{2,k}}\tilde{h}_{1,\bar{k}}|^2}{g_k^2 h_{3,\bar{k}}^2 + 1}. \tag{2.8}$$

It follows from (2.8) that $\beta_k = \alpha_{1,\bar{k}} - \alpha_{2,k} - \alpha_{3,\bar{k}}$ is the phase of $\tilde{g}_k$ that maximizes SNR_k. With the optimal phase β_k, (2.8) becomes

$$\text{SNR}_k = p_{1,k}h_{1,k}^2 + \frac{(\sqrt{p_{1,k}}g_k h_{2,k}h_{3,\bar{k}} + \sqrt{p_{2,k}}h_{1,\bar{k}})^2}{g_k^2 h_{3,\bar{k}}^2 + 1}. \tag{2.9}$$

Let source node transmit in relay phase will result in a better SNR especially when relay power is limited or direct channel is strong. The simulation results also show that the

optimized $p_{2,k}$'s are typically larger than zero. A more rigorous discussion will be given at the end of Section 4.

We will consider two types of cost functions. The first is

$$J_1 = -\min_k \mathrm{SNR}_k. \tag{2.10}$$

This cost could be particularly useful if each of the N subcarriers is occupied by a distinct downlink user (see Fig. 1.2) and we want to ensure a fair quality for all users. The second cost is

$$J_2 = \sum_{k=0}^{N-1} f_k(\mathrm{SNR}_k), \tag{2.11}$$

where $f_k(\mathrm{SNR}_k)$ is any decreasing convex function of $\mathrm{SNR}_k > 0$, i.e., $f_k' \doteq \frac{\partial f_k(x)}{\partial x}\Big|_{x=\mathrm{SNR}_k} < 0$ and $f_k'' \doteq \frac{\partial^2 f_k(x)}{\partial^2 x}\Big|_{x=\mathrm{SNR}_k} > 0$. A special form of J_2 is

$$J_2 = -\frac{1}{2N}\sum_{k=0}^{N-1} \log_2(1+\mathrm{SNR}_k), \tag{2.12}$$

which is the negative of the capacity of the relay system under the previously defined relay scheme. Clearly, there are many more variations of the cost functions. But we hope that our results for J_1 and J_2 can help solve other related problems.

The joint source and relay power allocation problem is formulated as:

$$\min_{p_{1,k},p_{2,k},g_k,\forall k} J. \tag{2.13}$$

subject to

$$\sum_{k=0}^{N-1}(p_{1,k}+p_{2,k}) \le P_s, \tag{2.14}$$

$$\sum_{k=0}^{N-1}\left(g_k^2 h_{2,k}^2 p_{1,k} + g_k^2\right) \le P_r. \tag{2.15}$$

along with $g_k \geq 0$, $p_{1,k} \geq 0$ and $p_{2,k} \geq 0$. Here, J is either J_1 or J_2, P_r is the power constraint at the relay, and P_s is the sum power constraint at the source.

The above problem differs from those in [4, 5, 6, 7, 8] in a fundamental way. As mentioned earlier, all those references assume that the source node is silent during the relay phase. As shown later in this paper, by allowing the source power to be distributed in both phases, a substantial performance gain can be achieved.

The exact solution to (2.13) is difficult to find because both the cost function and the relay power constraint in (2.15) are non-convex. In this paper, we provide a local optimal solution by adoptting an alternating optimization approach where we optimize g_k $\forall k$ with previously given $p_{1,k}$ and $p_{2,k}$ $\forall k$, then optimize $p_{1,k}$ and $p_{2,k}$ $\forall k$ with previously given g_k $\forall k$, and then repeat the process until convergence. For fixed source power allocation $p_{1,k}, p_{2,k} \forall k$, the relay power allocation problem (i.e., the optimization of $g_k \forall k$) is still non-convex. However, by exploiting the specific structure of the SNR expression in (2.9), we propose efficient algorithms to find the unique optimal solution for this non-covex problem in Section 3. For fixed relay amplifying factor g_k, the dual-phase source power allocation problem (i.e., the optimization of $p_{1,k}, p_{2,k} \forall k$) is convex and we propose efficient algorithms to find the optimal solution in Section 4. The overall algorithm to solve Problem (2.13) is given in Section 5.

Chapter 3

Optimal Relay Power Allocation given Source Power Allocation

For fixed $p_{1,k}$ and $p_{2,k}$, Problem (2.13) becomes

$$\min_{g_k \geq 0, \forall k} J, \tag{3.1}$$

subject to

$$\sum_{k=0}^{N-1} c_k g_k^2 \leq P_r. \tag{3.2}$$

where $c_k = h_{2,k}^2 p_{1,k} + 1$.

Neither J_1 nor J_2 is a convex functions of g_k $\forall k$. In particular, the SNR_k in (2.9) is not a concave function of g_k. However, it is easy to verify that

$$\begin{aligned} \frac{d\text{SNR}_k}{dg_k} &= 2(\sqrt{p_{1,k}} g_k h_{2,k} h_{3,\bar{k}} + \sqrt{p_{2,k}} h_{1,\bar{k}}) \\ &\quad \times \frac{(\sqrt{p_{1,k}} h_{2,k} h_{3,\bar{k}} - \sqrt{p_{2,k}} g_k h_{1,\bar{k}} h_{3,\bar{k}}^2)}{(g_k^2 h_{3,\bar{k}}^2 + 1)^2}. \end{aligned} \tag{3.3}$$

It follows that SNR_k is a quasi-concave function of g_k, which has a unique maximum at[1]

$$g_k^* = \frac{h_{2,k}\sqrt{p_{1,k}}}{h_{1,\bar{k}}h_{3,\bar{k}}\sqrt{p_{2,k}}}. \tag{3.4}$$

Namely, SNR_k is an increasing function of g_k for $g_k \in [0, g_k^*)$ and a decreasing function of g_k for $g_k \in (g_k^*, \infty)$. Because of the power constraint (3.2), we only need to search the optimal g_k within $[0, g_k^*]$. A typical plot of SNR_k is shown in Figure. 3.1.

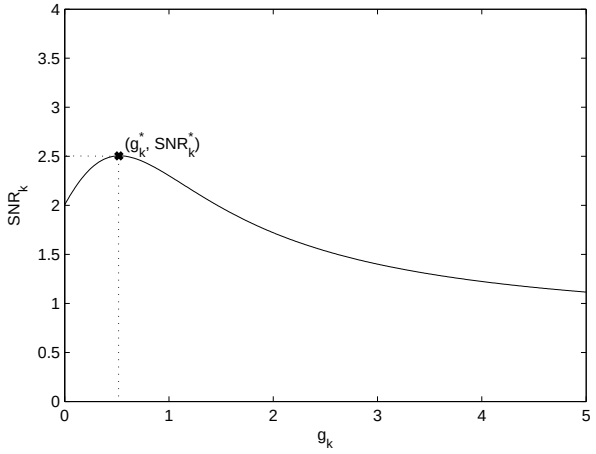

Figure 3.1: A typical plot of SNR_k vs. g_k where g_k^* is the position of the peak value SNR_k^*.

Note that if the source does not transmit in relay phase, then $p_{2,k} = 0$ and hence SNR_k is simply an increasing concave function of g_k (and J_1 and J_2 are convex functions of g_k $\forall k$).

3.1 Using the Cost $J = J_1$

Recall $J_1 = -\min_k \mathrm{SNR}_k$ and $\min_{\{g_k \forall k\}} J_1 = \max_{\{g_l \forall l\}} \min_k \mathrm{SNR}_k$. Denote $\mathrm{SNR}_k^* = \mathrm{SNR}_k|_{g_k = g_k^*}$. Also denote the solution to (3.1) by $\hat{g}_k$ and the corresponding optimal SNR

[1]Note that if $p_{2,k} = 0$, we let $g_k^* = \infty$.

by $\widehat{\mathrm{SNR}}_k \triangleq \mathrm{SNR}_k|_{g_k=\hat{g}_k}$. From (2.9), if we let $g_k = 0$, we have the corresponding $\mathrm{SNR}_k = p_{1,k}h_{1,k}^2 + p_{2,k}h_{1,\bar{k}}^2$. Since SNR_k is a monotonic increasing function of g_k over $[0, g_k^*)$, we must have:

$$p_{1,k}h_{1,k}^2 + p_{2,k}h_{1,\bar{k}}^2 \leq \widehat{\mathrm{SNR}}_k \leq \mathrm{SNR}_k^*, \ \forall k. \tag{3.5}$$

Also, because SNR_k is an increasing function of g_k for $g_k \in [0, g_k^*)$, it follows that

$$\widehat{\mathrm{SNR}}_k = \min_l \widehat{\mathrm{SNR}}_l, \forall k \in \left\{0 \leq k^{'} \leq N-1 : \ \hat{g}_{k'} > 0\right\}.$$

It is easy to verify from (2.9) that for each $\mu > 0$, the equation $\mathrm{SNR}_k = \mu$ can be reduced to a quadratic equation of g_k, which has two (closed-form) solutions $g_k^{(1)}$ and $g_k^{(2)}$. Furthermore, if $0 < \mu \leq \mathrm{SNR}_k^*$, one (and only one value) of $g_k^{(1)}$ and $g_k^{(2)}$ is less than or equal to g_k^*, which is denoted by $g_k(\mu)$.

With the above discussions, one can verify that the following algorithm yields the exact solution to (3.1) with $J = J_1$:

Algorithm 1:

1. Compute g_k^*, SNR_k^* and $\mu^* = \min_k \mathrm{SNR}_k^*$.

2. For each k, solve the equation $\mathrm{SNR}_k = \mu^*$ to obtain $g_k(\mu^*)$. If (3.2) is satisfied with $g_k = \max(0, g_k(\mu^*)) \ \forall k$, then set $\hat{g}_k = \max(0, g_k(\mu^*)) \ \forall k$ and stop. Otherwise, go to the next step.

3. Use the bisection search method[2] [15] to find $\hat{\mu}$ within $(0, \mu^*)$ such that (3.2) is satisfied with equality as $\sum_{k=0}^{N-1} c_k g_k^2 = P_r$ and $g_k = \max(0, g_k(\hat{\mu})) \ \forall k$. Then, set $\hat{g}_k = \max(0, g_k(\hat{\mu})) \ \forall k$, and stop.

[2]It converges exponentially fast.

3.2 Using the Cost $J = J_2$

Recall $J_2 = \sum_k f_k(\text{SNR}_k)$ where $f_k(x)$ is a decreasing convex function of $x \geq 0$. To find the solution to (3.1), the KKT conditions [15] are the necessary conditions (but not sufficient conditions due to non-convexity of J_2 with respect to g_k $\forall k$). But we can still distill the exact solution from the KKT conditions as follows. Among the KKT conditions[3], we have

$$f_k^{'} \frac{d\text{SNR}_k}{dg_k} + 2\mu g_k c_k^2 - \gamma_k = 0, \ \forall k, \tag{3.6}$$

where $f_k^{'} = \frac{df_k(\text{SNR}_k)}{d\text{SNR}_k} < 0$ and $\frac{d\text{SNR}_k}{dg_k}$ is given in (3.3), μ is the Lagrange multiplier associated with the relay power constraint in (3.2), and γ_k is the Lagrange multiplier for the constraint $g_k \geq 0$. Also, $\mu > 0$ if the equality in (3.2) holds, and $\gamma_k = 0$ if $g_k > 0$.

The following proposition characterizes the properties of the solution of the KKT conditions.

Proposition 1 *The KKT conditions of the relay power allocation problem in* (3.1) *with* $J = J_2$ *has a unique solution denoted by* $\hat{\mu}, \{\hat{\gamma}_k, \hat{g}_k : \forall k\}$. *Moreover,* $\hat{\mu}, \{\hat{\gamma}_k, \hat{g}_k : \forall k\}$ *has the following properties:*

1. $g_k = 0, \gamma_k = 0, \ \forall k \in \mathcal{K}_0 \triangleq \left\{k^{'} : p_{1,k^{'}} = 0\right\}$ *and* $g_k > 0, \gamma_k = 0, \ \forall k \in \overline{\mathcal{K}}_0 \triangleq \left\{k^{'} : p_{1,k^{'}} > 0\right\}$.

2. *If* $\sum_{k=0}^{N-1} c_k g_k^{*2} \leq P_r$, *we have* $\hat{g}_k = g_k^*, \forall k$; *otherwise* $\hat{g}_k = 0, \forall k \in \mathcal{K}_0$ *and* $\hat{\mu}, \left\{\hat{g}_k : \forall k \in \overline{\mathcal{K}}_0\right\}$

[3]For brevity, we do not list all KKT conditions. We assume that the reader understands the basic components of the KKT conditions.

is the unique solution of the following equations:

$$-f_k' \frac{d\mathrm{SNR}_k}{2g_k dg_k} = \mu c_k, \ \forall k \in \overline{\mathcal{K}}_0, \tag{3.7}$$

$$\sum_{k\in\overline{\mathcal{K}}_0} c_k g_k^2 = P_r. \tag{3.8}$$

3. *In* (3.7), $-f_k' \frac{d\mathrm{SNR}_k}{2g_k dg_k}$ *is positive and decreasing with* $g_k \in [0, g_k^*]$.

4. *Let* $g_k(\mu), \forall k \in \overline{\mathcal{K}}_0$ *denote the solution of* (3.7) *with fixed* μ. *Then we have* $g_k(\mu) \in [0, g_k^*]$ *and* $\sum_{k\in\overline{\mathcal{K}}_0} c_k g_k^2(\mu)$ *is decreasing with* μ.

Please refer to Appendix 8.1 for the proof.

By Result 3) in Proposition 1, for a given feasible μ, the solution $g_k(\mu), \forall k \in \overline{\mathcal{K}}_0$ of (3.7) can be easily found by a bisection search. On the other hand, if $\sum_{k=0}^{N-1} c_k g_k^{*2} > P_r$ the optimal Lagrange multiplier $\hat{\mu}$ is given by the solution of

$$\sum_{k\in\overline{\mathcal{K}}_0} c_k g_k^2(\mu) = P_r, \tag{3.9}$$

which can also be found by a bisection search according to the Result 4) in Proposition 1.

Based on Proposition 1, one can verify that the following algorithm yields the exact solution to Problem (3.1) with $J = J_2$:

Algorithm 2:

1. Compute g_k^* $\forall k$. If (3.2) holds with $g_k = g_k^*$, set $\hat{g}_k = g_k^*$ $\forall k$ and stop. Otherwise, go to the next step.

2. Use a bisection search to find $\hat{\mu}$ within $[0, \infty]$ such that Equation (3.9) is satisfied, where for a given μ, the $g_k(\mu), \forall k \in \overline{\mathcal{K}}_0$ in (3.9) is found as the solution to (3.7) via an inner-loop bisection search.

Chapter 4

Optimal Source Power Allocation given Relay Power Allocation

Given a relay power allocation (i.e., given a set of g_k $\forall k$), we now consider the optimization of the source power allocation by solving the following problem:

$$\min_{p_{1,k}\geq 0, p_{2,k}\geq 0, \forall k} J, \tag{4.1}$$

subject to (2.14) and (2.15) , which is later proved convex.

4.1 Using the Cost $J = J_1$

Since $J_1 = -\min_k \mathrm{SNR}_k$, Problem (4.1) can be reformulated as

$$\min_{\theta, p_{1,k}\geq 0, p_{2,k}\geq 0,\ \forall k} -\theta, \tag{4.2}$$

subject to (2.14), (2.15) and

$$\mathrm{SNR}_k \geq \theta, \forall k. \tag{4.3}$$

It follows from (2.9) that

$$\mathrm{SNR}_k = r_k p_{1,k} + s_k \sqrt{p_{1,k} p_{2,k}} + t_k p_{2,k}, \tag{4.4}$$

where $r_k = h_{1,k}^2 + \frac{g_k^2 h_{2,k}^2 h_{3,\bar{k}}^2}{g_k^2 h_{3,\bar{k}}^2 + 1}$, $s_k = \frac{g_k h_{1,\bar{k}} h_{2,k} h_{3,\bar{k}}}{g_k^2 h_{3,\bar{k}}^2 + 1}$ and $t_k = \frac{h_{1,\bar{k}}^2}{g_k^2 h_{3,\bar{k}}^2 + 1}$. It is obvious that SNR_k is increasing with $p_{1,k}$ and $p_{2,k}$.

It is also obvious that the optimal $p_{1,k}$ and $p_{2,k}$ must be such that the equality in (2.14) is satisfied. If $p_{1,k}$ and $p_{2,k}$ are such that the strict inequality in (2.14) holds, we can increase some or all of $p_{2,k}$ such that the equality in (2.14) is achieved and θ is increased while (2.15) is not affected.

Furthermore, the optimal $p_{1,k}$ and $p_{2,k}$ must be such that $\mathrm{SNR}_k = \theta$, $\forall k$. If there is SNR_l satisfying $\mathrm{SNR}_l > \min_k \mathrm{SNR}_k$, we can reduce $p_{1,l}$ to make $\mathrm{SNR}_l = \min_k \mathrm{SNR}_k$ without affecting θ and then we can increase some or all of $p_{2,k}$ such that the equality in (2.14) is achieved and θ is increased while (2.15) is not affected.

Applying the KKT conditions [15] to the problem (4.2), we have

$$-\lambda_k \left(r_k + \frac{s_k \sqrt{p_{2,k}}}{2\sqrt{p_{1,k}}} \right) + \mu_2 g_k^2 h_{2,k}^2 + \mu_1 = 0, \ \forall k, \tag{4.5}$$

$$-\lambda_k \left(t_k + \frac{s_k \sqrt{p_{1,k}}}{2\sqrt{p_{2,k}}} \right) + \mu_1 = 0, \ \forall k, \tag{4.6}$$

where λ_k is the k-th multiplier due to (4.3), μ_1 is the multiplier due to (2.14), and μ_2 is the multiplier due to (2.15). The discussions shown previously imply that $\mu_1 > 0$ and $\lambda_k > 0$, $\forall k$.

The following proposition gives the solution to the above KKT conditions for fixed μ_1, μ_2.

Proposition 2 *For fixed μ_1, μ_2, the solution to the KKT conditions of Problem* (4.2) *with* $J = J_1$ *is given by*

$$p_{1,k} = \begin{cases} 0, & t_k\gamma - r_k > 0, s_k = 0 \\ \frac{\theta}{r_k}, & t_k\gamma - r_k < 0, s_k = 0 \\ \frac{\theta}{r_k+\gamma t_k}, & t_k\gamma - r_k = 0, s_k = 0 \\ \frac{\theta}{r_k+\eta_k s_k+\eta_k^2 t_k}, & s_k > 0 \end{cases}, \tag{4.7}$$

$$p_{2,k} = \begin{cases} \frac{\theta}{t_k}, & t_k\gamma - r_k > 0, s_k = 0 \\ 0, & t_k\gamma - r_k < 0, s_k = 0 \\ \frac{\theta}{\gamma r_k+t_k}, & t_k\gamma - r_k = 0, s_k = 0 \\ \eta_k^2 p_{1,k}, & s_k > 0 \end{cases}, \tag{4.8}$$

where $\gamma = g_k^2 h_{2,k}^2 \frac{\mu_2}{\mu_1} + 1$; $\eta_k, \forall k \in \left\{k' : s_k > 0\right\}$ *is given by*

$$\eta_k = \sqrt{\frac{p_{2,k}}{p_{1,k}}} = \frac{1}{s_k}\left(t_k\gamma - r_k + \sqrt{(t_k\gamma - r_k)^2 + s_k^2\gamma}\right), \tag{4.9}$$

and θ is chosen such that (2.14) *is satisfied with equality.*

Please refer to Appendix 8.2 for the proof.

By Proposition 2, for fixed μ_1, μ_2, the solution of the KKT conditions only depends on the intermediate variable $\gamma = g_k^2 h_{2,k}^2 \frac{\mu_2}{\mu_1} + 1$. Hence, if the solution in Proposition 2 with $\gamma = 1$ (i.e., $\mu_2 = 0$) satisfies the relay power constraint (2.15), it is also the optimal solution for Problem (4.2) with $J = J_1$. Otherwise, we can use bisection search to find the γ such that the solution in Proposition 2 satisfies (2.15) with equality and this solution is optimal

for Problem (4.2). Note that the probability for $s_k = r_k = t_k = 0$ is virtually zero. So, the last expressions in (4.7) and (4.8) should be stable numerically.

From the above analysis, we obtain the following algorithm which finds the exact solution to (4.2) with $J = J_1$:

Algorithm 3:

1. Initialize $\gamma = 1$ and $\theta > 0$.

2. Determine η_k from (4.9) for all k where $s_k > 0$.

3. Determine $p_{1,k}$ and $p_{2,k}$ by (4.7) and (4.8).

4. One step bisection[1]: If the left side of (2.14) is smaller than its right side, increase[2] θ. If the opposite is true, decrease θ. Go to step 3) until convergence.

5. If $\gamma = 1$ and (2.15) is satisfied, stop. Otherwise, go to the next step.

6. One step bisection[3]: If the left side of (2.15) is larger than its right side, increase γ. If the opposite is true, decrease γ. Go to step 2) until convergence.

In our simulations, "convergence" means that the difference between the coefficients obtained in two consecutive iterations is less than a pre-set threshold.

[1]The lower bound of θ is obviously zero. An upper bound of θ for each γ can be found by doubling its previous (nonzero) value each time initially as θ is increased consecutively in the bisection search.

[2]In bisection, "increase a variable" means "increase the variable halfway towards its nearest larger estimate obtained previously", and "decrease a variable" means "decrease the variable halfway towards its nearest smaller estimate obtained previously".

[3]An upper bound of γ can be found by doubling its previous (nonzero) value each time initially as γ is increased consecutively in the bisection search.

4.2 Using the cost $J = J_2$

The cost function J_2 can be expressed as

$$J_2 = \sum_{k=0}^{N-1} f_k(r_k p_{1,k} + s_k\sqrt{p_{1,k}p_{2,k}} + t_k p_{2,k}). \tag{4.10}$$

Let $\mathbf{p} = [p_{1,0}, \cdots, p_{1,N-1}, p_{2,0}, \cdots, p_{2,N-1}]^T$ and let $\mathbf{H}$ be the Hessian matrix of J_2 with respect to $\mathbf{p}$. Then, one can verify that for any real vector $\mathbf{v} \in \mathbb{R}^{2N}$,

$$\begin{aligned}
\mathbf{v}^T\mathbf{H}\mathbf{v} &= \sum_{k=0}^{N-1}\Bigg\{ f_k^{''}\cdot\left(a_k\left[r_k + s_k\frac{\sqrt{p_{2,k}}}{2\sqrt{p_{1,k}}}\right]\right. \\
&\quad \left. +b_k\left[s_k\frac{\sqrt{p_{1,k}}}{2\sqrt{p_{2,k}}} + t_k\right]\right)^2 \\
&\quad -f_k^{'}\cdot a_k^2 s_k\frac{\sqrt{p_{2,k}}}{4\sqrt{p_{1,k}^3}} - f_k^{'}\cdot b_k^2 s_k\frac{\sqrt{p_{1,k}}}{4\sqrt{p_{2,k}^3}}\Bigg\} \\
&\geq 0,
\end{aligned} \tag{4.11}$$

where we have applied $f_k^{'} < 0$ and $f_k^{''} > 0$. Hence, J_2 is convex with respect to $\mathbf{p}$. The KKT conditions of (4.1) with $J = J_2$ include

$$f_k^{'}\cdot\frac{d\mathrm{SNR}_k}{dp_{1,k}} + \mu_2(g_k^2 h_{2,k}^2) + \mu_1 = 0, \forall k, \tag{4.12}$$

$$f_k^{'}\cdot\frac{d\mathrm{SNR}_k}{dp_{2,k}} + \mu_1 = 0, \forall k, \tag{4.13}$$

where, as discussed previously, $\mu_1 > 0$ and $\mu_2 \geq 0$. The following proposition gives the solution to the above KKT conditions for fixed μ_1, μ_2.

Proposition 3 *For fixed μ_1, μ_2, the solution to the KKT conditions of Problem* (4.2) *with*

$J = J_2$ is given by

$$p_{1,k} = \begin{cases} 0, & t_k\frac{a_2}{a_1} - r_k > 0 \\ \frac{\left(f_k'^{-1}\left(\frac{-\frac{a_2}{a_1}\mu_1}{\frac{a_2}{a_1}t_k + \left(t_k\frac{a_2}{a_1} - r_k\right)^2}\right)\right)^+}{r_k}, & t_k\frac{a_2}{a_1} - r_k < 0 \\ \frac{\left(f_k'^{-1}\left(\frac{-\mu_1}{t_k}\right)\right)^+}{r_k + \frac{a_2}{a_1}t_k}, & t_k\frac{a_2}{a_1} - r_k = 0 \\ \frac{\left(f_k'^{-1}\left(\frac{-\mu_1}{t_k + \frac{s_k}{2\eta_k}}\right)\right)^+}{r_k + \eta_k s_k + \eta_k^2 t_k}, & s_k > 0 \end{cases} \tag{4.14}$$

$$p_{2,k} = \begin{cases} \frac{\left(f_k'^{-1}\left(\frac{-\mu_1}{t_k}\right)\right)^+}{t_k}, & t_k\frac{a_2}{a_1} - r_k > 0 \\ 0, & t_k\frac{a_2}{a_1} - r_k < 0 \\ \frac{\left(f_k'^{-1}\left(\frac{-\mu_1}{t_k}\right)\right)^+}{\frac{a_1}{a_2}r_k + t_k}, & t_k\frac{a_2}{a_1} - r_k = 0 \\ \eta_k^2 p_{1,k}, & s_k > 0 \end{cases} \tag{4.15}$$

where $\gamma = g_k^2 h_{2,k}^2 \frac{\mu_2}{\mu_1} + 1$, and $\eta_k, \forall k \in \left\{k' : s_k > 0\right\}$ is given in (4.9).

Please refer to Appendix 8.3 for the proof.

Summarizing the above analysis, we have the following algorithm for finding the exact solution to (4.1) with $J = J_2$:

Algorithm 4:

1. Initialize $\gamma = 1$ and $\mu_1 > 0$.

2. Compute η_k from (4.9) for all k where $s_k > 0$. Compute $p_{1,k}$ and $p_{2,k}$ by (4.14) and (4.15) for all k.

3. One step bisection: if the left side of (2.14) is smaller than its right side, decrease μ_1. If the opposite is true, increase μ_1. Go to step 2) until convergence.

4. If $\gamma = 1$ and (2.15) is satisfied, stop. Otherwise, go to next step.

5. One step bisection: If the left side of (2.15) is larger than its right side, increase γ. If the opposite is true, decrease γ. Go to step 2) until convergence.

4.3 Discussion of the Optimal Source Power Ratio $\frac{p_{2,k}}{p_{1,k}}$

Some properties of the optimal source power ratio $\frac{p_{2,k}}{p_{1,k}}$ are shown below.

- **Conditions for non-zero source transmit power in the relay phase**: For any given g_k $\forall k$, the optimal $\frac{p_{2,k}}{p_{1,k}}$ is given in (4.9), which is larger than zero if $s_k > 0$. It follows from the definition of s_k, shown below (4.4), that $s_k > 0$ if and only if $g_k > 0$, $h_{1,\bar{k}} > 0$, $h_{2,k} > 0$ and $h_{3,\bar{k}} > 0$. If $s_k = 0$, it follows from (4.4) (i.e., $\max_{p_{1,k},p_{2,k}} \mathrm{SNR}_k$ subject to $p_{1,k} + p_{2,k} \leq p_k$ where p_k is any amount of power for the kth subcarrier) that $p_{1,k} = p_k$ and $p_{2,k} = 0$ if $r_k > t_k$, or otherwise $p_{1,k} = 0$ and $p_{2,k} = p_k$ if $r_k < t_k$. It is obvious from the definitions of r_k and t_k that $r_k > t_k$ if $k = \bar{k}$. But if $k \neq \bar{k}$, r_k may not always be larger than t_k.

- **Optimal $\frac{p_{2,k}}{p_{1,k}}$ under weak direct link channel gain $h_{1,k}$**: If the direct link has an infinite attenuation (or weak in the extreme), i.e., $h_{1,k} \approx 0$ $\forall k$, then $s_k = 0$, $r_k \geq t_k = 0$ and hence $\frac{p_{2,k}}{p_{1,k}} = 0$. In general, as the direct link becomes weaker, $\frac{p_{2,k}}{p_{1,k}}$ should become smaller.

- **Optimal $\frac{p_{2,k}}{p_{1,k}}$ under strong direct link channel gain $h_{1,k}$**: if the direct link ($h_{1,k}$ $\forall k$) becomes relatively strong compared to the relay links ($h_{2,k}$ and $h_{3,k}$ $\forall k$), then r_k

and t_k become more dominant than s_k. In this case, $\frac{p_{2,k}}{p_{1,k}}$ becomes either very large or very small depending on which of r_k and t_k is larger than the other.

Chapter 5

Overall Algorithm and Optimality Analysis

The overall algorithm (named Algorithm AO) for solving Problem (2.13) is summarized below.

Algorithm AO:

1. Use algorithm 1 (or algorithm 2) with a pre-select source power to find a new set of relay power, then go to Step 2);

2. Use algorithm 3 (or algorithm 4) with newly updated relay power to find a new set of source power, then go to Step 3);

3. Use algorithm 1 (or algorithm 2) with newly updated source power to find a new set of relay power, then go to Step 2) until converge, $|\triangle J| \leq \epsilon_I$.

In general, the alternating optimization method may fail to locate the stationary points, not

to mention the global convergence to the optimal solution. However, since the constraint functions in (2.14-2.15) are convex either for fixed $\{p_{1,k}, p_{2,k}\}$ or for fixed $\{g_k\}$, and Algorithm AO belongs to the nonlinear Gauss–Seidel (GS) method [16] where the optimization vector is only partitioned into two component vectors, it follows from [16] that Algorithm AO converges to a stationary point of Problem (2.13) as stated in the following theorem.

Theorem 1 (Local convergence of Alg. AO) *Any limit point* $\{\tilde{p}_{1,k}, \tilde{p}_{2,k}, \tilde{g}_k : \forall k\}$ *generated by Algorithm AO is a stationary point of Problem (2.13).*

In the following, we derive the asymptotically optimal solutions respectively for large relay transmit power P_r and large source-relay channel gain $h_2 \triangleq \min_k h_{2,k}$. Based on this, we show that the stationary point found by Algorithm AO is asymptotically optimal for large h_2 or P_r. Throughout this section, we will explicitly express the cost $J(\{p_{1,k}, p_{2,k}g_k\})$ as a function of $\{p_{1,k}, p_{2,k}g_k\}$ for clearness.

5.1 Asymptotically Optimal Solution for Large Relay Transmit Power

First, we give an upper bound for the SNR and show that the SNR upper bound can be approached as P_r grows large.

Lemma 1 *For fixed* $p_{1,k} + p_{2,k} = P_k$*, the SNR on the* k*-th subcarrier is upper bounded by*

$$\mathrm{SNR}_k \leq \mathrm{SNR}_k^{U1} \triangleq P_k max\left(h_{2,k}^2 + h_{1,k}^2, h_{1,\bar{k}}^2\right).$$

Moreover, if we let

$$p_{1,k} = P_k \mathrm{I}\left(h_{2,k}^2 + h_{1,k}^2 > h_{1,\bar{k}}^2\right), \tag{5.1}$$

$$p_{2,k} = P_k \mathrm{I}\left(h_{2,k}^2 + h_{1,k}^2 \leq h_{1,\bar{k}}^2\right), \tag{5.2}$$

$$g_k = \begin{cases} 0, & if\, h_{2,k}^2 + h_{1,k}^2 \leq h_{1,\bar{k}}^2, \\ \sqrt{\frac{P_r h_{2,k}^2}{N\left(1+h_{2,k}^2 p_{1,k}\right)}}, & otherwise, \end{cases} \tag{5.3}$$

then the corresponding SNR_k *satisfies* $\mathrm{SNR}_k^{U1} - \mathrm{SNR}_k = \mathcal{O}\left(\frac{1}{P_r}\right)$ *for sufficiently large* P_r*, where* $\mathrm{I}(\cdot)$ *denotes the indication function such that* $\mathrm{I}(E) = 1$ *if the event* E *is true and* $\mathrm{I}(E) = 0$ *otherwise.*

Please refer to Appendix 8.4 for the proof.

Using Lemma 1, we can obtain an asymptotically optimal solution of Problem (2.13) for large P_r by solving a convex optimization problem as stated in the following theorem.

Theorem 2 (Asymptotically optimal solution for large P_r) *Let* $\{P_k^\circ : \forall k\}$ *denote the optimal solution of the following convex optimization problem*

$$\min_{\{P_k \geq 0 : \forall k\}} \check{J},\ s.t.\ \sum_{k=0}^{N-1} P_k \leq P_s, \tag{5.4}$$

where either $\check{J} = -\min_k \mathrm{SNR}_k^{U1}$ *or* $\check{J} = \sum_{k=0}^{N-1} f_k\left(\mathrm{SNR}_k^{U1}\right)$*. Obtain* $\left\{p_{1,k}^\circ, p_{2,k}^\circ, g_k^\circ : \forall k\right\}$ *using (5.1-5.3) with* P_k *replaced by* P_k°*. Then for sufficiently large* P_r*,* $\left\{p_{1,k}^\circ, p_{2,k}^\circ, g_k^\circ : \forall k\right\}$ *is an asymptotically optimal solution of Problem (2.13), i.e.,* $\left\{p_{1,k}^\circ, p_{2,k}^\circ g_k^\circ : \forall k\right\}$ *satisfies the power constraints in (2.14-2.15) and*

$$J\left(\left\{p_{1,k}^\circ, p_{2,k}^\circ g_k^\circ\right\}\right) - J^* = \mathcal{O}\left(\frac{1}{P_r}\right), \tag{5.5}$$

where J^* is the optimal value of Problem (2.13).

Please refer to Appendix 8.5 for the proof.

Based on Theorem 2, we establish the asymptotic optimality of Algorithm AO for large P_r.

Theorem 3 (Asymptotic optimality of Alg. AO for large P_r) *Suppose that in Algorithm AO, the initial point is chosen such that $p_{1,k} = \mathcal{O}(1)$, $p_{2,k} = \mathcal{O}\left(\frac{1}{P_r}\right)$ if $h_{2,k}^2 + h_{1,k}^2 > h_{1,\bar{k}}^2$ and $p_{1,k} = \mathcal{O}\left(\frac{1}{P_r}\right)$, $p_{2,k} = \mathcal{O}(1)$ otherwise. Then for sufficiently large P_r, any limit point $\{\tilde{p}_{1,k}, \tilde{p}_{2,k}, \tilde{g}_k : \forall k\}$ generated by Algorithm AO is an asymptotically optimal solution of Problem (2.13), i.e.,*

$$J\left(\{\tilde{p}_{1,k}, \tilde{p}_{2,k}, \tilde{g}_k\}\right) - J^* = \mathcal{O}\left(\frac{1}{P_r}\right), \tag{5.6}$$

and $\{\tilde{p}_{1,k}, \tilde{p}_{2,k}, \tilde{g}_k : \forall k\}$ satisfies the power constraints in (2.14-2.15).

Please refer to Appendix 8.6 for the proof.

5.2 Asymptotically Optimal Solution for Large Source-Relay Channel Gain

We first give an upper bound for the SNR and show that the SNR upper bound can be approached as h_2 grows large.

Lemma 2 *For given non-negative $p_{1,k}, p_{2,k}, g_k$, the SNR on the k-th subcarrier is upper bounded by $\mathrm{SNR}_k(p_{1,k}, p_{2,k}, g_k) \leq \mathrm{SNR}_k^{U2}(p_{1,k}, p_{2,k}, \rho_k)$, where*

$$\mathrm{SNR}_k^{U2}(p_{1,k}, p_{2,k}, \rho_k) \triangleq h_{1,k}^2 p_{1,k} + \left(h_{3,\bar{k}}\sqrt{\rho_k} + h_{1,\bar{k}}\sqrt{p_{2,k}}\right)^2,$$

and $\rho_k = g_k^2 h_{2,k}^2 p_{1,k}$. *Moreover, for sufficiently large* h_2 *and given non-negative* $p_{1,k}^{'}, g_k^{'}$, *if* $g_k^{'} = \mathcal{O}\left(\frac{1}{\sqrt{h_2}}\right)$, $p_{1,k}^{'} - p_{1,k} = \mathcal{O}\left(\frac{1}{h_2}\right)$ *and* $g_k^{'2} h_{2,k}^2 p_{1,k}^{'} = \rho_k$, *then*

$$\mathrm{SNR}_k^{U2}\left(p_{1,k}, p_{2,k}, \rho_k\right) - \mathrm{SNR}_k\left(p_{1,k}^{'}, p_{2,k}, g_k^{'}\right) = \mathcal{O}\left(\frac{1}{h_2}\right).$$

Lemma 2 follows straightforward and the proof is omitted for conciseness.

Using Lemma 2, we can obtain an asymptotically optimal solution of Problem (2.13) for large h_2 by solving a convex optimization problem as stated in the following theorem.

Theorem 4 (Asymptotically optimal solution for large h_2**)** *Let* $\left\{p_{1,k}^{\circ}, p_{2,k}^{\circ}, \rho_k^{\circ} : \forall k\right\}$ *be an optimal solution of the following convex optimization problem*

$$\begin{aligned} &\min_{\left\{p_{1,k}\geq 0, p_{2,k}\geq 0, \rho_k \geq 0 : \forall k\right\}} \hat{J}, \\ &s.t. \sum_{k=0}^{N-1} \rho_k \leq P_r, \sum_{k=0}^{N-1} \left(p_{1,k} + p_{2,k}\right) \leq P_s, \end{aligned} \tag{5.7}$$

where either $\hat{J} = -\min_k \mathrm{SNR}_k^{U2}$ *or* $\hat{J} = \sum_{k=0}^{N-1} f_k\left(\mathrm{SNR}_k^{U2}\right)$. *Define*

$$\hat{g}_k^{\circ} = \begin{cases} \frac{1}{h_{2,k}} \sqrt{\frac{\rho_k^{\circ}}{p_{1,k}^{\circ}}}, & if\, p_{1,k}^{\circ} > 0, \\ \frac{\left(\rho_k^{\circ}\right)^{\frac{1}{4}}}{\sqrt{h_2}}, & otherwise. \end{cases}$$

$$\hat{p}_{1,k}^{\circ} = \begin{cases} p_{1,k}^{\circ}, & if\, p_{1,k}^{\circ} > 0, \\ \frac{\sqrt{\rho_k^{\circ}}}{h_2}, & otherwise. \end{cases}$$

Then for sufficiently large h_2, $\left\{\hat{p}_{1,k}^{\circ}, p_{2,k}^{\circ}, \hat{g}_k^{\circ} : \forall k\right\}$ *is an asymptotically optimal solution of Problem (2.13), i.e.,*

$$J\left(\left\{\hat{p}_{1,k}^{\circ}, p_{2,k}^{\circ}, \hat{g}_k^{\circ}\right\}\right) - J^* = \mathcal{O}\left(\frac{1}{h_2}\right), \tag{5.8}$$

and $\sum_{k=0}^{N-1}\left(\hat{p}_{1,k}^{\circ}+p_{2,k}^{\circ}\right)-P_s\leq\mathcal{O}\left(\frac{1}{h_2}\right)$, $\sum_{k=0}^{N-1}\left(h_{2,k}^2\hat{p}_{1,k}^{\circ}+1\right)(\hat{g}_k^{\circ})^2-P_r\leq\mathcal{O}\left(\frac{1}{h_2}\right)$.

Please refer to Appendix 8.7 for the proof.

Obviously, if we use the $\left\{\hat{p}_{1,k}^{\circ},p_{2,k}^{\circ},\hat{g}_k^{\circ}\right\}$ in Theorem 4 as initial point, the solution $\{\tilde{p}_{1,k},\tilde{p}_{2,k},\tilde{g}_k:\forall k\}$ found by Algorithm AO will be an asymptotically optimal solution of Problem (2.13), i.e.,

$$J\left(\{\tilde{p}_{1,k},\tilde{p}_{2,k},\tilde{g}_k\}\right)-J^*=\mathcal{O}\left(\frac{1}{h_2}\right). \tag{5.9}$$

Chapter 6

Implementation Issue and Simulation Result

6.1 Implementation Issue

In a real system, the AO algorithm could be executed at the source node. The global channel state information (CSI) must be supplied to this node. In relay systems, the source-relay/source-destination and relay-destination channels can be estimated directly at the destination node by utilizing pilot signals [17]. The destination must then feedback the CSI to the source node.

- **Complexity Analysis:** Here, each of addition, subtraction, multiplication and division is counted as one FLOP. The operations for comparisons are neglected.
  - **Complexity of Algorithm 1:** Step 1 requires $6N$ FLOPs (floating point operation), while Step 2 and 3 together require $21N$ FLOPs, where N is the

number of subcarrier. Then the complexity order of the overall bisection search process is $\mathcal{O}\left(21N\log_2\left(\frac{\mu^*}{\epsilon}\right)+6N\right)$, where μ^* is the length of the search range in Algorithm 1 and ϵ is the tolerable error.

– **Complexity of Algorithm 2:** Step 1 requires $8N$, while step 2 requires $(21+M_1)N$, where the M_1 additional FLOPs per subcarrier is introduced by convex function f. A different function f may require a different number of FLOPs in calculating f', f'^{-1} and f''. Given $\mu \leq \mu^*$, the complexity order of the overall bisection search process is upper-bounded by $\mathcal{O}\left((21+M_1)N\log_2\left(\frac{\mu^*}{\epsilon}\right)\log_2\left(\frac{\mu^*}{\epsilon}\right)+8N\right)$

– **Complexity of Algorithm 3:** Steps 1 through 3 require $46N$ FLOPs. The search ranges for θ and γ are denoted by R_θ and R_γ, respectively. The complexity order is upper-bounded by $\mathcal{O}\left(\left(37N+9N\log_2\left(\frac{R_\theta}{\epsilon}\right)\right)\log_2\left(\frac{R_\gamma}{\epsilon}\right)+46N\right)$. The complexity order increases logarithmically with R_θ and R_γ.

– **Complexity of Algorithm 4:** Step 1 through 2 require $40N+M_2$, where the additional M_2 FLOPs are introduced by the convex function f. Then, the complexity order is upper-bounded by

$$\mathcal{O}\left(\left(26N+M_2N+14N\log_2\left(\frac{R_\theta}{\epsilon}\right)\right)\times\log_2\left(\frac{R_\gamma}{\epsilon}\right)+40N+M_2N\right) \tag{6.1}$$

– **Overall Complexity of Algorithm AO:** With the above analysis, one can obtain the total number of FLOPS per iteration of the AO algorithm. Basically, the complexity grows linearly with the number of carrier and logarithmically with precision requirement. The number of iterations of the AO algorithm is

difficult to quantify, which depends on the stop criterion. In our simulation, the required number of iterations to achieve $|\triangle J| \leq \epsilon_I$ with $\epsilon_I = 0.005$ is about 2-4, where $\triangle J$ is the difference of J between two consecutive iterations.

6.2 Simulation Results

We have tested Algorithms 1-4 individually. They all converged rapidly to the exact optimal solutions.

For problem (2.13) with $J = J_1$, we apply Algorithms 1 and 3 alternately until convergence. For problem (2.13) with $J = J_2$, we apply Algorithms 2 and 4 alternately until convergence. We determine the convergence when both μ_1 and μ_2 satisfy $|\mu_1^r - \mu_1^{(r-1)}| < 10^{-5}$ and $|\mu_2^r - \mu_2^{(r-1)}| < 10^{-5}$ where r is the current index of alternation. For all tested cases, the convergence was reached within three to six alternations. The initialization of the source power allocation was chosen to be uniform, i.e., $p_{1,k} = p_{2,k} = \frac{P_s}{2N}$.

The optimization of the permutation function $\bar{k}$ is computationally costly. In our simulation, we have compared three choices of $\bar{k}$: 1) $\bar{k} = k$, 2) $\bar{k}$ is such that $h_{3,\bar{k}}$ is aligned with $h_{1,k}$ $\forall k$, and 3) $\bar{k}$ is such that $h_{3,\bar{k}}$ is aligned with $h_{2,k}$ $\forall k$. Two sequences S_1 and S_2 are said to be aligned if the largest element in S_1 is located at the same position as the largest element in S_2, the second largest element in S_1 is located at the same position as the second largest element in S_2, and so on. We have found that the third choice of $\bar{k}$ always yields slightly better result than the first two. Also note that with the third choice of $\bar{k}$, the overall relay channel gains defined by $h_{2,k}h_{3,\bar{k}}$ $\forall k$ have a larger dynamics than $h_{2,k}h_{3,k}$, which intuitively makes the relay power scheduling more effective. In the following, we use

the third choice of $\bar{k}$.

We generated the channel parameters $\tilde{h}_{1,k}$, $\tilde{h}_{2,k}$ and $\tilde{h}_{3,k}$ $\forall k$ as independent circular complex Gaussian random variables of zero means. We choose $\tilde{h}_{2,k}$ and $\tilde{h}_{3,k}$ $\forall k$ to have the variance two, and $\tilde{h}_{1,k}$ $\forall k$ to have the variance $2 \times 10^{\frac{\alpha}{10}}$. When $\alpha = 0$, the direct link has the same strength as the relay links. As α decreases from zero, the direct link weakens. The value of α measures a relative (averaged) strength in dB of the direct link over the relay links.

In Fig. 6.1, we show the minimum capacity among all subchannels versus α. This capacity was averaged over ten independent channel realizations. For each channel realization (of $\tilde{h}_{1,k}$, $\tilde{h}_{2,k}$ and $\tilde{h}_{3,k}$ $\forall k$), Algorithms 1 and 3 were used to maximize $\min_k \mathrm{SNR}_k$ (or minimize $-\min_k \mathrm{SNR}_k$). The resulting $\min_k \mathrm{SNR}_k$ is used to determine the minimum capacity (in bits/s/Hz) by $\frac{1}{2}\log_2(1 + \min_k \mathrm{SNR}_k)$. We see a significant gap of capacity between the case of free (optimal) η_k and the case of $\eta_k = 0$ when the direct link is not much weaker than the relay links. When the direct link becomes much weaker than the relay links, the gap diminishes as expected.

The distribution of the optimal $\log_{10} \eta_k$ $\forall k$ determined by Algorithms 1 and 3 for a typical channel realization is shown in Fig. 6.2. As predicted by the analysis shown in Section 4.3, when the direct link becomes weaker (α smaller), η_k approaches to zero. And when the direct link becomes stronger (α larger), η_k is either very large or very small. For the plot, any value of $\log_{10} \eta_k$ larger than 4 is set to 4, and any value of $\log_{10} \eta_k$ less than -4 is set to -4.

Fig. 6.3 shows the averaged subchannel capacity determined by Algorithms 2 and

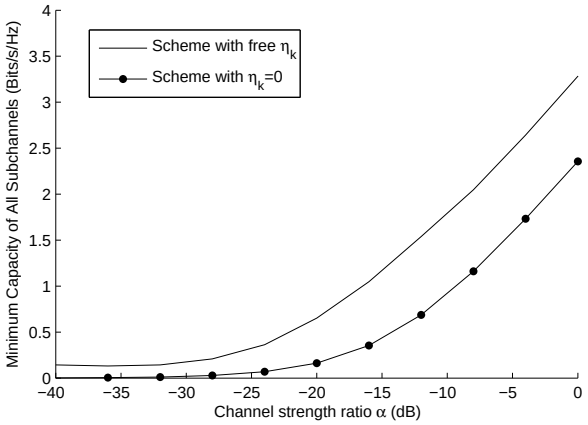

Figure 6.1: Minimum subchannel capacity determined by Algorithms 1 and 3 (for J_1) with $N = 300$ and $P_s = P_r = 50$. The scheme with free η_k is based on Algorithms 1 and 3 with no constraint on η_k. The scheme with $\eta_k = 0$ is based on Algorithms 1 and 3 with $\eta_k = 0$.

4 versus α. For each channel realization, Algorithms 2 and 4 were used to minimize J_2 shown in (2.12). The resulting $-J_2$ was further averaged over ten independent channel realizations and then plotted into this figure. Once again, we see an important gap between the case of free (optimal) η_k and the case of $\eta_k = 0$ when the direct link is not very weak.

The distribution of the optimal η_k $\forall k$ determined by Algorithms 2 and 4 for a typical channel realization is shown in Fig. 6.4. The general trends of the values of η_k as α increases or decreases are consistent with the analysis shown in Section 4.3.

Comparing the two costs J_1 and J_2, or equivalently, comparing Figs. 6.1 and 6.2 versus Figs. 6.3 and 6.4, we see that allowing η_k to be nonzero is more important for J_1 than for J_2, i.e., the capacity gap for J_1 is larger than that for J_2. It takes a much weaker direct link, for J_1 than for J_2, that η_k approaches to zero. We also see that the distribution of η_k becomes more binary for J_1 than for J_2 as the direct link becomes stronger.

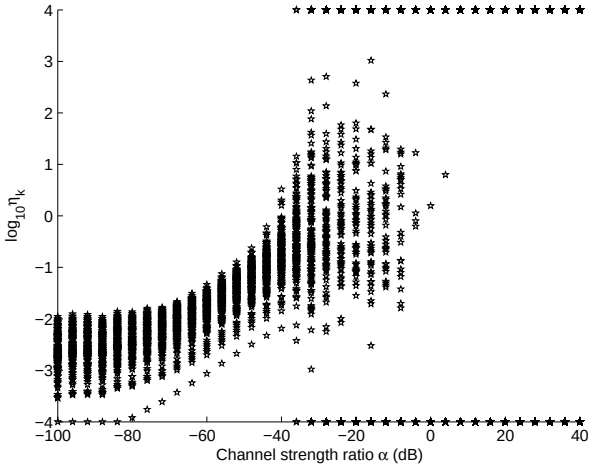

Figure 6.2: Distribution of the optimal η_k $\forall k$ determined by Algorithms 1 and 3 (for J_1) with $N = 300$ and $P_s = P_r = 50$.

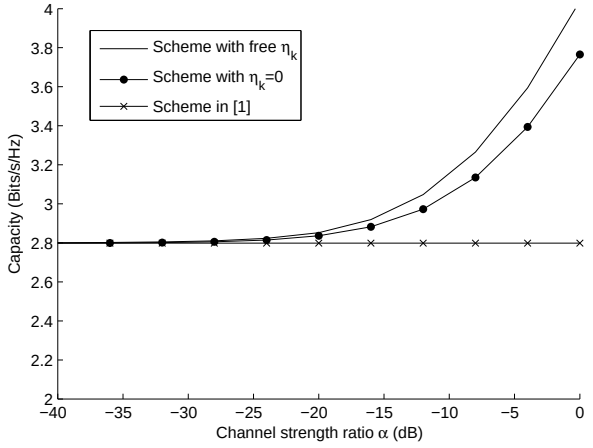

Figure 6.3: Average subchannel capacity determined by Algorithms 2 and 4 (for J_2) with $N = 300$ and $P_s = P_r = 50$. The scheme with free η_k is that by Algorithms 2 and 4 with no constraint on η_k, the scheme with $\eta_k = 0$ is that by Algorithms 2 and 4 with $\eta_k = 0$, and the scheme in [1] is the WF-MCAF method in [1] which ignores the direct link completely.

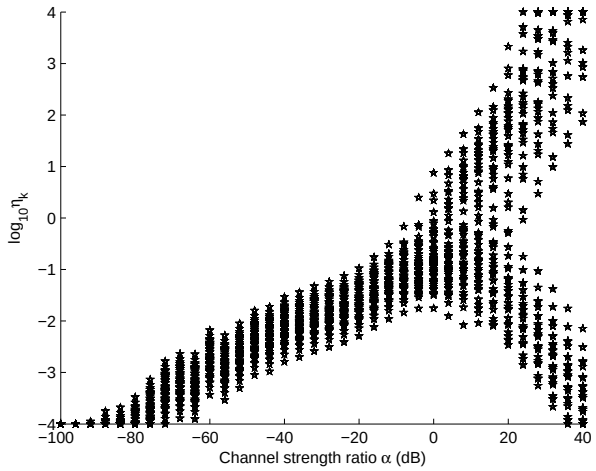

Figure 6.4: Distribution of optimal η_k $\forall k$ determined by Algorithms 2 and 4 (for J_2) with $N = 300$ and $P_s = P_r = 50$.

Chapter 7

Conclusion

We have studied a dual-phase power allocation problem for a multicarrier relay system with direct link. We have developed four efficient algorithms that yield the exact solutions to the four corresponding optimization problems, including two that are not convex. Unlike the previous works, we allow the source power to be distributed in both phases for each carrier. Our analysis and simulation show that this additional freedom is important when the direct link is not too weak compared to the relay links.

Chapter 8

Proof of Lemma and Theorem

8.1 Proof of Proposition 1

1. It follows from $\frac{d\mathrm{SNR}_k}{dg_k^2} = \frac{d\mathrm{SNR}_k}{2g_k dg_k}$ and (3.3) that $\frac{d\mathrm{SNR}_k}{dg_k^2} = \infty$ when $g_k = 0$, and $\frac{d\mathrm{SNR}_k}{dg_k^2} < \infty$ when $g_k > 0$. Also note that the left-side function of the power constraint (3.2) is a (finitely) weighted sum of g_k^2. As a result, if there is a $g_k = 0$, we can always increase g_k and decrease a positive $g_{k'}$ without affecting the power constraint but decreasing the cost J_2. Therefore, the optimal g_k for the cost J_2 must be positive for all k, and hence $\gamma_k = 0$, $\forall k \in \overline{\mathcal{K}}_0$.

2. Since the optimal g_k (also denoted by $\hat{g}_k$) to Problem (3.1) must fall in $[0, g_k^*]$ where J_2 is decreasing with g_k, the optimal g_k $\forall k$ must be such that either (3.2) holds with $\hat{g}_k = g_k^*$ $\forall k$ or the equality in (3.2) holds with $\hat{g}_k < g_k^*$ for at least one k.

3. It follows from (3.3) that

$$\frac{d\mathrm{SNR}_k}{2g_k dg_k} = \frac{(h_{3,\bar{k}}h_{2,k}g_k + h_{1,\bar{k}}\eta_k)}{g_k} \times \frac{(h_{3,\bar{k}}h_{2,k} - \eta_k h_{3,\bar{k}}^2 h_{1,\bar{k}}g_k)}{(h_{3,\bar{k}}^2 g_k^2 + 1)^2} p_{1,k}, \tag{8.1}$$

where both factors in the right-hand side are positive and decreasing with $g_k \in [0, g_k^*]$. Since $f_k(x)$ is a decreasing convex function, $-f_k^{'}$ is also positive and decreasing with $g_k \in [0, g_k^*]$. For a given feasible μ, the corresponding g_k for each k can be easily found by a bisection search based on (3.7), the solution of which is denoted by $g_k(\mu)$.

8.2 Proof of Proposition 2

The constraint (2.15) may or may not be active (i.e., the equality may or may not hold at the optimal solution). If the solution to all the KKT conditions, except with $\mu_2 = 0$, satisfies (2.15) with equality, then $\mu_2 = 0$ is optimal. Otherwise, we need to have $\mu_2 > 0$.

Let $a_1 = \mu_1$ and $a_2 = \mu_2 g_k^2 h_{2,k}^2 + \mu_1$. Then, for each pair of μ_1 and μ_2, (4.5) and (4.6) become

$$r_k + s_k \frac{\eta_k}{2} = \frac{a_2}{\lambda_k}, \tag{8.2}$$

$$t_k + s_k \frac{1}{2\eta_k} = \frac{a_1}{\lambda_k}. \tag{8.3}$$

Taking the ratio of the above two equations leads to a quadratic equation in terms of η_k, from which we have one unique (positive) solution in (4.9).

One can verify from (4.9) that η_k is a monotonically increasing function of $\frac{\mu_2}{\mu_1}$, i.e., $\frac{\partial \eta_k}{\partial\left(\frac{\mu_2}{\mu_1}\right)} > 0$.

For any given η_k in $\sqrt{p_{2,k}} = \eta_k \sqrt{p_{1,k}}$, we have from (4.4) that $\text{SNR}_k = (r_k + \eta_k s_k + \eta_k^2 t_k) p_{1,k}$ and hence for each given θ we can choose

$$p_{1,k} = \frac{\theta}{r_k + \eta_k s_k + \eta_k^2 t_k} \tag{8.4}$$

to achieve $\text{SNR}_k = \theta \ \forall k$.

The search for θ should be such that the equality in (2.14) is satisfied. Obviously, the left side of (2.14) is also a monotonically increasing function of θ subject to given η_k $\forall k$.

If the inequality in (2.15) is satisfied by the optimal solution to (4.2), $\frac{\mu_2}{\mu_1} = 0$ is optimal. Otherwise, we must have $\frac{\mu_2}{\mu_1} > 0$. So, we should start the search for $\frac{\mu_2}{\mu_1}$ from $\frac{\mu_2}{\mu_1} = 0$. The left side of (2.15) is a decreasing function of $\frac{\mu_2}{\mu_1}$ subject to (4.9) and the equality in (2.14).

The expression of η_k in (4.9) is numerically unstable when s_k is small (especially since g_k, and hence s_k, for some k can be exactly zero). To solve the numerical problem, we need to consider the case when s_k is arbitrarily small. As $s_k \to 0$, we can use the Taylor series expansion of (4.9) and write that

$$\eta_k = \begin{cases} \frac{2}{s_k}\left(t_k \frac{a_2}{a_1} - r_k\right) \to \infty, & t_k \frac{a_2}{a_1} - r_k > 0 \\ \frac{s_k \frac{a_2}{a_1}}{2\left(t_k \frac{a_2}{a_1} - r_k\right)^2} \to 0, & t_k \frac{a_2}{a_1} - r_k < 0 \\ \sqrt{\frac{a_2}{a_1}}, & t_k \frac{a_2}{a_1} - r_k = 0 \end{cases} \tag{8.5}$$

and using this in (8.4) leads to (4.7) and (4.8).

8.3 Proof of Proposition 3

The (4.12) and (4.13) are equivalent to

$$r_k + s_k \frac{\eta_k}{2} = -\frac{a_2}{f_k'}, \tag{8.6}$$

$$t_k + s_k \frac{1}{2\eta_k} = -\frac{a_1}{f_k'}, \tag{8.7}$$

which are virtually the same as (8.2) and (8.3).

Taking the ratio of (8.6) and (8.7) and solving the resulting quadratic equation in terms of η_k, we have the same solution as shown in (4.9). Hence, for any given $\frac{\mu_2}{\mu_1}$, we can find η_k $\forall k$ from (4.9).

Since f_k' is monotonically increasing with SNR_k, it is also monotonically increasing with $p_{1,k}$ subject to $\sqrt{p_{2,k}} = \eta_k \sqrt{p_{1,k}}$. Hence, if we are also given $\mu_1 = a_1$ (in addition to γ), we can find from (8.7) a unique $p_{1,k}$, and then the corresponding $p_{2,k}$, $\forall k$. Specifically, we recall $\mathrm{SNR}_k = (r_k + \eta_k s_k + \eta_k^2 t_k) p_{1,k}$, and hence have from (8.7) that $f_k' \doteq f_k'(\mathrm{SNR}_k) = f_k'((r_k + \eta_k s_k + \eta_k^2 t_k) p_{1,k}) = \frac{-\mu_1}{t_k + \frac{s_k}{2\eta_k}}$. Therefore,

$$p_{1,k} = \frac{\left({f_k'}^{-1} \left(\frac{-\mu_1}{t_k + \frac{s_k}{2\eta_k}} \right) \right)^+}{r_k + \eta_k s_k + \eta_k^2 t_k}, \tag{8.8}$$

where ${f_k'}^{-1}(x)$ is the inverse function of $f_k'(x)$, and $(x)^+ = \max(x, 0)$.

It is clear from (8.8) that $p_{1,k}, p_{2,k}, \forall k$ increase as μ_1 deacrese, subject to any given γ. So, we can use the bisection search to determine μ_1 such that the equality in (2.14) holds.

The equality in (2.15) may or may not be satisfied by the optimal solution subject to $\gamma = 1$ (or equivalently $\mu_2 = 0$). If it is satisfied, $\gamma = 1$ is optimal and no further search

is needed. Otherwise, we need to increase γ. Since $\sqrt{\frac{p_{2,k}}{p_{1,k}}}$ increases with γ, the left side of (2.15) is monotonically decreasing with γ subject to the equality in (2.14). Hence, we can use the bisection search to find γ such that the equality in (2.15) is satisfied.

Similar to the discussions for (4.7) and (4.8), as $s_k \to 0$, we should apply (8.5) to (8.8), which yields

$$p_{1,k} = \begin{cases} 0, & t_k \frac{a_2}{a_1} - r_k > 0 \\ \frac{\left(f_k'^{-1}\left(\frac{-\frac{a_2}{a_1}\mu_1}{\frac{a_2}{a_1} t_k + \left(t_k \frac{a_2}{a_1} - r_k \right)^2} \right) \right)^+}{r_k}, & t_k \frac{a_2}{a_1} - r_k < 0 \\ \frac{\left(f_k'^{-1}\left(\frac{-\mu_1}{t_k} \right) \right)^+}{r_k + \frac{a_2}{a_1} t_k}, & t_k \frac{a_2}{a_1} - r_k = 0 \end{cases} \tag{8.9}$$

and

$$p_{2,k} = \begin{cases} \frac{\left(f_k'^{-1}\left(\frac{-\mu_1}{t_k} \right) \right)^+}{t_k}, & t_k \frac{a_2}{a_1} - r_k > 0 \\ 0, & t_k \frac{a_2}{a_1} - r_k < 0 \\ \frac{\left(f_k'^{-1}\left(\frac{-\mu_1}{t_k} \right) \right)^+}{\frac{a_1}{a_2} r_k + t_k}, & t_k \frac{a_2}{a_1} - r_k = 0 \end{cases} \tag{8.10}$$

(8.8), (8.9) and (8.10) together conclude the proof.

8.4 Proof of Lemma 1

For fixed $p_{1,k}, p_{2,k}$, we have $\mathrm{SNR}_k \leq \mathrm{SNR}_k^* = p_{1,k}\left(h_{2,k}^2 + h_{1,k}^2 \right) + p_{2,k} h_{1,\bar{k}}^2$. Then for fixed $p_{1,k} + p_{2,k} = P_k$, the SNR upper bounded can be obtained by solving

$$\max_{p_{1,k}, p_{2,k}} \mathrm{SNR}_k^*, \text{ s.t. } p_{1,k} + p_{2,k} = P_k. \tag{8.11}$$

It is easy to see that the optimal solution of (8.11) is given by (5.1-5.2) and the optimal value is $\mathrm{SNR}_k^{\mathrm{U1}}$. Substituting (5.1-5.3) into the SNR expression in (2.9), it can be verified that $\mathrm{SNR}_k^{\mathrm{U1}} - \mathrm{SNR}_k = \mathcal{O}\left(\frac{1}{P_r} \right)$.

8.5 Proof of Theorem 2

By Lemma 1, we have

$$\check{J}\left(P_k^{\circ}\right) \leq J^*. \tag{8.12}$$

$$\mathrm{SNR}_k^{\mathrm{U1}}\left(P_k^{\circ}\right) - \mathrm{SNR}_k\left(p_{1,k}^{\circ}, p_{2,k}^{\circ}, g_k^{\circ}\right) = \mathcal{O}\left(\frac{1}{P_r}\right). \tag{8.13}$$

From (8.13), we have

$$\check{J}\left(P_k^{\circ}\right) - J\left(\left\{p_{1,k}^{\circ}, p_{2,k}^{\circ}, g_k^{\circ}\right\}\right) = \mathcal{O}\left(\frac{1}{P_r}\right). \tag{8.14}$$

Then (5.5) follows immediately from (8.12) and (8.14). Finally, using the definition of $\left\{p_{1,k}^{\circ}, p_{2,k}^{\circ}, g_k^{\circ} : \forall k\right\}$, it can be verified that $\left\{p_{1,k}^{\circ}, p_{2,k}^{\circ}, g_k^{\circ} : \forall k\right\}$ also satisfies the power constraints in (2.14-2.15).

8.6 Proof of Theorem 3

Using the KKT condition in (3.7), it can be shown that for any initial point $\{p_{1,k}, p_{2,k}\}$ that satisfies the condition in Theorem 3, the optimal $g_k^{(1)}$ obtained in step 1 of Algorithm AO satisfies $g_k^{(1)} = \mathcal{O}\left(\frac{1}{\sqrt{P_r}}\right)$ if $h_{2,k}^2 + h_{1,k}^2 \leq h_{1,\bar{k}}^2$, and $g_k^{(1)} = \mathcal{O}\left(\sqrt{P_r}\right)$ otherwise. Following similar analysis as in the proof of Lemma 1, it can be shown that

$$\check{J}\left(\{P_k^{\circ}\}\right) - J\left(\left\{p_{1,k}^{\circ}, p_{2,k}^{\circ}, g_k^{(1)}\right\}\right) = \mathcal{O}\left(\frac{1}{P_r}\right). \tag{8.15}$$

By Lemma 1, we have

$$\check{J}\left(\{P_k^{\circ}\}\right) \leq J^*. \tag{8.16}$$

For fixed $g_k^{(1)}$, the optimal $\left\{p_{1,k}^{(1)}, p_{2,k}^{(1)}\right\}$ obtained in step 2 of Algorithm AO satisfies

$$J\left(\left\{p_{1,k}^{(1)}, p_{2,k}^{(1)}, g_k^{(1)}\right\}\right) \leq J\left(\left\{p_{1,k}^{\circ}, p_{2,k}^{\circ}, g_k^{(1)}\right\}\right). \tag{8.17}$$

From (8.15-8.17), we have $J\left(\left\{p_{1,k}^{(1)}, p_{2,k}^{(1)}, g_k^{(1)}\right\}\right) - J^* = \mathcal{O}\left(\frac{1}{P_r}\right)$, i.e., after the first iteration of Algorithm AO, the solution is already asymptotically optimal for large P_r. The rest iterations will only decrease the cost function. This completes the proof.

8.7 Proof of Theorem 4

Using Lemma 2 and the fact that the constraint $\sum_{k=0}^{N-1} \rho_k \leq P_r$ in (5.7) is a more relaxed relay power constraint compared to the original one in (2.15), we have

$$\hat{J}\left(p_{1,k}^{\circ}, p_{2,k}^{\circ}, \rho_k^{\circ}\right) \leq J^*. \tag{8.18}$$

Note that $\left(\hat{g}_k^{\circ}\right)^2 h_{2,k}^2 \hat{p}_{1,k}^{\circ} = \rho_k^{\circ}$. Then it follows from Lemma 2, $\hat{g}_k^{\circ} = \mathcal{O}\left(\frac{1}{\sqrt{h_2}}\right)$ and $\hat{p}_{1,k}^{\circ} - p_{1,k}^{\circ} = \mathcal{O}\left(\frac{1}{h_2}\right)$ that

$$\mathrm{SNR}_k^{\mathrm{U2}}\left(p_{1,k}^{\circ}, p_{2,k}^{\circ}, \rho_k^{\circ}\right) - \mathrm{SNR}_k\left(\hat{p}_{1,k}^{\circ}, p_{2,k}^{\circ}, \hat{g}_k^{\circ}\right) = \mathcal{O}\left(\frac{1}{h_2}\right). \tag{8.19}$$

From (8.19), we have

$$\hat{J}\left(p_{1,k}^{\circ}, p_{2,k}^{\circ}, \rho_k^{\circ}\right) - J\left(\left\{\hat{p}_{1,k}^{\circ}, p_{2,k}^{\circ}, \hat{g}_k^{\circ}\right\}\right) = \mathcal{O}\left(\frac{1}{h_2}\right). \tag{8.20}$$

Then (5.8) follows immediately from (8.18) and (8.20). Finally, using $\hat{g}_k^{\circ} = \mathcal{O}\left(\frac{1}{\sqrt{h_2}}\right)$, $\hat{p}_{1,k}^{\circ} - p_{1,k}^{\circ} = \mathcal{O}\left(\frac{1}{h_2}\right)$, and the definition of $\left\{p_{1,k}^{\circ}, p_{2,k}^{\circ}, \rho_k^{\circ} : \forall k\right\}$, it can be verified that $\left\{\hat{p}_{1,k}^{\circ}, p_{2,k}^{\circ}, \hat{g}_k^{\circ} : \forall k\right\}$ satisfies $\sum_{k=0}^{N-1}\left(\hat{p}_{1,k}^{\circ} + p_{2,k}^{\circ}\right) - P_s \leq \mathcal{O}\left(\frac{1}{h_2}\right)$,

Part II

A Practical Exploration of Full-Duplex Radio Communication

Chapter 9

Introduction

Currently the radio used in cellular communication, radio, microwave back-haul, WiFi, bluetooth technology are half-duplex. Either a frequency-devision (FD), time-devision (TD), or other division, such as code-division (CD), is used for multiple access. Nowadays the spectrum become more and more previous as the demands increases. Many researches have been done to improvement the management of spectrum. Traditionally, the sub-channel used for transmitting is different from the sub-channel used for receiving due to self-interference. Full-duplex, a new approach with theoretically double efficiency of spectrum, has received growing interests in research and commercial applications [18, 19]. Full-duplex will bring a great advantage over half-duplex in terms of capacity and interference coordination, etc and has the potential for sustain the LTE 5G [20]. The key to full-duplex is to remove the self-interference caused by the local transmitter, referred as self-interference cancellation (SIC). One can cancel the self-interference using the following techniques:

- Passive Cancellation. Passive cancellation includes antenna separation and fixed an-

tenna null. Obviously the more attenuation between the receiver and the local transmitter, better the cancellation. However, the cancellation is at the expense of increasing the size of the nodes, which is limited in practice.

- Active Digital cancellation. This technique are DSP based cancellation achieved in digital domain. If only active digital cancellation is applied, strong self-interference will still be presented at the LNA and the ADC. The saturation of LNA and the reduction of dynamic range of ADC limit the performance of full-duplex link capacity, or even destroy the connection.

- Active analog cancellation. This cancellation is aimed to cancel the self-interference before the digital domain to prevent the saturation or dynamic range wastes. This method has a higher implementation cost comparing to active digital cancellation due to the difficulties to manipulating signal in analog domain.

These three main techniques are not mutually exclusive. In fact, the best result is achieved using the combination of them. Previously several research are conducted to verify the performance of each technique and the combination of them. Self-interference cancellation achieved by antenna placement are discussed in [21, 22, 23, 24, 25, 26]. In [21, 22, 23], the antenna were specifically placed to create a pair of path with same attenuation and opposite phase, resulting in a RF null at receiver. [24] proposed a relay antenna domain isolation technique, [25] was based on antenna mutual coupling model and [26] used a directional antenna to achieve the null at the receiver.

In [27], noise cancellation chip Intersil QHX220 was used for digital active cancellation.

However, the cancellation was limited by the dynamic range. In [28], the passive cancellation was used to break this limits. The active analog cancellation was adopted in [21] with two additional antenna. To reduce the additional hardware requirement, in [29], a design with two antenna full-duplex radio was proposed using a Balun circuit. Though this method didn't have a bandwidth constrain, the performance degraded as the bandwidth increases. This limits the application of the proposed structure in a scenario where the self-interference channel is frequency selective. Another method for frequency selective self-interference channel method was proposed in [30] for orthogonal frequency division multiplexing (OFDM) system. This method processed the cancellation in digital domain and the cancellation happened in analog domain. In [31], we proposed a more general technique for any system with this advantage. An mathematically analysis of 20MHz FD OFDM wireless system was presented in [32]. [33] proposed an analytical optimal solution for wideband multitap self-interference channel cancellation.

For active analog cancellation, [34, 35, 36] proposed open loop techniques on narrow or wide band. The open-loop made the system vulnerable to the transmitter and receiver impairment. A more robust approach was proposed in [37] using closed-loop. Since the self-interference was much stronger than the desired signal, an iterative cancellation would improve the robustness to the error estimation of the self-interference channel. A two- stage cancellation was proposed in [38]. While the above method were using multiple antenna (or directional antenna) for active analog cancellation, [39] proposed a single antenna solution. [40] also proposed a single antenna solution but only allowed simultaneous transmitting and reception on different adjacent channel/subcarrier. In [41], an 110 dB cancellation

was achieved by a combination of digital and analog cancellation technique. The proposed method had a significant less cancellation in strongly frequency selective self-interference channel.

MIMO system that support multiple streams were considered in [42, 43, 44, 45, 46, 31]. The possibility of full-duplex MIMO was discussed in [42]. A 20 MHz full-duplex MIMO OFDM WiFi radio was proposed in [43]. An mixture of SISO and MIMO scenario was discussed in [44]. [45] also presented a full-duplex WiFi radio with complexity scales linearly with the number of antenna. [46] presented a solution that can flexibly select the number of RF chains based on the network topology. In [31], we proposed a time domain transmit beamforming method without the assumption of the frequency-flat self-interference channel. This method also got rid of the prefix-region problem associated with the OFDM beamforming method.

While most of the active analog method weree cancel the self-interference at the RF stage, [47, 48, 49, 50, 51] discussed the analog baseband cancellation. [47] showed a significant improve with an additional complementary analog baseband cancellation stage. [48] fed back the cancellation signal before the input of ADC. [49] used an adaptive auxiliary transmitter. [50, 51] implemented an adaptive filter using the information from digital domain. In [52], we categorized them into 1) all-analog method, such as [21, 40, 33, 41, 37], 2) all-digital method, such as [48] and 3) hybrid method, such as [28, 36, 31, 52]. In an all-analog method, RF interference was canceled at RF front-end by using its RF interference source. In an all-digital method, interference was canceled only after the RF interference had been converted into baseband and digitized. A hybrid method might use either a baseband-controlled trans-

mit beamforming method to cancel interference at the RF front-end of receivers [31] or use the RF signals tapped from the output of RF power amplifiers to cancel the interference after down-conversion to a lower frequency [52]. In Figure 9.1, four approaches for SIC critical for full-duplex radio are presents. The dash lines denote the cancellation paths. The all-analog path denotes a path with analog input interface, analog filter and analog output interface. The all-digital path denotes a path with digital input interface, digital filter and digital output interface. The hybrid-1 path denotes a path with digital input interface, digital filter and analog output interface. The hybrid-2 path denotes a path with analog input interface, digital filter and analog output interface. The two antennas can be merged into one by using a circulator.

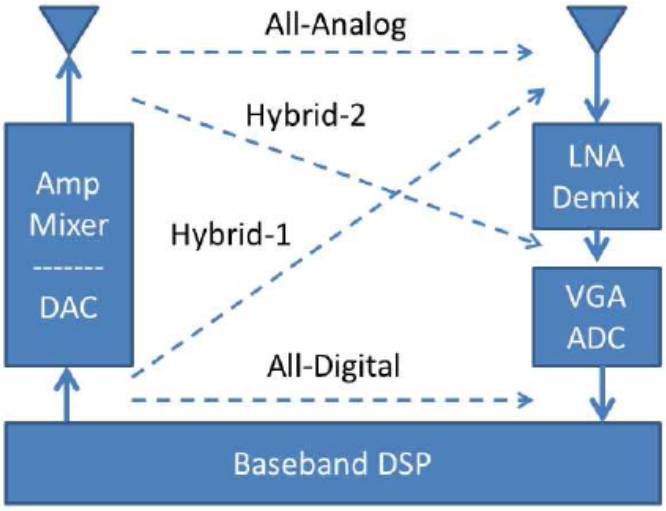

Figure 9.1: Four approaches for self-interference cancellation.

Analog active cancellation is affected by the impairment of the transmitter and receiver such as phase noise, non-linear distortion and thermal noise. This had been an bottle

neck for full-duplex in the past. [53, 54, 55, 56] showed that the effect caused by the phase noise could also be mitigated. [53] showed that the main bottle neck in self-interference cancellation was the local oscillator phase noise. [54] considered both shared oscillator and independent ones. [55] developed a digital domain cancellation under oscillator phase noise. [56] investigated the amplify-and-forward repeater link in the presents of the oscillator phase noise. In [52], we proposed a new analog-digital hybrid method without the limitation of the transmitting noise. A blind system identification and equalization algorithm for finding the optimal configuration was discussed and provided. [57, 58, 59, 60, 61] considered the effect caused by nonlinear distortion. [60] provided a comprehensive analysis of the effects of nonlinear distortion in transmitter power amplifier. [61] analyzed the performance of full-duplex MIMO OFDM transceivers under non-ideal ADCs. In [62], impact of thermal noise on full-duplex radio was analyzed. Tabel 9.1 shows the topic covered by each paper

We have proposed novel architecture for all-analog cancellation using a clustered taps in [63] and compared its performance with the uniformly distributed RF attnuator in [41, 37]. This method method would taken care of all the impairment of the transmitter, which is the main source of noise. The following section shows the detail of our contribu-

Category	Reference
Passive Cancellation	[21, 22, 23, 24, 25, 26, 27, 28, 34, 43]
Active Digital Cancellation	[20, 21, 27, 28, 29, 30, 31, 32, 33, 34, 35, 36, 37, 38] [39, 41, 43, 45, 46, 47, 52, 61]
Actice Analog Cancellation	[21, 28, 29, 34, 35, 38, 41, 43, 45, 46, 48, 49, 50, 51] [55, 58, 59, 61]

Table 9.1: Topics covered by the reference paper.

tion. First, the transmitting beamforming method is discussed and the experiment data is presented, second a new adaptive method is presented and the algorithm associate with it is also demonstrated.

Chapter 10

Transmitting Beamfoming Method

Since the transmitted signal are known and the interference channel can be estimated, we can subtract the self-interference from the received waveform. It is the most straightforward method to remove the self-interference. The model can be expressed as:

$$y[n] = r[n] - \hat{i}[n] = x[n] * h_i[n] + d[n] * h_d[n] - x[n] * \hat{h}_i[n] \tag{10.1}$$

where $r[n]$ is the received signal, $i[n]$ is the estimated interference signal, $x[n]$ is the transmitted signal, $d[n]$ is the desired remote signal, $h_i[n]$ is the self-interference channel, $h_d[n]$ is the remote channel and the $\hat{h}_i[n]$ is the estimated self-interference channel in baseband complex form. With an accurate enough estimation of the self-interference channel, we can achieve full-duplex radio communication. However, the cancellation happens in digital domain, which means that the strong self-interference will be presented at the front end of the LNA and ADC. This will caused the saturation of LNA. Even the the LNA is not saturated, the dynamic range of ADC will be great reduced. For example, assume we have two communication nodes with channel strength shown in Figure 10.1. The path loss (with

everything lumped together) between the transmitter and the remote receiver is 90 dB, the path loss between the transmitter and the local receiver is 40dB, both receivers, remote or the local ones, require 20dB to decode, and has a noise floor at -100dBm. Therefore to ensure the SNR of both the receiver, the receiving signal should at least be -80dBm, with the transmitting power at 10dBm and the self-interference power at -30dBm. In this case, the self-interference is 50dB larger than the desired signal. This will saturate the amplifier and/or waste the dynamic range of ADC as we will discussed in detail later. An example of power level at the receiver is shown in Figure 10.2. As we can see the desired remote signal is deeply buried by the self-interference.

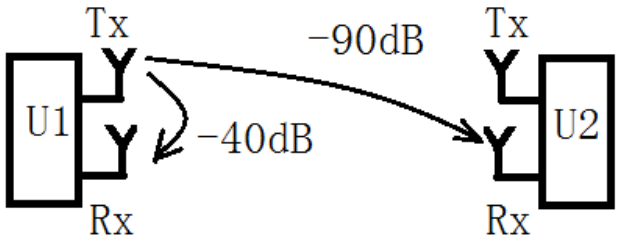

Figure 10.1: Remote Channel Gain vs. Self-Interference Channel Gain

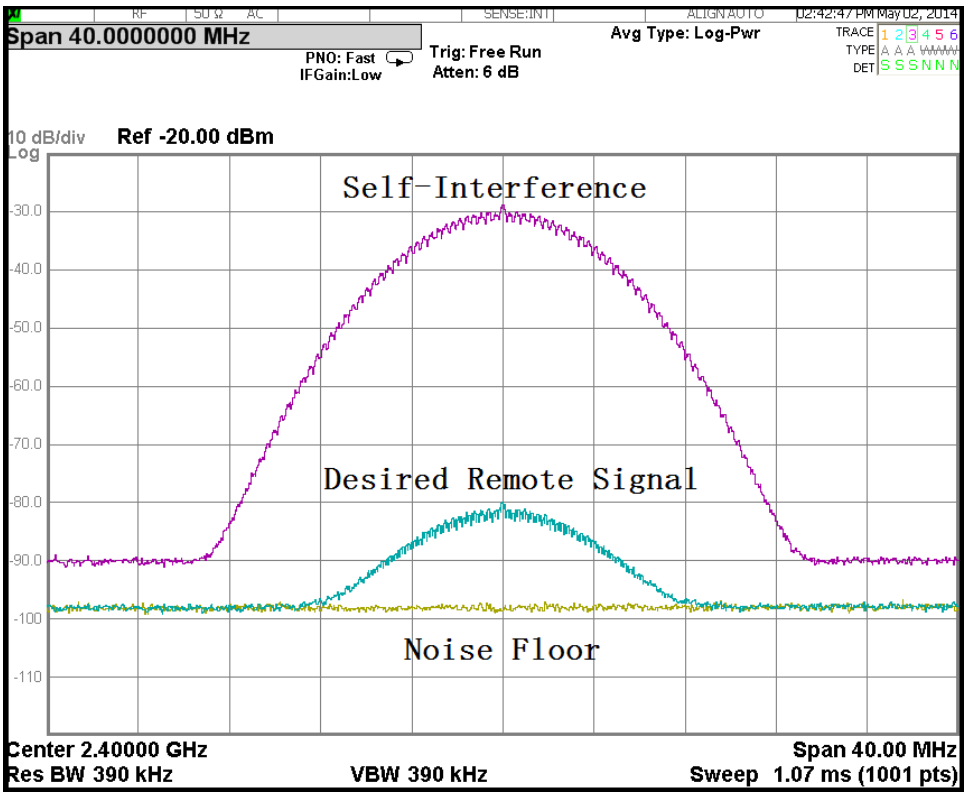

Figure 10.2: Power levels at receiver.

To achieve fullduplex, interference has to be canceled. Initially, digital cancellation is applied and cancellation is limited. This is due to the saturation power of the front-end LNA amplifier is limited. Then RF/analog domain cancellation is studied. We have to cancel the interference before the input of the LNA amplifier, which can not be achieved by digital cancellation. A variety structures have been designed for the RF/analog domain cancellation, so are the corresponding control algorithm for the structures. As shown in Figure 10.2, the self-interference is 50dB stronger than the desired remote signal. Assume

we are using a 14-bit ADC, the whole dynamic range is

$$DR = 20\log_{10}\left(\frac{Max\ Value}{Min\ Value}\right) = 20\log\frac{2^{14}-1}{2^0} \approx 84dB \tag{10.2}$$

By subtracting the self-interference, we removed the larger 50 dB range from the dynamic range, therefore leaving 34dB for decoding desired remote signal, which is equivalent to $N = 5.6$ bits ADC without self-interference, as shown in Equ. (10.3)

$$N = \log_2 10^{34\times 0.05} \approx 5.6 \tag{10.3}$$

With much less digits available in the ADC, the quantization error become significant and the whole communication is compromised. In reality, sometime self-interference could be more than 100 dB higher than the desired signal. It is not practical to use a digital interference removal to achieve full-duplex radio alone.

10.1 Structure and Procedure in SISO Mode

As stated earlier, digital interference cancellation is not practical due to the saturation of LNA and reduction of the dynamic range of ADC. In [31], we presented a method for full duplex Radio. This method cancels the self-interference at antenna to avoid saturation effect. The fullduplex needs an additional transmitting antenna to cancel the self-interference. This antenna is called cancelmitter (Cx). The full-duplex node has one transmitter (Tx), one cancelmitter (Cx) and one receiver (Rx). The hardware experimental schematic is shown in Figure 10.3, where, two Signal Generator, Agilent MXG N5182A (SG1 and SG2), and one Signal Analyzer, Agilent MXA N9020A (SA) are deployed as Cx, Tx and Rx, respectively.

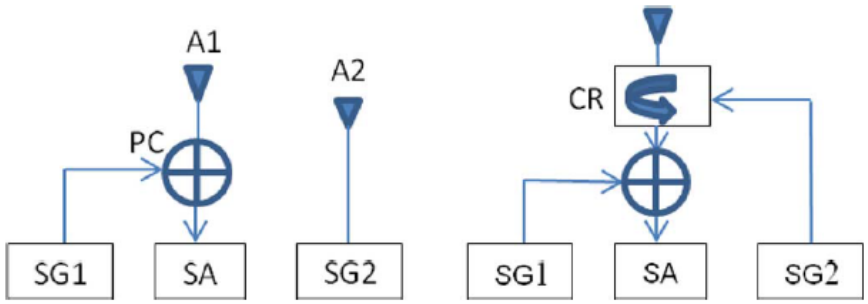

Figure 10.3: Schematic of experiment using Agilent MXA N9020A and MXG N5182A for Full Duplex Hardware Experiment. Two MXG and one MXA are used as Tx, Cx and Rx.

During channel estimation phase, broadband signal is transmitted from Tx and Rx. The received signal is processed for channel estimation. During full-duplex phase, according to the estimated channel, a transmitting beamforming method is applied to make an null at the Rx. Another important issue is the alignment. The interference signal and the cancel signal should arrive the receiver at the same time. This requires additional effort to record the delay of each path. The accuracy of the alignment is critical and sometimes is smaller than the sample interval. Though we can align the signal using fractional sampling method, a novel procedure without alignment is proposed in [31] as:

1 Tx transmits a delta signal $p[n]$ and Cx transmits $p[n]$, Rx captures it as $p_1[n]$;

2 Tx transmits $p[n]$ and Cx transmits $-p[n]$ and Rx captures them using the same delay as $p_2[n]$;

3 To transmit $s[n]$ in full-duplex mode, Tx transmits $s[n] * (p_2[n] - p_1[n])$ and Cx transmits $s[n] * (p_1[n] + p_2[n])$

By using this procedure, interference and the cancellation goes through self-interference channel and cancellation channel in different orders. After permutation, they both go through the same channel therefore all the delay are identical. We can show that

$$p_1[n] = p[n] * h_1[n] + p[n] * h_2[n] \tag{10.4}$$

$$p_2[n] = p[n] * h_1[n] - p[n] * h_2[n] \tag{10.5}$$

where $h_1[n]$ is the baseband complex channel between Tx and Rx, $h_2[n]$ is the baseband complex channel between Cx and Rx. The interference at the Rx is expressed as:

$$\begin{aligned} I[n] &= s[n] * (p_2[n] - p_1[n]) * h_1[n] + s[n] * (p_1[n] + p_2[n]) * h_2[n] \\ &= 2s[n] * (-p[n] * h_2[n] * h_1[n] - p[n] * h_1[n] * h_2[n]) = 0 \end{aligned} \tag{10.6}$$

The transmitted full-duplex radio signal goes through an additional pre-filter $p_2[n] + p_1[n]$ or $p_2[n] - p_1[n]$. This length of the filter is small since it's a response of the self-interference channel, and can be lumped into the real channel. Therefore this additional filter won't affect the reception and decoding for the remote receiving node. The reception of the remote signal is not affected.

10.2 Pre-Filter Design in MIMO Mode

The procedure for general MIMO full-duplex radio is also discussed in [31]. Assume the full-duplex node has N_t transmitter, the first N_r are auxiliary Tx used for self-interference cancellation, last $N_s = N_t - N_r$ are primary Tx, and N_l receiver. The received self-interference can be represented as

$$\mathbf{i}[n] = \mathbf{H}[n] * \mathbf{x}[n] = \mathbf{H}[n] * \mathbf{G}[n]\mathbf{s}[n] \tag{10.7}$$

where, $\mathbf{i}[n]$ is $N_l \times 1$ column vector composed by the received self-interference at each Rx, $\mathbf{H}[n]$ is $N_l \times N_t$ matrix, whose (i, j) element is the self-interference channel response between, the jth Tx and ith Rx, $\mathbf{x}[n]$ is $N_t \times 1$ vector contains the transmitted signal from each Tx, $G[n]$ is the $N_t \times N_s$ transmitting beamforming matrix and $\mathbf{s}[n]$ is the transmitted signal in half-duplex radio. We have to develop $\mathbf{G}[n]$ with the knowledge of $\mathbf{H}[n]$ so that

$$\mathbf{H}[n] * \mathbf{G}[n] = \mathbf{0} \tag{10.8}$$

For the kth Tx in half-duplex radio, we should have

$$\mathbf{i}_k[n] = \mathbf{H}[n] * \mathbf{g}_k[n] = \mathbf{0} \tag{10.9}$$

then we can have

$$\mathbf{i}[n] = \sum_{k=1}^{N_s} \mathbf{i}_k[n] = \mathbf{0} \tag{10.10}$$

where bold $g_k[n]$ is the kth column of $\mathbf{G}[n]$, to cancel the self-interference cancellation, we should satisfy Equ. (10.9) for all k. Now we can discuss the condition for the existence of the solution to the aforementioned equation. If $\sum_{i=1}^{I} \mathbf{a}_i[n] * \mathbf{f}_i[n] = \mathbf{0}$ implies $\mathbf{a}_1[n] = \mathbf{a}_2[n] = \cdots = \mathbf{a}_I[n] = \mathbf{0}$, $\mathbf{f}_i$ are convolutively independent. The convolution rank $r_{conv}(\mathbf{H}[n])$ of matrix $\mathbf{H}[n]$ is the largest number of columns (rows) in $\mathbf{H}[n]$ that are convolutively independent. It's more or less like the linear independent concept. Similarly we have the $r_{conv}(\mathbf{H}[n]) \leq \min\{N, N_t\} = N_r$. The dimension of the solution space of Equ. (10.9), similarly called the right null space of $\mathbf{H}[n]$, is the number of the convolutively independent solution to Equ. (10.9), $d_{null} = N_t - r_{conv}(\mathbf{H}[n]) \geq N_s$. In practice, typically we will have $d_{null} = N_s$, given the rich scatter environment. Therefore when the data stream is less than the number of primary Tx, we can find solution to Equ. (10.9). The choice of $g_k[n]$ is not

unique. One of the solution we provide in [31] is described as:

$$\mathbf{g}_k[n] = \begin{bmatrix} \bar{\mathbf{g}_k}[n] \\ \mathbf{0}_{k-1,1} \\ g_{0,k}[n] \\ \mathbf{0}_{N_r-1,1} \end{bmatrix} \tag{10.11}$$

where $\mathbf{0}_{m,1}$ is the $m \times 1$ zero vector, $\bar{\mathbf{g}_k}[n]$ and $g_{0,k}[n]$ are the solution to

$$\mathbf{A}[n] * \bar{\mathbf{g}_k}[n] + \mathbf{b}_k[n] * g_{0,k}[n] = \mathbf{0} \tag{10.12}$$

where $\mathbf{A}[n]$ is a square matrix equal to the first N_r columns of $\mathbf{H}[n]$ and $\mathbf{b}_k[n]$ is the N_{r+k}th column of $\mathbf{H}[n]$. Therefore one straightforward solution is

$$\bar{\mathbf{g}_k}[n] = -adj\{\mathbf{A}[n]\} * \mathbf{b}_k[n] \tag{10.13}$$

and

$$g_{0,k}[n] = det\{\mathbf{A}[n]\} \tag{10.14}$$

All the values can be obtained analytically and no division is involved.

10.3 Experimental Results and Conclusion

The transmitting beamforming method is test using 1) Agilent MXA and MXG with time-invariant channel and 2) WARP board in real time-variant channel. The details are recored below.

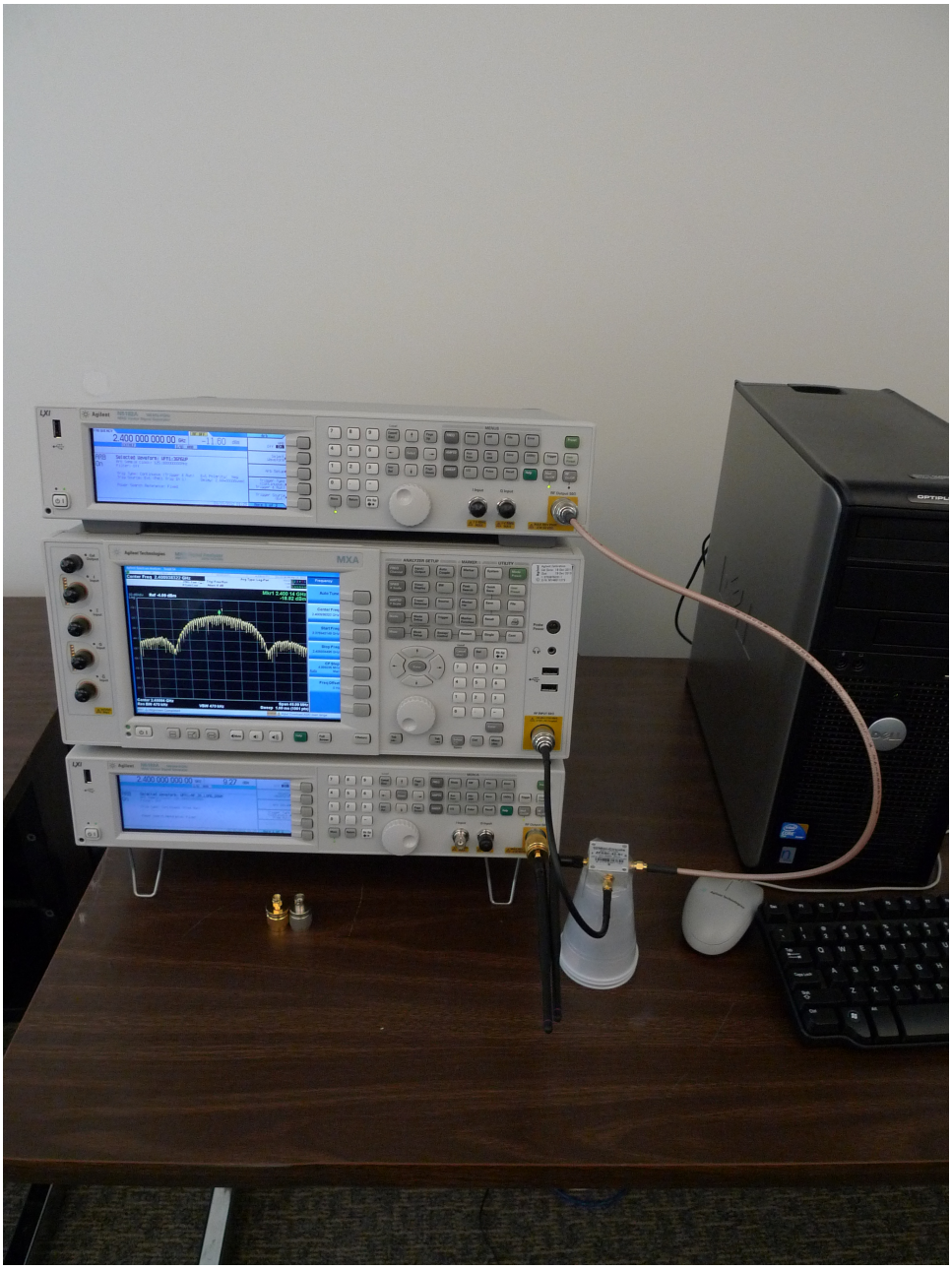

Figure 10.4: Agilent MXA N9020A and MXG N5182A. Two MXG and one MXA are used as Tx, Cx and Rx. A 10 MHz local oscillator is shared. We used 40 MHz broadband signal at 2.4 GHz on this platform. Details of the component are listed in Appendix A. The schematic is shown in Figure 10.3.

Figure 10.4 shows the Agilent MXA and MXG used in this experiment. Power

combiner ZAPD-4-S+ from mini-circuit is used. The time and frequency domain full-duplex radio self-interference caused by the transmitted signal are shown in Figure 10.5 and Figure 10.6, respectively. time and frequency domain residual are shown in Figure 10.7 and Figure 10.8.

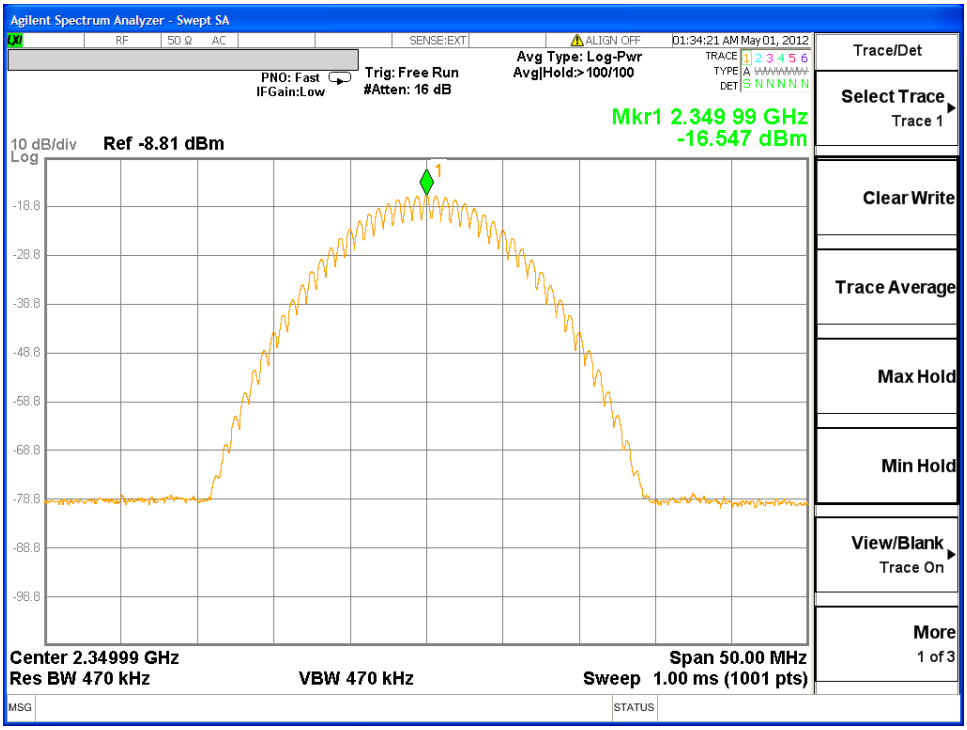

Figure 10.5: Self-Interference in Frequency Domain in Agilent MXA and MXG Experiment

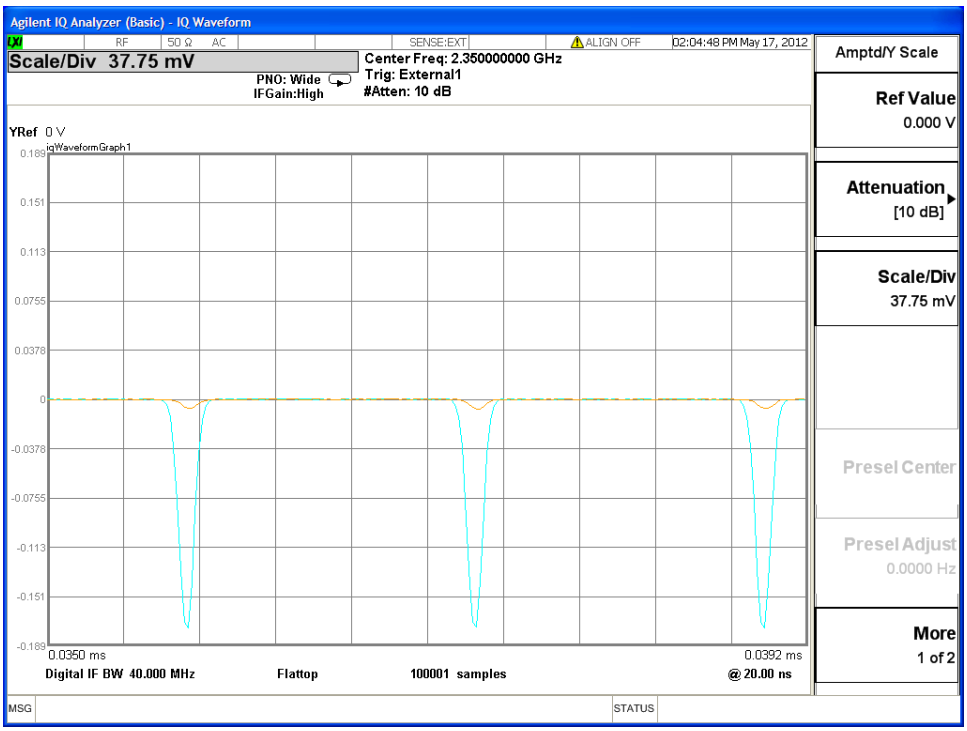

Figure 10.6: Self-Interference in Time Domain in Agilent MXA and MXG Experiment

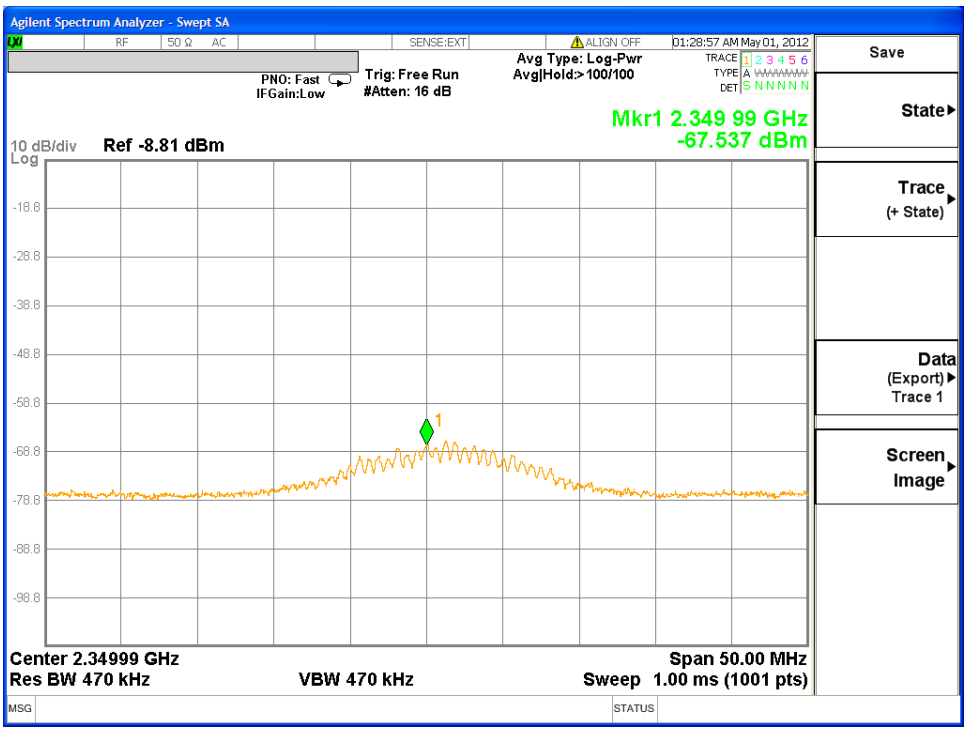

Figure 10.7: Residual in Frequency Domain in Agilent MXA and MXG Experiment

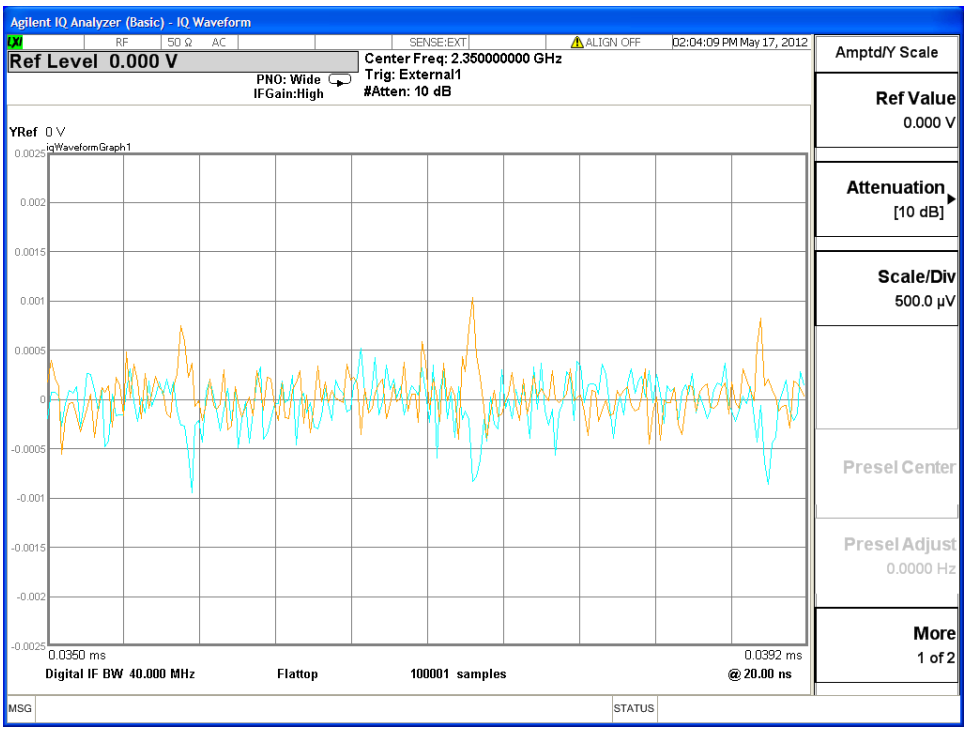

Figure 10.8: Residual in Time Domain in Agilent MXA and MXG Experiment

As we can see that the signal at the central frequency is canceled by 50dB. However, we cannot do a real time experiment in this system due to the limitation of the interface provided by the equipment. Also, the RF chain of Agilent MXA and MXG is much superior than the off-the-shelf commercial. For the real time experiment, we use WARP radio hardware plat form Mango communication [64] as shown in Figure 10.9.

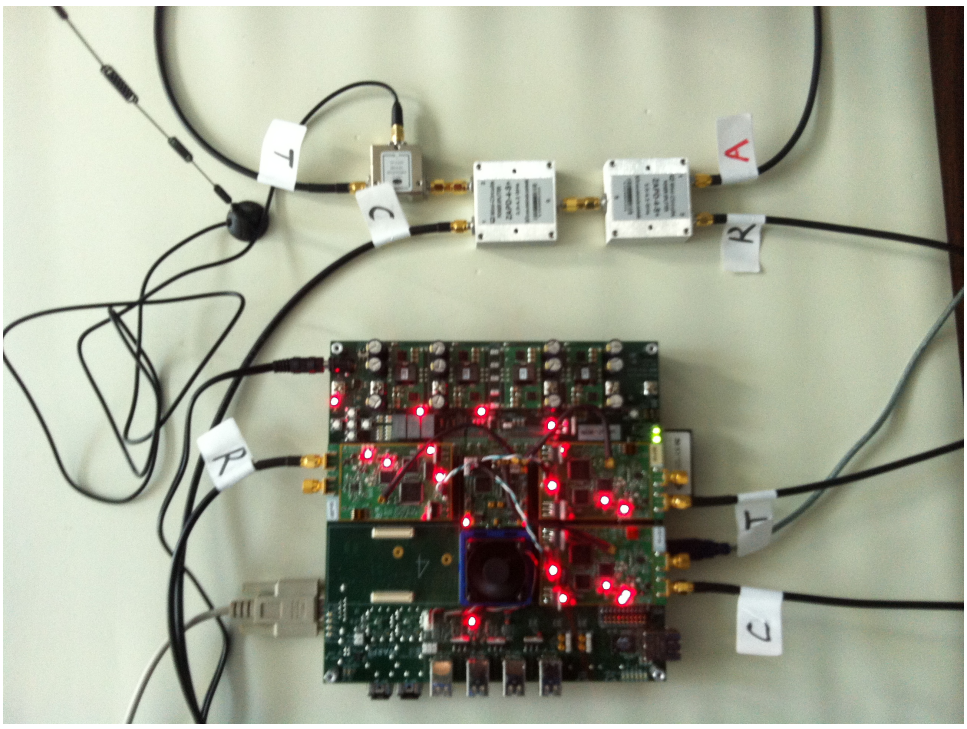

Figure 10.9: WARP board for Full Duplex Node Hardware Experiment. On this platform we test the self-interference cancellation for 20MHz signal at 2.4GHz. Three radio board is configured as Tx, Cx an Rx. The local oscillator and clock is shared. Details of the component and the related hardware are listed in Appendix A.

The key components of the platform is listed below:

1. Xilinx Virtex- FX100 FPGA (XC4VFX100-11FFG1517C)

2. 20MHz and 40 MHz temperature compensated oscillators for RF carrier reference and logic and converter clocks respectively.

3. Dual AD9510 low jitter buffers for clocks.

4. Dual 65MS/sec 14-bit analog-digital-converter (ADC) for Rx I/Q (AD9248)

5. Dual 125 MS/sec 16-bit digital-analog-converter (DAC) for Tx I/Q (AD9777)

6. 20MS/sec 10-bit ADC for receiver signal strength indicator (RSSI) (AD9200)

7. 2.4 & 5GHz RF transceiver (MAX2829)

8. 18dBm power amplifier.

9. Power combiner ZAPD-4-S+

10. 2.4GHz antenna

More details of the involved component are listed in Appendix A. Comparing with the Aigilent MXA and MXG experiment, the RF and analog component are less expensive and accurate. This experiment is more practical given that most of the component are commercial off-the-shelf ones. Firmware and software were developed based on the reference design of WARP project. The concept schematic is shown in Figure 10.10 with most of the interface neglected for convenience. Similar to the Angilent MXA and MXG experiment, three radio chain is shown as transmitter, cancelmitter and receiver.

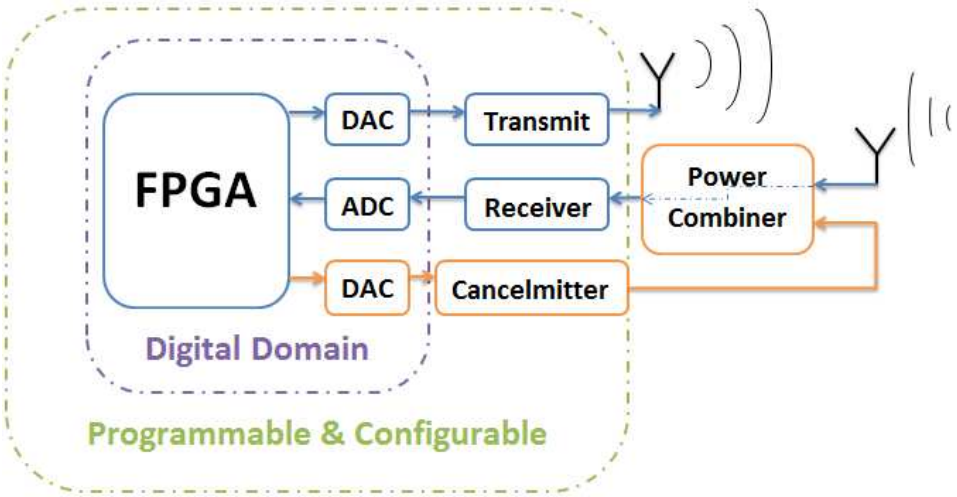

Figure 10.10: The structure of the experiment system.

An example of the time domain waveform in a single experiment is shown in Figure 10.11. We can see from the upper-left plot that without transmitting beamforming, self-interference signal saturated the receiver (notice the clipping at the peak of the waveform.) While in the lower-left plot the residual interference is within the dynamic range, which can be further removed by applying baseband digital method.

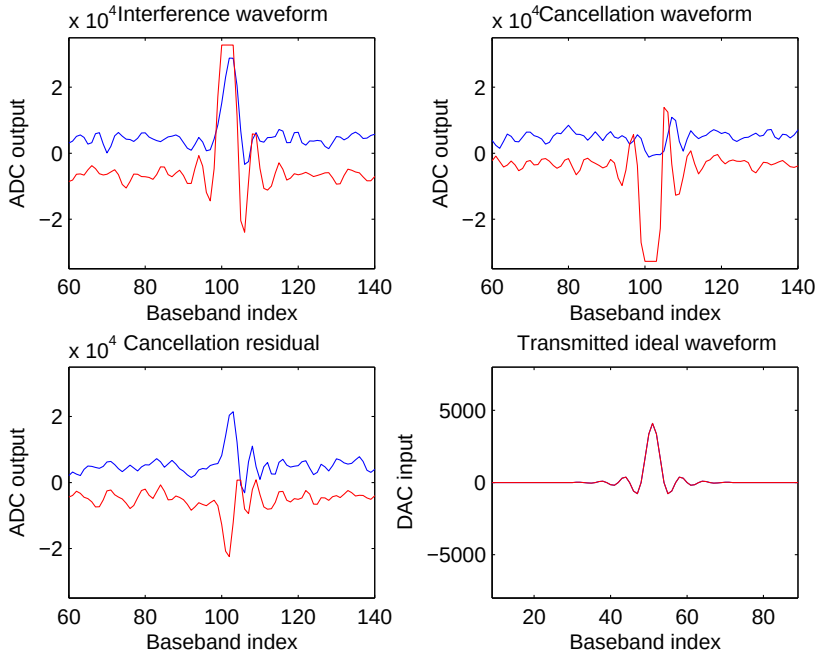

Figure 10.11: The upper left plot shows the received Rx waveform when only Tx is transmitting(interference waveform), the upper right plot shows received Rx waveform when only Cx is transmitting (cancellation waveform), the lower left plot shows the received Rx waveform when Tx and Cx are both transmitting, and the lower right plot shows the transmitted ideal waveform. All the plots are captured within 25.6ns.

In this experiment we use four antenna position with repeated test to get the statistics of the cancellation. As shown in Figure 10.12, Tx is placed in the same location (Marked with Tx) while Rx has four locations (Marked with Rx1, Rx2, Rx3 and Rx4). The corresponding results are the curve labeled with C1, C2, C3 and C4 in Figure 10.13.

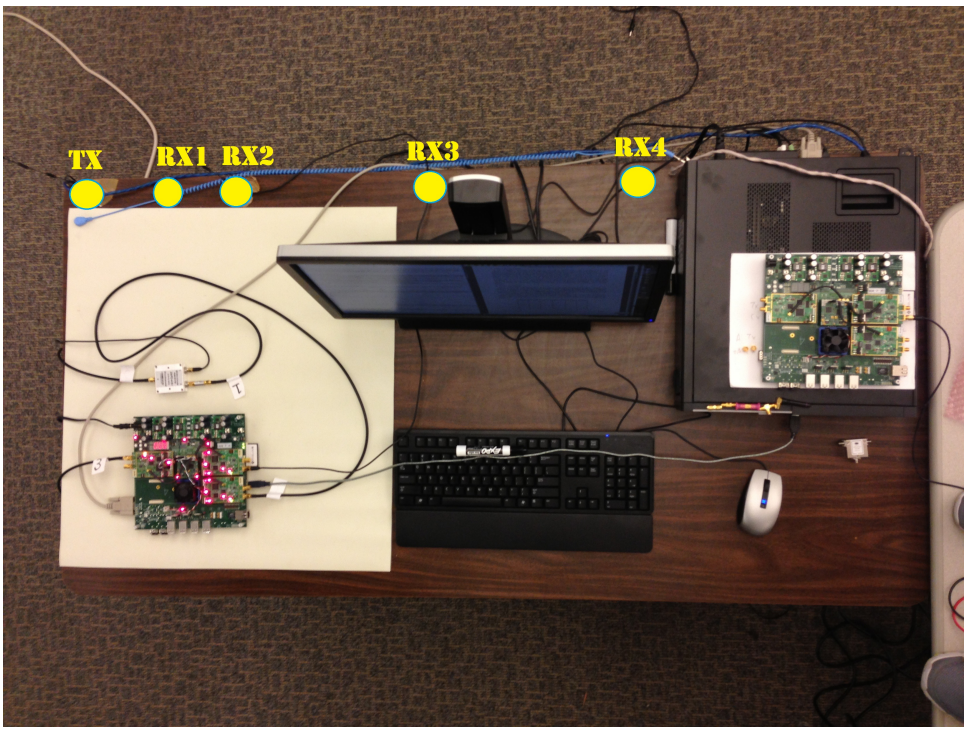

Figure 10.12: Photo of the equipment and position of Tx and Rx antenna. To verify the cancellation performance with multiple different surrounding structure. The Tx is placed in a fixed location and Rx has four location as shown. Cx is connected via circulator therefore no Cx antenna. Identical power, bandwidth, carrier frequency are used for all the test.

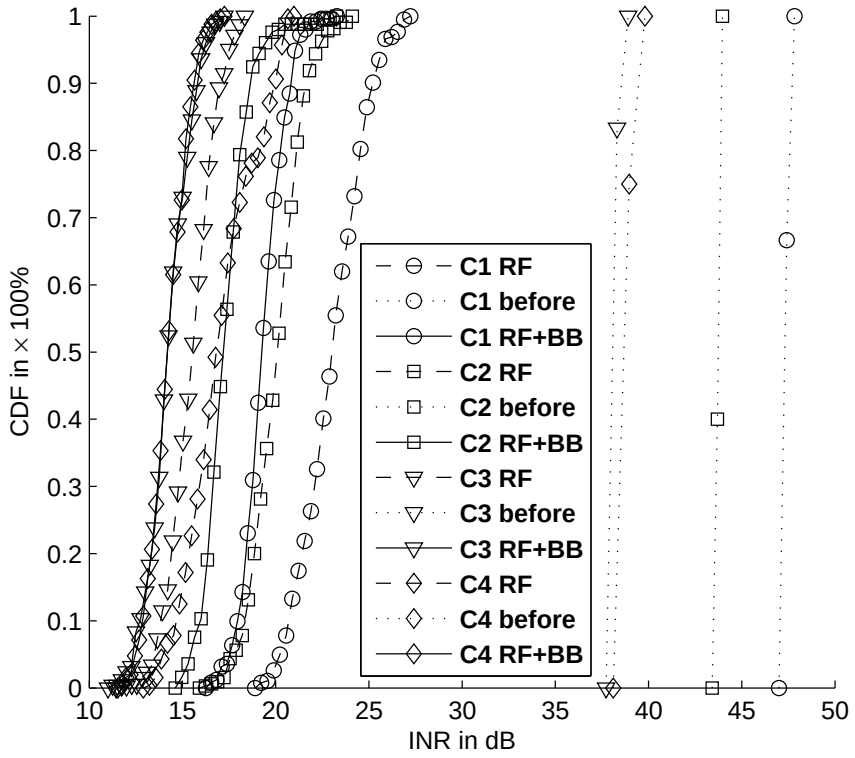

Figure 10.13: In the legend, 'Before' stands for self-interference, 'RF' stands for the proposed cancellation method, 'BB' stands for the baseband cancellation and 'Cn' stands for the configuration of antenna position with index n in Figure 10.12.

As we can see that the cancellation amount is less than the Agilent MXA and MXG experiment. Roughly 27dB is canceled before digitizing. This leaves the residual in the dynamic range that can be further removed by digital signal processing method. This method prevent the LNA from saturation and reduce the dynamic range loss by 27dB.

10.4 Limitation of transmitting Beamforming: transmitting Noise

The dominating random noise floor is not introduced at the receiver side. Instead the noise floor raised with the transmitting power. As shown in Figure 10.2, the noise floor of self-interference is about 9 dB higher than the receiver noise floor. Traditionally, the noise floor from remote transmitter is buried by the receiver noise floor. However, in full-duplex radio, the transmitter noise is dominant. Since we cannot cancel the random transmitting noise, this effect puts an upper limits of the cancellation we can achieve using transmitter beamforming method. In other words, the actual transmitted signal $\tilde{p}[n]$is not exactly $p[n]$. It can be modeled as:

$$\tilde{p}[n] = p[n] + r[n] \tag{10.15}$$

And the transmitting SNR is defined as

$$SNR_T = 20 \log \frac{||p[n]||}{||r[n]||} \tag{10.16}$$

where $r[n]$ is a random noise, whose power increases with the transmitting power. We verified the transmitting noise with MXA and MXG, as shown in Figure 10.4, is 60dB, while the transmitting of WARP board is only about 30dB. Also the transmitting noise will brought extra error in self-interference channel estimation, but the main effect is that the transmitting noise cannot be canceled during full-duplex communication. This barrier limits the transmitting power for a full-duplex node. Without a method to overcome this barrier, the full-duplex radio will not be practical.

Chapter 11

Adaptive Filter Method

Beamforming method can cancel the self-interference down to the transmitting noise floor. For long distance communication, the attenuation between the Tx and remote Rx is larger. With larger power gap between the transmitting and the receiving power, beamforming method become less practical for long distance full-duplex radio. For practical long distance full-duplex radio, we have to cancel the self-interference beyond the transmitting SNR. One option is to use transmitter with less transmitting noise, just like the Agilent MXG. This solution may become feasible in the future. Since we cannot reproduce the transmitting noise, the only way to cancel it is to use filtered version of that noise to cancel itself. Another method we proposed later is to use an adaptive filter to create an "opposite" self-interference channel to cancel the self-interference.

11.1 Adaptive Filter Architecture

The essence is to construct a "opposite" channel, which cancels the actual self-interference channel. In [52], we provide a detailed model with detailed block for the adaptive filter method. The basic structure is shown in Figuire. 11.1.

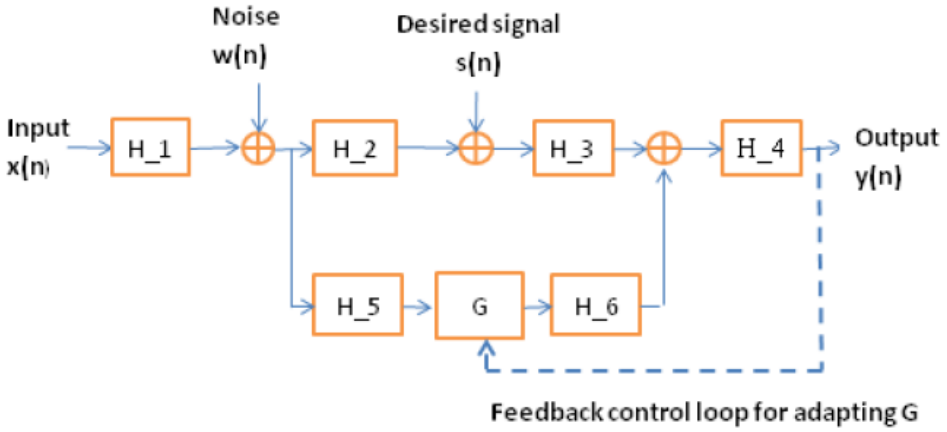

Figure 11.1: Adaptive filter for self-interference cancellation

The input signal $x[n]$ is the digital source interference signal before DAC in the transmit chain. $w[n]$ is the transmitting noise from the entire transmit chain. $s[n]$ is the desired remote signal. $y[n]$ is the only observed signal after ADC. $y[n]$ has two component, one is the self-interference, the other is the desired remote signal. H_k represents the transfer function of all the path, and none of them is known. The detailed description of each H are as follow:

1. H_1 represents the equivalent baseband channel between the digital domain and the output of the RF power amplifier. All the noise is added after H_1 for convenience.

2. H_2 represents the channel between the transmit antenna and the receive antenna. If other component, such as circulator is used, H_2 would represent the combination of isolation path of the RF circulator and the local reflect channel.

3. H_3 represents the channel between the receive antenna and an analog baseband signal combiner before LNA.

4. H_4 represents the channel between the signal combiner and the output $y[n]$, including LNA, VGA and ADC.

5. H_5 represents the channel between the output of the transmit power amplifier in the transmit chain and the input of the digital-controlled filter.

6. H_6 represents the channel between the output of the digital controlled filter G and the signal combiner.

If the transfer function G satisfied that

$$H_6 G H_5 = -H_3 H_2 \tag{11.1}$$

then both $x[n]$ and $w[n]$ will not affect $y[n]$. We can cancel the transmitting noise by using the adaptive filter. To avoid introducing additional noise, it is preferred that only passive component are used in the adaptive filter. Below we first show that the attenuator-delay combination is adequate for construct the adaptive filter G. Our discussion is based on a most accepted structure of adaptive filter G as shown in Figure 11.2, named as all-analog canceler.

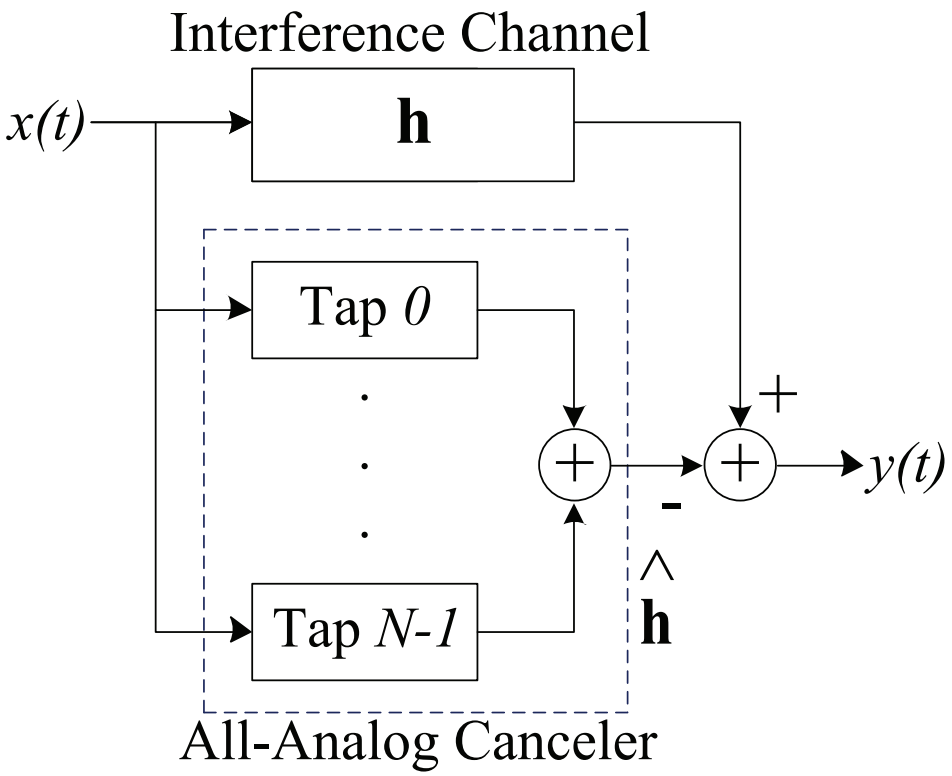

Figure 11.2: Architecture of adaptive G filter with taps

11.1.1 Single Tone Signal Cancellation

If there is only one radio path between the transmitter and receiver and single tone is used for wireless transmitting. The received signal can be express as

$$y(t) = x(t - \tau)A\exp(j\theta) \tag{11.2}$$

where $y(t)$ is the received signal, $x(t)$ is transmitted signal, A is the amplitude attenuation of the path, and θ is the phase caused by the path. We can construct a cancel path using

one attenuator to create a path with the received signal being:

$$\hat{y}(t) = x(t-\tau)A\exp(j\hat{\theta}) = -x(t-\tau)A\exp(j\theta) \tag{11.3}$$

If multiple path are presented, we can use multiple cancellation path. The ideal sum of interference and cancellation can be expressed as:

$$y(t) + \hat{y}(t) = \sum_{n=1}^{N} A_n \exp(j\theta_n)x(t-\tau_n) + \sum_{n=1}^{N} A_n \exp(j\hat{\theta}_n)x(t-\tau_n) = 0 \tag{11.4}$$

The method for finding the attenuation and delay and constructing the cancel filter in practice will be discussed later. This concept is verified using RF signal generator(SG) Agilent MXG N5182A and RF spectrum analyzer(Sa) Agilent MXA N9020A. We connect SG and SA using two cable with different length and RF combiner, splitter and attenuator. This block provides us a two path channel with similar attenuation and different delay. In practical design, without the knowledge of the delay and the attenuation, we can connect a sequence tunable step attenuator, each with a different fixed delay for the cancel block. With small enough step and difference between delay, the ideal cancel channel can be arbitrarily accurate approximated.

11.1.2 Broadband Signal Cancellation

Broadband can be view as the combination of plenty of single tone signal. Each attenuation path will result in a different phase and similar attenuation for each tones. For example, $x(t)$ with two tones at f_1 and f_2 are transmitted, and received as

$$y(t) = x_{f_1}(t-\tau)A_{f_1}\exp(j\theta_{f_1}) + x_{f_2}(t-\tau)A_{f_2}\exp(j\theta_{f_2}) \tag{11.5}$$

In this case, we need at least two independent cancel path to cancel the self-interference. Let the received signal of the cancel path be:

$$\hat{y}_a(t) = x_{f_1}(t-\tau)A_a \exp(j\theta_{af_1}) + x_{af_2}(t-\tau)A_a \exp(j\theta_{af_2}) \tag{11.6}$$

$$\hat{y}_b(t) = x_{f_1}(t-\tau))A_b \exp(j\theta_{bf_1}) + x_{bf_2}(t-\tau)A_b \exp(j\theta_{bf_2}) \tag{11.7}$$

Adjust A_a, A_b, θ_{af_1}, θ_{af_2}, θ_{bf_1} and θ_{bf_2}

$$-A_{f_1} \exp(j\theta_{f_1}) = A_a \exp(j\theta_{af_1}) + A_b \exp(j\theta_{bf_1}) \tag{11.8}$$

and

$$-A_{f_2} \exp(j\theta_{f_2}) = A_a \exp(j\theta_{af_2}) + A_b \exp(j\theta_{bf_2}) \tag{11.9}$$

Then the interference from the two-tone signal can be canceled. Multiple-tone or broadband signal interference can be canceled similarly. It is also straightforward to achieve similar result for multiple path case. For each path, we use a set of cancel channel to cancel the broadband signals. The conclusion is that, with enough cancel path, we can construct a inverted broadband channel to cancel the self-interference.

11.2 Evaluation Criteria

The adaptive filter is could be composed with several tap, each is a tunable step-attenuator connected with fixed delay. Or it could contains other component such as phase splitter, circulator and/or RF switches. The adaptive filter changes as the value of the attenuators. And currently there is no tunable delay available. There are many other possible ways to construct the adaptive filter. Before discussing the variety of the structures,

we discuss the evaluation criteria of the adaptive filter$G$ first. Since the resolution of the step attenuator, or other tunable component, are limited, the number of possible adaptive filter G is limited. We call each configuration of adaptive filter G a channel candidate. To compensate the actual interference channel, which is random and time-variant, we are favor in the structure that provide more channel candidate with diversity. For example, we put 4 step digital-attenuator in series as shown on the left side of figure 11.4. Let each attenuator have 0 to 31.5dB with step size 0.5dB and assume the phase associated with the attenuation is linear as shown in Figure 11.3.

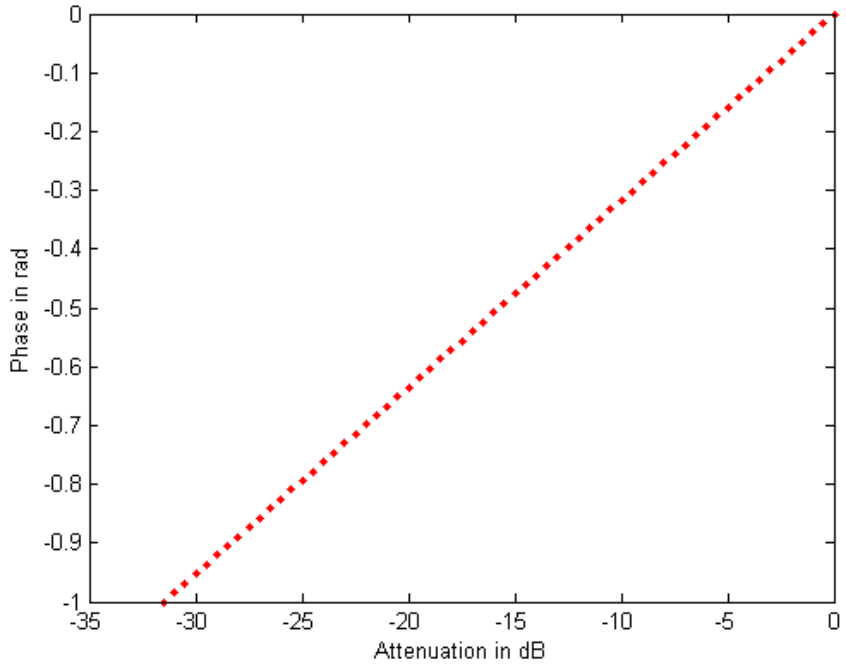

Figure 11.3: Relay phase vs Attenuation

In other words, each attenuator has 2^6 possible values. The whole structure has totally 2^{24} possible settings. However, a lot of these setting results in same attenuation.

The structure can only be 0dB to 126dB, 2^8 possible values, much smaller than the possible settings. If we connect as on the right side of figure 11.4, it would have more possible values.

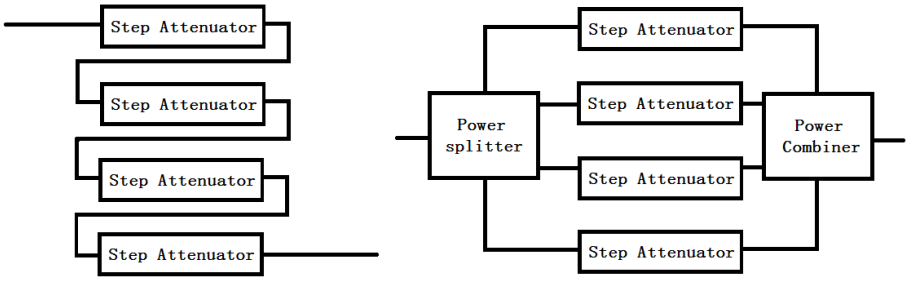

Figure 11.4: Two different taps composed by four step attenuator

Even though both tap have same number of the relay configurations, the combined candidates shows a different distribution as shown in Figure 11.5.

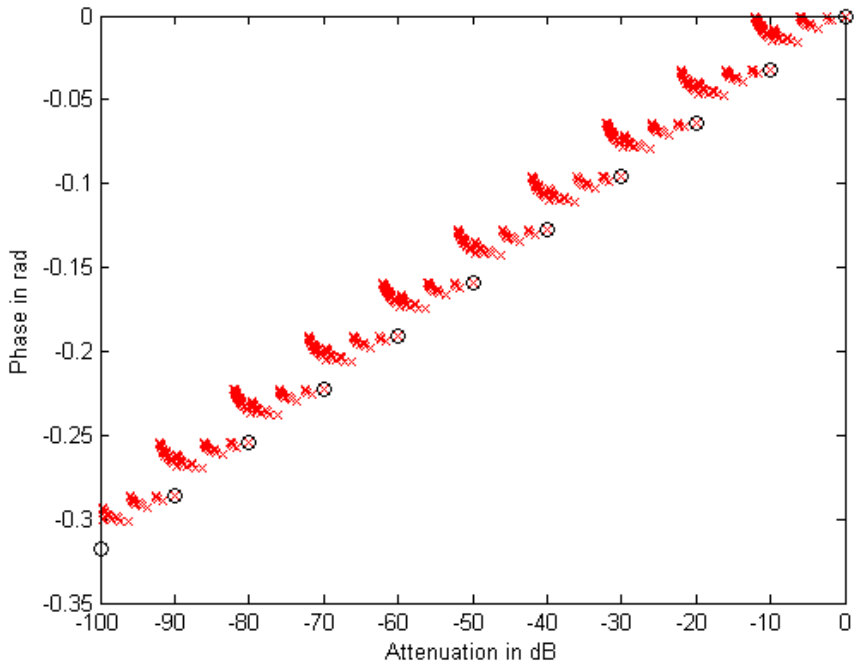

Figure 11.5: Distribution of different configuration of attenuators.

In the figure, the black circle shows the candidates from series connected attenuator while the red cross shows the candidates from the parallel connected attenuator. Besides the number of the channel candidates, other features such as cost, additional modification for upgrading the current radio is also important evaluation criteria, but that is beyond the scope of this dissertation.

11.3 Adaptive Filter G with Complex Taps

One of the adaptive filter proposed by us in [63] is to construct complex taps as shown in Figure 11.6. As we know that the equivalent baseband channel is a complex chan-

nel. If we can construct a complex baseband channel, then we can create the corresponding RF channel accordingly.

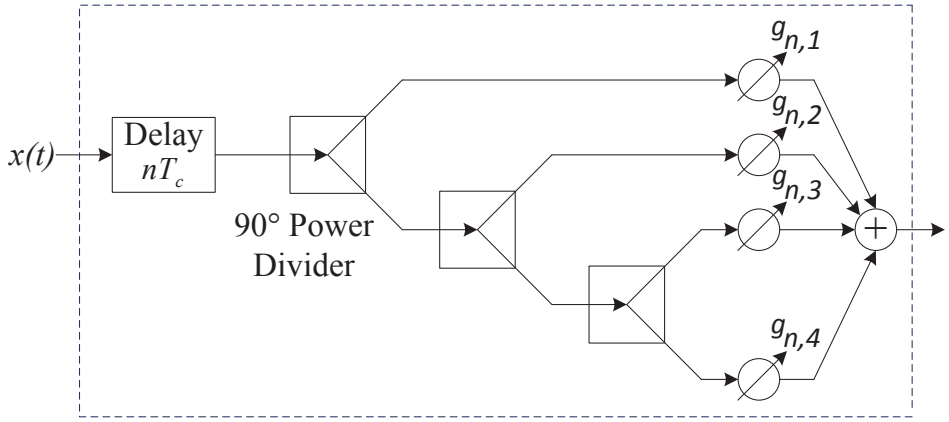

Figure 11.6: Complex tap

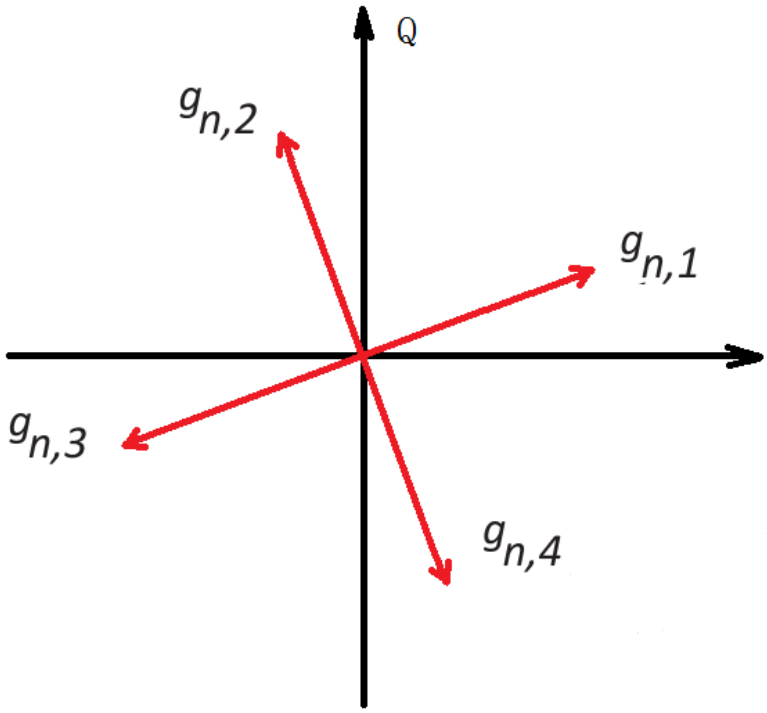

Figure 11.7: The baseband equivalent Complex tap

However, the attenuator we have only provides certain attenuation and a fixed delay associated with it. Assume the phase is linearly associated with the attenuation (in dB), Figure 11.7 shows the equivalent complex vector contributed by the step attenuator in Figure 11.6 with smallest attenuation. The x axis is the response projected to I channel and y axis is the response projected to Q channel. Larger the amplitude, smaller the attenuation. If the attenuator has infinite small resolution, then the achievable area would be the convex combination of vector $g_{n,1}$, $g_{n,2}$, $g_{n,3}$ and $g_{n,4}$. The convex combination is defined as:

$$\hat{g}_n = \alpha_1 g_{n,1} + \alpha_2 g_{n,2} + \alpha_3 g_{n,3} + \alpha_4 g_{n,4} \tag{11.10}$$

where $\alpha_i \in [0, 1], \forall i$. The reason that α_i cannot be negative is because the attenuation must be non-negative, otherwise it invert the signal. Therefore we can acquire arbitrary phase with complex tap. By connecting the complex taps in series with small enough interval, we can achieve arbitrary bandwidth of the adaptive filter G. Comparing to other structure, such as uniform distributed delay in [41], complex taps performances better. Details of the comparison can be founded in [63] . The off-the-shell step attenuator from Mini-Circuits ZX76-31R5-SP-S+ has a non-linear phase associated with the attenuation. The test results of ZX76-31R5-SP-S+ phase vs attenuation is shown in Figure 11.8

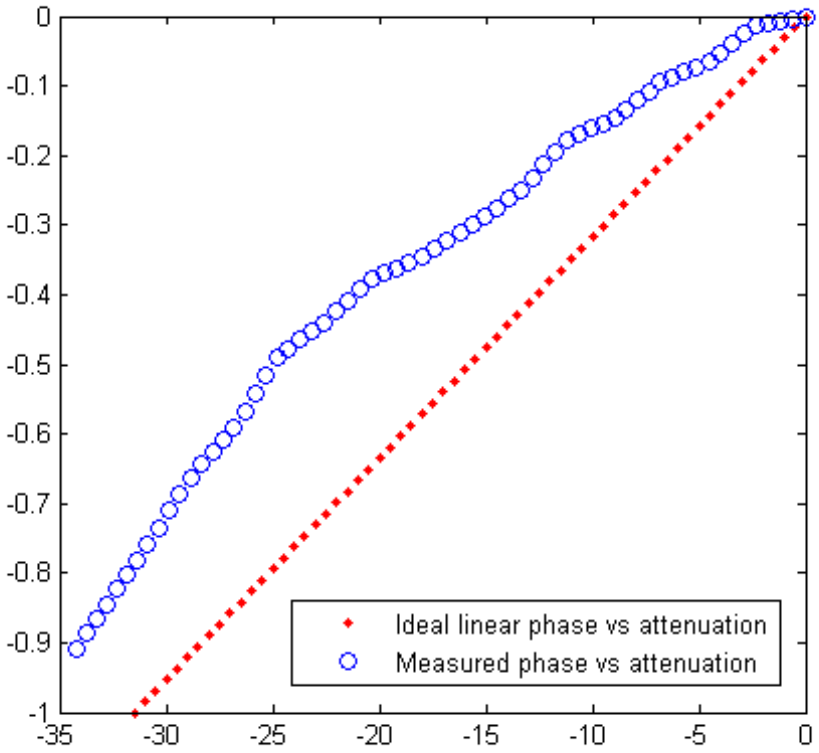

Figure 11.8: Ideal pase vs attenuation and the measured one

This non-linear phase will affect the distribution of the candidates provided by the complex taps. A simulation are shown in

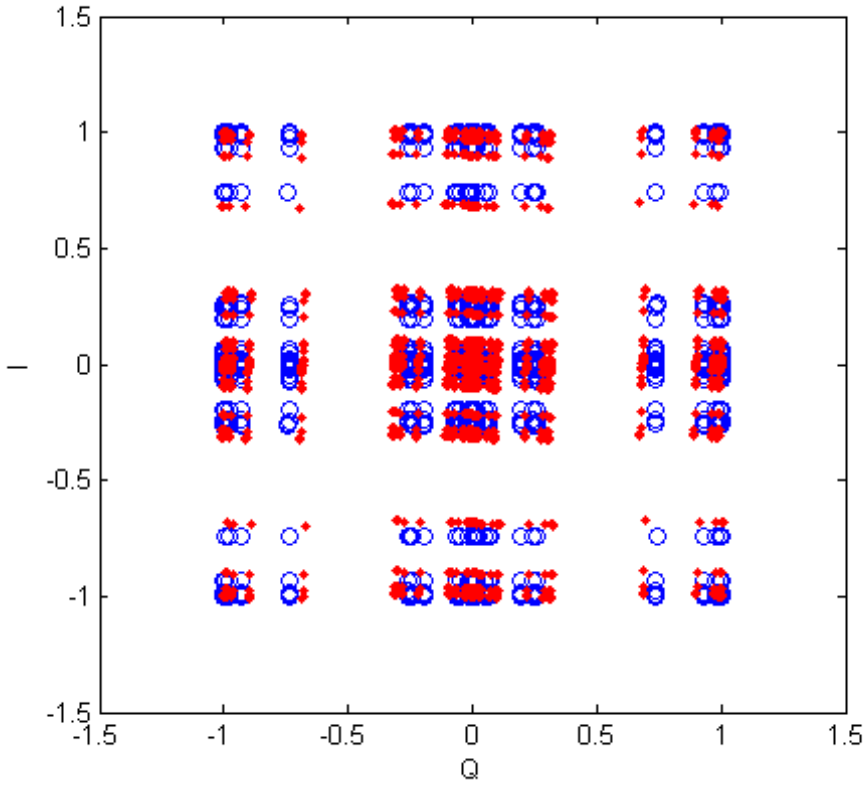

Figure 11.9: Candidates of complex tap using ideal and non-ideal attenuator

The red dots are the candidates from the ideal attenuator complex tap and the blue circles are from the non-ideal attenuator.

11.4 Experiments

We have built a single complex tap to verify the aforementioned idea. As shown in Figure 11.10, the complex tap is made by 90^o splitter, step attenuator, power combiner and controlled by USB I/Q interface provided by Mini Circuits.

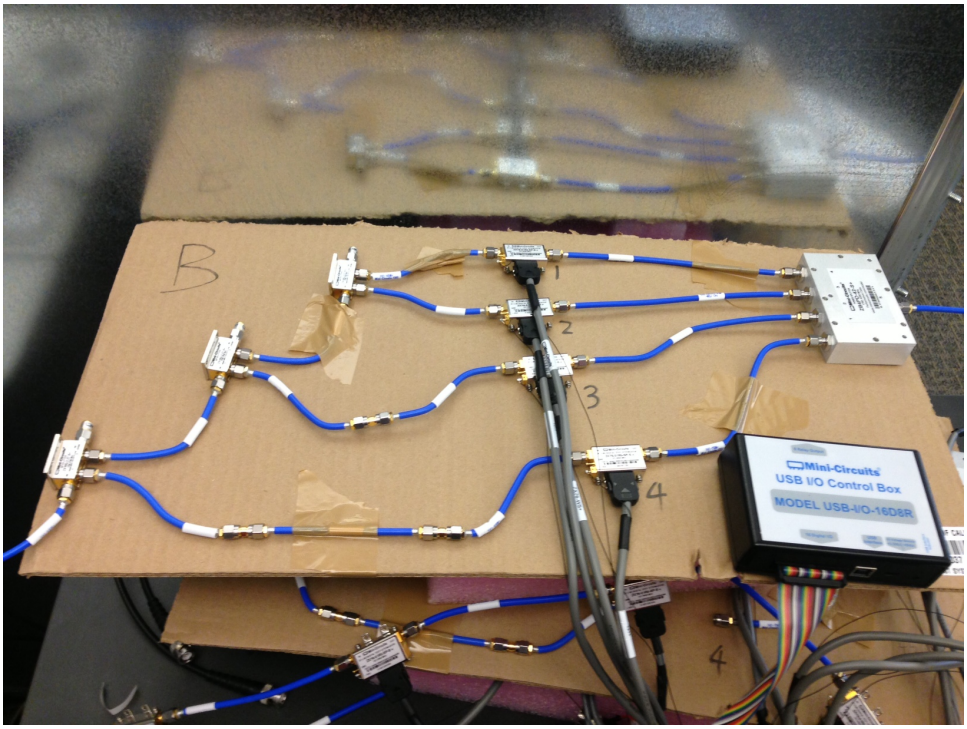

Figure 11.10: Single complex tap. The component is connected as shown in Figure 11.6. Attenuator is ZX76-31R5-SP-S+ from mini circuit. All attenuator is controlled by the USB I/Q interface with shared data and clock. We tested 40 MHz broadband signal at 2.4 GHz. Details of the component and USB I/Q interface are listed in Appendix A.

We use this simple complex tap to cancel the single path self-interference. With the limits of the step size of the attenuator and non-real-time interface, we achieved 30 dB cancellation. Another solution we are currently working on is a complex multi-tap cancellation board with real time control. We integrated several complex taps on a single

PCB board with the control interface for FPGA, up to 32 complex tap can be configured in real time for self-interference cancellation. The PCB of the complex multi-tap cancellation board is shown in Figure 11.11. Details of the component are listed in Appendix A.

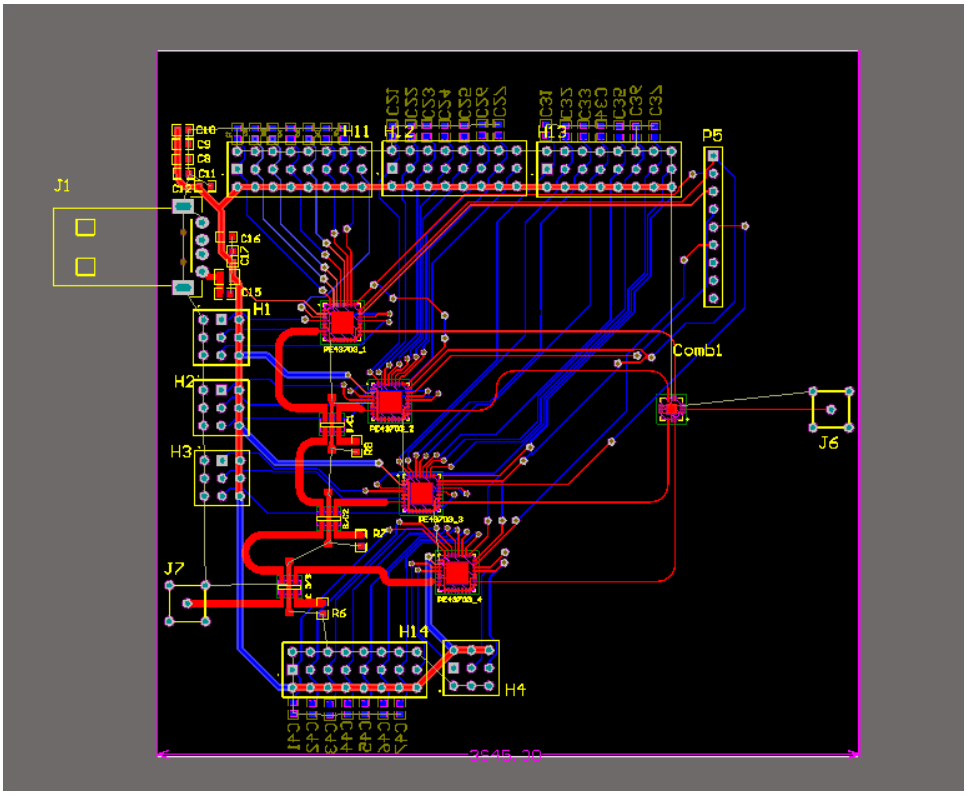

Figure 11.11: PCB of the complex multi-tap cancellation board. Attenuator is PE43703 from Peregrine Semiconductor. Details of the component are listed in Appendix A.

11.5 Adaptive Filter with Active Component

One way to build this filter G is using another Rx sample the transmitting noise with an attenuator. Then the received self-interference is processed with DSP technique and send out with another Tx to combine before H_4 in Figure 11.1. In this way, the sampling Rx the self-interference could use all the dynamic range for the self-interference.

The combination before H_4 would cancel the the self-interference up to the dynamic range of the sampling Rx and the Rx can use all its dynamic range for the remote desired signal and the residual of the self-interference. This is more like concatenated the dynamic range of two Rx. And multiple layer of this Rx can be used if necessary. The advantage of this method are:

1. G can be easily manipulated in complex baseband form.
2. Multiple Rx can be used together to achieve totally high dynamic range.
3. The algorithm is well understood as success interference cancellation.

However, this method is also suffered from the following disadvantage:

1. The delay of path contain adaptive filter G is extreme short since the self-interference channel has a short path.
2. The additional Rx and Tx will introduce noise. Though this noise is less significant than the original transmitting noise, it will degrade the performance.
3. Additional Rx and Tx increase the cost and heat dissipation.

Chapter 12

Tuning Algorithm for Adaptive Filter

With the previous analysis, we showed that the adaptive filter architecture is capable of creating a opposite channel. The following discussion is about how to find the optimal solution of adaptive filter G. Here is the system model in terms of G, represented in the complex baseband form. During the training, we assume no desired remote signal, the received $y[n]$ in Figure 11.1 is purely caused by the self-interference $x[n]$. We model $y[n]$ as the linear function of $x[n]$ and $w[n]$ and affine function of impulse response of $G[n]$

12.1 Complex Linear System

Let's denote the impulse response of filter G as $g[0]$, $g[1]$, $\cdots$, $g[L]$. With the linear system assumption, which is reasonable, for any given training pulse $x[n]$, $n = 0, 1, 2, \cdots$,

$N-1$ and a proper guard interval, we have

$$\mathbf{y}_i = (\mathbf{F} + \mathbf{W}_i)\mathbf{g} + \mathbf{f} + \mathbf{w}_i \tag{12.1}$$

where $\mathbf{y}_i = [y[0],\ y[1],\ \cdots,\ y[N-1]]^T$ is the vector of the corresponding outputs in the ith realization, $\mathbf{g} = [g[0],\ g[1], \cdots,\ g[L]]^T$, $\mathbf{F}$ and $\mathbf{f}$ are unknown linear function of $x[n]$, and $\mathbf{W}$ and $\mathbf{w}_i$ are unknown linear function of noise $\mathbf{w}[n]$.The same training sequence $x[n]$ is used repeatedly. Denote the energy of $\mathbf{y}_i$ by $||\mathbf{y}||^2$, $i \in [1,\ M]$. For large M, the average energy of the self-interference is given by

$$e = \frac{1}{M}\sum_{i=1}^{M} ||\mathbf{y}_i||^2 = \mathbf{g}^H(\mathbf{R}_F + \mathbf{R}_W)\mathbf{g} + 2Re\{(\mathbf{r}_F + \mathbf{r}_W)\mathbf{g}\} + \mathbf{r}_f + \mathbf{r}_w \tag{12.2}$$

where $\mathbf{R}_F = \mathbf{F}^H\mathbf{F}$, $\mathbf{R}_W = \frac{1}{M}{}^{M}_{i=1}\mathbf{W}_i^H\mathbf{W}_i$, $\mathbf{r}_F^H = \mathbf{f}^H\mathbf{F}$, $\mathbf{r}_W^H = \frac{1}{M}\sum_{i=1}^{M}\mathbf{w}_i\mathbf{W}_i$, $\mathbf{r}_f = \mathbf{f}^H\mathbf{f}$, and $\mathbf{r}_w = \frac{1}{M}\sum_{i=1}^{M}\mathbf{w}_i^H\mathbf{w}_i$. Equivalently, we can lump some notations together, the previous equation becomes:

$$e = \mathbf{g}^H\mathbf{A}\mathbf{g} + Re\{\mathbf{g}^H\mathbf{b}\} + c \tag{12.3}$$

where $\mathbf{A} = \mathbf{A}^H$, $\mathbf{b}$ and c are unknowns to be determined during training before determine the optimal $\mathbf{g}$. Define

$$\bar{\mathbf{A}} = \begin{bmatrix} \mathbf{A}_r & -\mathbf{A}_i \\ \mathbf{A}_i & \mathbf{A}_r \end{bmatrix} \tag{12.4}$$

$$\bar{\mathbf{g}} = \left[\mathbf{g}_r^T,\ \mathbf{g}_i^T\right]^T \tag{12.5}$$

$$\bar{\mathbf{b}} = \left[\mathbf{b}_r^T,\ \mathbf{b}_i^T\right]^T \tag{12.6}$$

where $\mathbf{A}_r = Re\{\mathbf{A}\} = \mathbf{A}_r^T$, $\mathbf{A}_i = Im\{\mathbf{A}\} = \mathbf{A}_i^T$, $\mathbf{g}_r = Re\{\mathbf{g}\}$, $\mathbf{g}_i = Im\{\mathbf{g}\}$, $\mathbf{b}_r = Re\{\mathbf{b}\}$ and $\mathbf{b}_i = Im\{\mathbf{b}\}$. Equ. (12.3) can be rewrite as:

$$e = \bar{\mathbf{g}}^T\bar{\mathbf{A}}\bar{\mathbf{g}} + \bar{\mathbf{g}}^T\bar{\mathbf{b}} + c \tag{12.7}$$

Furthermore, we can write

$$e = \bar{\mathbf{g}}^T \otimes \bar{\mathbf{g}}^T vec(\bar{\mathbf{A}}) + \bar{\mathbf{g}}^T \bar{\mathbf{b}} + c$$

$$= [\mathbf{g}_r^T,\ \mathbf{g}_i^T] \otimes [\mathbf{g}_r^T,\ \mathbf{g}_i^T] \begin{bmatrix} vec\begin{pmatrix} \mathbf{A}_r \\ \mathbf{A}_i \end{pmatrix} \\ vec\begin{pmatrix} -\mathbf{A}_i \\ \mathbf{A}_r \end{pmatrix} \end{bmatrix} + \bar{\mathbf{g}}^T \bar{\mathbf{b}} + c$$

$$\mathbf{g}_r^T \otimes [\mathbf{g}_r^T,\ \mathbf{g}_i^T] vec\begin{pmatrix} \mathbf{A}_r \\ \mathbf{A}_i \end{pmatrix} + \mathbf{g}_i^T \otimes [\mathbf{g}_r^T,\ \mathbf{g}_i^T] vec\begin{pmatrix} -\mathbf{A}_i \\ \mathbf{A}_r \end{pmatrix} + \bar{\mathbf{g}}^T \bar{\mathbf{b}} + c$$

$$= \left\{ \mathbf{g}_r^T \otimes [\mathbf{g}_r^T,\ \mathbf{g}_i^T] + \mathbf{g}_i^T \otimes [\mathbf{g}_i^T,\ -\mathbf{g}_r^T] \right\} vec\begin{pmatrix} \mathbf{A}_r \\ \mathbf{A}_i \end{pmatrix} + \bar{\mathbf{g}}^T \bar{\mathbf{b}} + c \tag{12.8}$$

where $\otimes$ is the outer product, and $vec(\cdot)$ is the vectorization function Let $\mathbf{P}$ be a permutation function that

$$vec\begin{pmatrix} \mathbf{A}_r \\ \mathbf{A}_i \end{pmatrix} = \mathbf{P} \begin{pmatrix} vec(\mathbf{A}_r) \\ vec(\mathbf{A}_i) \end{pmatrix} \tag{12.9}$$

Then

$$e = \left\{ \mathbf{g}_r^T \otimes [\mathbf{g}_r^T,\ \mathbf{g}_i^T] + \mathbf{g}_i^T \otimes [\mathbf{g}_i^T,\ -\mathbf{g}_r^T] \right\} \mathbf{P} \begin{pmatrix} vec(\mathbf{A}_r) \\ vec(\mathbf{A}_i) \end{pmatrix} + \bar{\mathbf{g}}^T \bar{\mathbf{b}} + c$$

$$= \left\{ [\mathbf{g}_r^T \otimes \mathbf{g}_r^T,\ \mathbf{g}_r^T \otimes \mathbf{g}_i^T] + [\mathbf{g}_i^T \otimes \mathbf{g}_i^T,\ -\mathbf{g}_i^T \otimes \mathbf{g}_r^T] \right\} \begin{pmatrix} vec(\mathbf{A}_r) \\ vec(\mathbf{A}_i) \end{pmatrix} + \bar{\mathbf{g}}^T \bar{\mathbf{b}} + c$$

$$= \left\{ [\mathbf{g}_r^T \otimes \mathbf{g}_r^T + \mathbf{g}_i^T \otimes \mathbf{g}_i^T,\ \mathbf{g}_r^T \otimes \mathbf{g}_i^T - -\mathbf{g}_i^T \otimes \mathbf{g}_r^T] \right\} \begin{pmatrix} vec(\mathbf{A}_r) \\ vec(\mathbf{A}_i) \end{pmatrix} + \bar{\mathbf{g}}^T \bar{\mathbf{b}} + c \tag{12.10}$$

Since $\bar{A}_r = \bar{A}_r^T$ and $\bar{A}_i = -\bar{A}_i$, only lower triangular, including the diagonal, element of $\mathbf{A}_r$ are independent and only the strictly lower triangle, excluding, the diagonal, elements of $\mathbf{A}_i$ are independent. We now define the selection matrices $\mathbf{S}_{r,L+1}$ and $\mathbf{S}_{i,L+1}$ that $\mathbf{S}_{r,L+1}vec(\mathbf{A}_r)$ and $\mathbf{S}_{i,L+1}vec(\mathbf{A}_i)$ only contains the independent element. Then

$$e = \mathbf{u}^T\mathbf{v} \tag{12.11}$$

where

$$\mathbf{v} = \left[\mathbf{S}_{r,L+1}vec(\mathbf{A}_r)\mathbf{S}_{i,L+1}vec(\mathbf{A}_i)\bar{\mathbf{b}}c\right] \tag{12.12}$$

$$\mathbf{u}^T = [\mathbf{u}_1^T\ \mathbf{u}_2^T\ \bar{\mathbf{g}}^T\ 1] \tag{12.13}$$

where $\mathbf{u}_1^T = (\mathbf{g}_r^T \otimes \mathbf{g}_r^T + \mathbf{g}_i^T \otimes \mathbf{g}_i^T)\mathbf{S}_{r,\ L+1}^T\mathbf{D}_{L+1}$, $\mathbf{u}_2^T = 2(\mathbf{g}_r^T \otimes \mathbf{g}_i^T - \mathbf{g}_i^T \otimes \mathbf{g}_r^T)\mathbf{S}_{i,\ L+1}$ and for example

$$\mathbf{D}_4 = diag[\ 1\ 2\ 2\ 2|\ 1\ 2\ 2\ |\ 1\ 2\ |\ 1] \tag{12.14}$$

Assume we use a unique $\mathbf{g}[k]$, $k \in [1,\ K]$ for every M realizations. Then we get a corresponding $\mathbf{e}[k]$ that

$$\mathbf{e} = \mathbf{G}\mathbf{v} \tag{12.15}$$

where $\mathbf{e} = [e[1],\ \cdots,\ e[K]]$ and

$$\mathbf{G} = \begin{bmatrix} \mathbf{u}[1]^T \\ \cdots \\ \mathbf{u}[K]^T \end{bmatrix} \in\ R^{K\times((L+1)^2+2L+3)} \tag{12.16}$$

and $\mathbf{u}[k]$ is defined in Equ. 12.13. If $\mathbf{G}$ has a full-column-rank, the least square solution of $\mathbf{v}$ is given by

$$\mathbf{v} = (\mathbf{G}^T\mathbf{G})^{-1}\mathbf{G}^T\mathbf{e} \tag{12.17}$$

Vector $\mathbf{v}$ has all the information of estimates of $\bar{\mathbf{A}}$, $\bar{\mathbf{b}}$ and c. According to Equ. (12.7), with the estimates $\bar{\mathbf{A}}$, $\bar{\mathbf{b}}$ and c, the optimal adaptive filter $\bar{\mathbf{g}}$ is given by

$$\bar{\mathbf{g}} = -\frac{1}{2}\bar{\mathbf{A}}^{-1}\bar{\mathbf{b}} \tag{12.18}$$

12.2 Real Linear System

If there is an I/Q imbalance phenomena in the circuit, the complex linear model fails. We can use a real linear model to replace the complex one. I/Q imbalance phenomena is discussed later. The real linear model is more relax problem than the complex one, since the in phase and quadrature signal are decoupled. But realize an adaptive filter for real linear model is much more difficult and therefore less practical. Luckily the I/Q imbalance is not severe practically and complex model can be applied generally. The linear model can be written as:

$$e = \bar{\mathbf{g}}^T\hat{\mathbf{A}}\bar{\mathbf{g}} + \bar{\mathbf{g}}\bar{\mathbf{b}} + c \tag{12.19}$$

were the real matrix $\hat{\mathbf{A}}$ only has the symmetric property $\hat{\mathbf{A}}^T = \hat{\mathbf{A}}$. Similarly

$$e = \hat{\mathbf{u}}^T\hat{\mathbf{v}} \tag{12.20}$$

where

$$\mathbf{v} = \left[\mathbf{S}_{2L+2}vec(\hat{\mathbf{A}})\bar{\mathbf{b}}c\right] \tag{12.21}$$

$$\hat{\mathbf{v}} = [(\bar{\mathbf{g}}^T \otimes \bar{\mathbf{g}}^T)\mathbf{S}_{2L+2}^T\mathbf{D}_{2L+2} \mid \bar{\mathbf{g}}^T \mid 1\ ] \tag{12.22}$$

12.3 Training vector $g[k]$ Design

One critical condition for finding the optimal adaptive filter G is to form the aforementioned matrix G with full-column-rank. With more realization of training, G will be full-column-rank. However, using the minimum number of training sequence to find a full-column-rank G with a small condition number worth discussion. One way to construct G is to make it as orthogonal as possible. In [52], a choice of training vector is introduced, which results in a sparse matrix G. The sparseness is also useful for reduced computation.

12.3.1 Real System

For real system, $\hat{\mathbf{A}}$ is a symmetric matrix. Let $\bar{\mathbf{g}}$ have the dimension $m \times 1$. Therefore the number of unknown real parameters in the systems is $N_m = m(m+1)/2 + m + 1$. Denote the corresponding $\mathbf{G}$ as $\mathbf{G}_m$ and $\bar{\mathbf{g}}[n] = [g_1[n],\ g_2[n],\ ,\cdots,\ g_m[n]]^T$ with $n \in [1,\ N]$. If m=2, $N_2 = 6$ and

$$\mathbf{G}_2 = \left[\begin{array}{c|c|c|c|c|c} g_1[1]^2 & 2g_1[1]g_2[1] & g_2[1]^2 & g_1[1] & g_2[1] & 1 \\ g_1[2]^2 & 2g_1[2]g_2[2] & g_2[2]^2 & g_1[2] & g_2[2] & 1 \\ g_1[3]^2 & 2g_1[3]g_2[3] & g_2[3]^2 & g_1[3] & g_2[3] & 1 \\ g_1[4]^2 & 2g_1[4]g_2[4] & g_2[4]^2 & g_1[4] & g_2[4] & 1 \\ g_1[5]^2 & 2g_1[5]g_2[5] & g_2[5]^2 & g_1[5] & g_2[5] & 1 \\ g_1[6]^2 & 2g_1[6]g_2[6] & g_2[6]^2 & g_1[6] & g_2[6] & 1 \end{array}\right] \tag{12.23}$$

To construct a nonsingular $\mathbf{G}_2$, one of the choice could be

1. $\bar{\mathbf{g}}[1] = [0,\ 0]$

2. $\bar{\mathbf{g}}[2] = [1,\ 0]$

3. $\bar{\mathbf{g}}[3] = [-1,\ 0]$

4. $\bar{\mathbf{g}}[4] = [0,\ 1]$

5. $\bar{\mathbf{g}}[5] = [0,\ -1]$

6. $\bar{\mathbf{g}}[6] = [1,\ 1]$

The corresponding $\mathbf{G}_2$ is

$$\mathbf{G}_2 = \left[\begin{array}{c|c|c|c|c|c} 0 & 0 & 0 & 0 & 0 & 1 \\ 1 & 0 & 0 & 1 & 0 & 1 \\ 1 & 0 & 0 & -1 & 0 & 1 \\ 0 & 0 & 1 & 0 & 1 & 1 \\ 0 & 0 & 1 & 0 & -1 & 1 \\ 1 & 2 & 1 & 1 & 1 & 1 \end{array}\right] \tag{12.24}$$

It is easy to verify that $\mathbf{G}_2$ has full rank and the $det(\mathbf{G}_2) = 1$. For any given m, we can show that using the following procedure will make a full rank $\mathbf{G}_m$:

1. $g_i[1] = 0$, for $i \in [1,\ ,\cdots,\ m]$

2. $g_i[2i] = 1$, for $i \in [1,\ ,\cdots,\ m]$

3. $g_i[2i+1] = -1$, for $i \in [1,\ ,\cdots,\ m]$

4. $g_{ik}[k+m+1] = g_{jk}[k+m+1]$=1, $k \in [1,\cdots,\ N_m - m - 1]$, where $(i_k,\ j_k)$ is the kth pair of elements out of $\{1,\ ,\ldots,\ m\}$ and $i_k < j_k$

5. $g[n] = 0$ otherwise.

To prove this procedure will generate the full rank $\mathbf{G}_m$, assume $N_{m-1} \times N_{m-1}$ matrix $\mathbf{G}_{m-1}$, generated using the aforementioned procedure has full rank N_{m-1}. Given $N_m = m(m+1)/2 + m + 1$, $N_m = N_{m-1} + m + 1$, $\mathbf{G}_m$ has $m+1$ additional columns and rows. One can then verify that there are a row permutation matrix $\mathbf{P}_1$, a column permutation matrix $\mathbf{P}_2$ and an elimination-by-row matrix $\mathbf{T}_m$ such that

$$\mathbf{P}_1\mathbf{T}_m\mathbf{G}_m\mathbf{P}_2 = \begin{bmatrix} \mathbf{G}_{m-1} & & \\ & \mathbf{J} & \\ & & 2\mathbf{I}_{m-1} \end{bmatrix} \tag{12.25}$$

where the two rows associated with the component

$$\mathbf{J} = \begin{bmatrix} 1 & 1 \\ 1 & -1 \end{bmatrix} \tag{12.26}$$

in the above are due to the two entries in $\mathbf{G}_m$: $\bar{\mathbf{g}}(2m) = [0, \cdots, 0, 1]^T$ and $\bar{\mathbf{g}}(2m+1) = [0, \cdots, 0, -1]^T$. The $m-1$ rows associated with the component $2\mathbf{I}_{m-1}$ in the above are due to the $m-1$ entries in $\mathbf{G}_m$: $\bar{\mathbf{g}}(N_m - m + 1 + i) = [\mathbf{e}_i^T, 1]^T$, $i = 1, \cdots, m-1$, where $\mathbf{e}_i$ is the $(m-1) \times 1$ vector of all zeros except the one value at its ith position. Hence, $\det(\mathbf{G}_m) = -2^m \det(\mathbf{G}_{m-1})$. Given $\det(\mathbf{G}_2) = 2^3$, we have $\det(\mathbf{G}_m) = (-1)^m 2^{\frac{m(m+1)}{2}}$.

12.3.2 Complex System

For the complex system, the matrix $\mathbf{G}$ has an additional structure. If we let $\bar{\mathbf{g}}$ have the dimension $k \times 1$ where $k = 2m$, then there are total $M_k = (k/2)^2 + k + 1$ unknown real parameters in the system. Note that $\bar{\mathbf{g}}(n) = [\mathbf{g}_r^T(n), \mathbf{g}_i^T(n)]^T$ where $\mathbf{g}_r(n) =$

$[g_{r,1}(n), \cdots, g_{r,m}(n)]^T$ and $\mathbf{g}_i(n) = [g_{i,1}(n), \cdots, g_{i,m}(n)]^T$. Also note that $M_k = N_m + \frac{(m-1)m}{2} + m$. We will denote the corresponding $\mathbf{G}$ by $\mathbf{G}_{(k)}$. We will propose a choice of $\bar{\mathbf{g}}(n)$ for $n = 1, \cdots, M_k$ to construct a nonsingular $M_k \times M_k$ matrix $\mathbf{G}_{(k)}$.

There is a permutation matrix $\mathbf{P}_{(k)}$ such that as follows:

$$\mathbf{G}_{(k)}\mathbf{P}_{(k)} = \begin{bmatrix} \mathbf{G}_{1,1} & \mathbf{G}_{1,2} \\ \\ \mathbf{G}_{2,1} & \mathbf{G}_{2,2} \end{bmatrix} \tag{12.27}$$

where the first block column only depends on $\mathbf{g}_r(n)$ and the second block column depends on both $\mathbf{g}_r(n)$ and $\mathbf{g}_i(n)$. Furthermore, $\mathbf{G}_{1,1} \in R^{N_m \times N_m}$ has the exactly same structure as $\mathbf{G}_m$ in the real system with $\bar{\mathbf{g}}(n)$ replaced by $\mathbf{g}_r(n)$.

For $1 \leq n \leq N_m$, we propose to choose $\mathbf{g}_i(n) = 0$ but at the same time choose $\mathbf{g}_r(n)$ in the same way as for the real system. Then, we know that $\mathbf{G}_{1,1}$ is nonsingular and $\mathbf{G}_{1,2} = 0$. Furthermore, for any $\mathbf{G}_{2,2}$, there is an elimination-by-row matrix $\mathbf{T}_{(k)}$ such that

$$\mathbf{T}_{(k)}\mathbf{G}_{(k)}\mathbf{P}_{(k)} = \begin{bmatrix} \mathbf{G}_{1,1} & 0 \\ \\ 0 & \mathbf{G}_{2,2} \end{bmatrix} \tag{12.28}$$

It is now sufficient to choose $M_k - N_m = \frac{(m-1)m}{2} + m$ additional $\bar{\mathbf{g}}(n)$ to make $\mathbf{G}_{2,2}$ full rank.

For $m = 3$, the structure of the nth row of $\mathbf{G}_{2,2}$ is

$$(\mathbf{G}_{2,2})_{n,:} = \left[\begin{array}{c|c|c|c} 2\delta g_{r,i}(1,2) & 2\delta g_{r,i}(1,3) & 2\delta g_{r,i}(2,3) & \hat{\mathbf{g}}_i^T \end{array} \right] \tag{12.29}$$

where $\delta g_{r,i}(k,l) = g_r(k)g_i(l) - g_i(k)g_r(l)$ and $\hat{\mathbf{g}}_i^T = [g_i(1), g_i(2), g_i(3)]$. If we choose

1. $\bar{\mathbf{g}}(N_3 + 1) = [0, 0, 0, 1, 0, 0]^T$

2. $\bar{\mathbf{g}}(N_3 + 2) = [0, 0, 0, 0, 1, 0]^T$

3. $\bar{\mathbf{g}}(N_3+3) = [0,0,0,0,0,1]^T$

4. $\bar{\mathbf{g}}(N_3+4) = [1,0,0,0,1,0]^T$

5. $\bar{\mathbf{g}}(N_3+5) = [1,0,0,0,0,1]^T$

6. $\bar{\mathbf{g}}(N_3+6) = [0,1,0,0,0,1]^T$

then we have (up to a column permutation)

$$\mathbf{G}_{2,2} = diag\left(\mathbf{I}_3, 2\mathbf{I}_3\right) \tag{12.30}$$

For any given m, we choose $\bar{\mathbf{g}}(n)$ for $N_m + 1 \leq n \leq M_k$ as follows:

1. $g_{i,n}(n+N_m) = 1$ for $n = 1, \cdots, m$

2. $g_{r,n_k}(N_m+m+k) = g_{i,m_k}(N_m+m+k) = 1$ for $1 \leq k \leq \frac{(m-1)m}{2}$ where (n_k, m_k) is the kth pair of elements from $\{1, \cdots, m\}$ satisfying $n_k < m_k$

3. $g_{r,j}(n) = 0$ and $g_{i,j}(n) = 0$ otherwise.

One can verify that up to a column permutation we have

$$\mathbf{G}_{2,2} = diag\left(\mathbf{I}_m, 2\mathbf{I}_{\frac{(m-1)m}{2}}\right) \tag{12.31}$$

which implies that $\det(\mathbf{G}_{2,2}) = 2^{\frac{(m-1)m}{2}}$.

Therefore, $\det(\mathbf{G}_{(k)}) = \det(\mathbf{G}_{1,1})\det(\mathbf{G}_{2,2}) = \det(\mathbf{G}_m)\det(\mathbf{G}_{2,2}) = 2^{m^2}$.

12.4 IQ Imbalance Issue

IQ imbalance is a phenomenon that a different phase and/or amplitude is introduced to in phase and quadrature component. We conduct an analysis and tested the results

using hardware to show that IQ imbalance could affect self-interference cancellation and it also can be canceled properly using proper designed filterer.

12.4.1 Model and Procedure

Gaussian pulse is used during this experiment for its dramatical contrast between the passband and the stopband. Figure 12.1 shows the time domain and frequency domain representation of the Gaussian pulse adopted in this experiment.

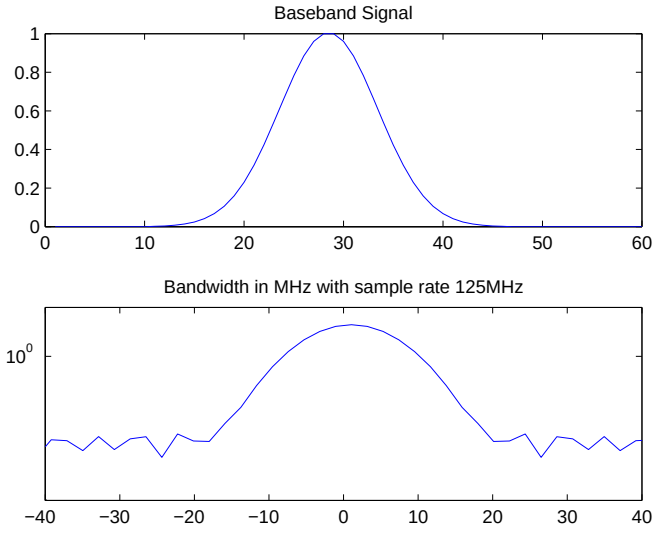

Figure 12.1: Time domain and frequency domain representation of Gaussian pulse used in this experiment

12.4.2 Tranining Phase

Before fullduplex transmitting starts, a training phase is needed to estimate the channel and preparing the cancel waveform. During training phase, waveform transmitted by Tx, Cx and the corresponding received waveform at Rx is listed in Table 12.1 below.

Four consecutive time slots are used for transmitting pilot signal during the training phase. W(-W) indicates that the Tx or Cx transmits the Gaussian pulse $w[n]$, $n \in [1,\ N]$ in Figure 12.1(or the negtive Gaussian pulse). RxR_1 denotes the received in-phase signal at slot 1 while RxI_3 indicates the received quadrature at slot 3. Index n is omitted for convenience. Therefore, the channel responses can be calculated as in Table 12.2.

The prefilterred signal generated with real model for fullduplex can be described as the following equation:

$$\overline{x_r} = \begin{bmatrix} x_{ar} \\ x_{ai} \\ x_{br} \\ x_{bi} \end{bmatrix} = \begin{bmatrix} h_{12} * h_{23} - h_{22} * h_{13} & h_{12} * h_{24} - h_{22} * h_{14} \\ h_{21} * h_{13} - h_{11} * h_{23} & h_{21} * h_{14} - h_{11} * h_{24} \\ h_{22} * h_{11} - h_{12} * h_{21} & 0 \\ 0 & h_{22} * h_{11} - h_{12} * h_{21} \end{bmatrix} \begin{bmatrix} s_r \\ s_i \end{bmatrix} \tag{12.32}$$

	Slot 1	Slot 2	Slot 3	Slot 4
TxR	W	0	W	0
TxI	0	W	0	W
CxR	W	0	-W	0
CxI	0	W	0	-W
RxR	RxR_1	RxR_2	RxR_3	RxR_4
RxI	RxI_1	RxI_2	RxI_3	RxI_4

Table 12.1: Transmitting scheduled for training phase

$$
\begin{array}{ll}
2h_{11} = RxR_1 + RxR_3 & 2h_{21} = RxI_1 + RxI_3 \\
2h_{12} = RxR_2 + RxR_4 & 2h_{22} = RxI_2 + RxI_4 \\
2h_{13} = RxR_1 - RxR_3 & 2h_{23} = RxI_1 - RxI_3 \\
2h_{14} = RxR_2 - RxR_4 & 2h_{24} = RxI_2 - RxI_4
\end{array}
$$

Table 12.2: Prefiltered signal for Fullduplex Waveform

In other hand, prefilterred signal generated with complex model for fullduplex can be described as the following equation:

$$
\overline{x_c} = \begin{bmatrix} x_{ar} \\ x_{ai} \\ x_{br} \\ x_{bi} \end{bmatrix} = \begin{bmatrix} h_{13} + h_{14} & -(h_{23} + h_{24}) \\ h_{23} + h_{24} & h_{13} + h_{14} \\ -(h_{11} + h_{12}) & h_{21} + h_{22} \\ -(h_{21} + h_{22}) & -(h_{11} + h_{12}) \end{bmatrix} \begin{bmatrix} s_r \\ s_i \end{bmatrix} \tag{12.33}
$$

12.4.3 Experiment and Result

To compare the cancel effect, $\overline{x_{cn}} = [x_{ar}\ x_{ai}\ 0\ 0]^T$ is transmitted to show the strength of the uncanceled self-interference for the complex model. The corresponding real model signal is $\overline{x_{rn}} = [x_{ar}\ x_{ai}\ 0\ 0]^T$. The received self interference waveform by transmitting $\overline{x_c}$, $\overline{x_r}$, $\overline{x_{cn}}$ and $\overline{x_{rn}}$ are denoted as $\overline{r_c}$, $\overline{r_r}$, $\overline{r_{cn}}$ and $\overline{r_{rn}}$, respectively. We can also apply baseband cancellation filter to further reduce the interference residual. The baseband cancellation filter problem for complex method can be described as:

$$
\min_{\overline{b_c}} \quad ||\overline{r_c} - \overline{W_c b_c}||_2^2 \tag{12.34}
$$

where $\overline{W_c}$ is

$$\overline{W_c} = \begin{bmatrix} w_c[1] & 0 & 0 & 0 & 0 \\ w_c[1] & w_c[2] & 0 & 0 & 0 \\ w_c[1] & w_c[2] & w_c[3] & 0 & 0 \\ \vdots & \vdots & \vdots & \vdots & \vdots \\ 0 & 0 & 0 & w_c[N] & w_c[N-1] \\ 0 & 0 & 0 & 0 & w_c[N] \end{bmatrix} \tag{12.35}$$

$\overline{b_c}$ is the adaptive complex filter for baseband cancellation and $w_c[n]$ is the nth complex sample of the transmitted waveform. The optimal $\overline{b_c}$ can be expressed as:

$$\overline{b_c} = (\overline{W_c}^H \overline{W_c})^{-1} \overline{W_c}^H \overline{r_c} \tag{12.36}$$

Traditional convolution complex sequence can be expressed as:

$$c[n] = a[n] * b[n] = \sum_{k=1}^{K} a[k] \times b[n-k]$$

$$= \sum_{k=1}^{K} \{ [Re(a[k]) \times Re(b[n-k]) - Im(a[k]) \times Im(b[n-k])]$$

$$+ j\,[Re(a[k]) \times Im(b[n-k]) + Im(a[k]) \times Re(b[n-k])] \} \tag{12.37}$$

It can also be expressed in matrix form

$$\bar{c} = \begin{bmatrix} c[1] \\ c[2] \\ \vdots \\ c[K] \end{bmatrix} = \bar{A}\bar{b} = \begin{bmatrix} a[1] & 0 & 0 & 0 & 0 \\ a[2] & a[1] & 0 & 0 & 0 \\ \vdots & \vdots & \vdots & \vdots & \vdots \\ 0 & 0 & 0 & 0 & a[K_a] \end{bmatrix} \begin{bmatrix} b[1] \\ b[2] \\ \vdots \\ b[K_b] \end{bmatrix} \tag{12.38}$$

$$Re(\bar{c}) = Re(\bar{A})Re(\bar{b}) - Im(\bar{A})Im(\bar{b}) \tag{12.39}$$

$$Im(\bar{c}) = Re(\bar{A})Im(\bar{b}) + Im(\bar{A})Re(\bar{b}) \tag{12.40}$$

where K_a and K_b are the length of $a[n]$ and $b[n]$ and $K = K_a + K_b - 1$. Use $\hat{a}[n]$ as the input and $\hat{c}[n]$ as output, the process of real method complex filter $\hat{b}$ can be described as

$$\hat{c} = \begin{bmatrix} Re(c[1]) & Im(c[1]) \\ Re(c[2]) & Im(c[2]) \\ \vdots & \vdots \\ Re(c[K]) & Im(c[K]) \end{bmatrix} = \hat{A}\hat{b} \tag{12.41}$$

where

$$\hat{A} = \begin{bmatrix} Re(a[1]) & Im(a[1]) & 0 & 0 & 0 & 0 \\ Re(a[2]) & Im(a[2]) & Re(a[1]) & Im(a[1]) & 0 & 0 \\ \vdots & \vdots & \vdots & \vdots & \vdots & \vdots \\ 0 & 0 & 0 & 0 & Re(a[K_a]) & Im(a[K_a]) \end{bmatrix} \tag{12.42}$$

$$\hat{b} = \begin{bmatrix} b_{11}[1] & b_{12}[1] \\ b_{21}[1] & b_{22}[1] \\ b_{11}[2] & b_{12}[2] \\ b_{21}[2] & b_{22}[2] \\ \vdots & \vdots \\ b_{11}[K_b] & b_{12}[K_b] \\ b_{21}[K_b] & b_{22}[K_b] \end{bmatrix} \tag{12.43}$$

Here $\hat{b}$ has twice number as $\bar{b}$. Consider the optimization problem below:

$$\min_{\widehat{b}} \quad ||\widehat{r} - \widehat{A}\widehat{b}||_2^2 \tag{12.44}$$

We can manipulate the expression and use traditional least square results to solve this problem. Let

$$\tilde{r} = [\widetilde{r_{re}}^T \ \widetilde{r_{im}}^T]^T = [Re(r[1]),\ Re(r[2]),\ Re(r[K_r]),\ \cdots,\ Im(r[1]),\ Im(r[2]),\ \cdots,\ Im(r[K_r])]^T \tag{12.45}$$

$$\tilde{b} = [\widetilde{b_{re}}^T \ \widetilde{b_{im}}^T]^T = [b_{11}[1],\ b_{21}[1],\ b_{11}[2],\ b_{21}[2],\ \cdots,\ b_{11}[K_b],\ b_{21}[K_b],\ \cdots$$

$$b_{12}[1],\ b_{22}[1],\ b_{12}[2],\ b_{22}[2],\ \cdots,\ b_{12}[K_b],\ b_{22}[K_b]]^T \tag{12.46}$$

and

$$\tilde{A} = \begin{bmatrix} \hat{A} & \hat{0} \\ \hat{0} & \hat{A} \end{bmatrix} \tag{12.47}$$

where $\hat{0}$ is the zero matrix same size as $\hat{A}$. Now the optimization problem can be written as:

$$\min_{\tilde{b}} \quad ||\tilde{r} - \tilde{A}\tilde{b}||_2^2 \tag{12.48}$$

Further more it can ge written as two independent optimization with smaller matrix size:

$$\min_{\widetilde{b_{re}}} \quad ||\widetilde{r_{re}} - \widetilde{\hat{A}}\widetilde{b_{re}}||_2^2 \tag{12.49}$$

and

$$\min_{\widetilde{b_{im}}} \quad ||\widetilde{r_{im}} - \widetilde{\hat{A}}\widetilde{b_{im}}||_2^2 \tag{12.50}$$

Experiments under two environment are conducted. The first experiment shows the cancellation results of RF, RF combined with traditional baseband cancel filter and RF combined with the real method complex filter. The MXG is set up without IQ adjustment. The second experiment shows the similar results. However, the IQ adjustment is set as 1dB in

IQ amplitude and 10 degree in phase for Tx and -1dB in IQ amplitude and -10 degree for Cx, which is the largest IQ adjustment that allowed on the system.

The result of the first experiment is shown in Figure 12.2 and second shown in Figure 12.3. A comparison over of the RF cancellation over two experimental environment is also shown in Figure 12.4

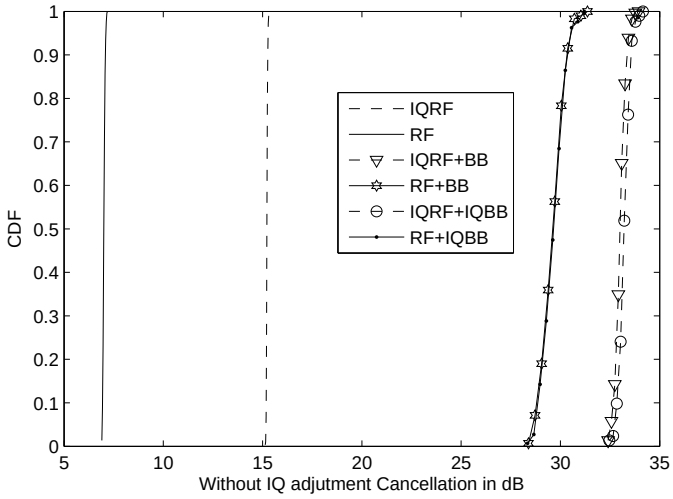

Figure 12.2: Cancellation comparison without IQ adjustment.

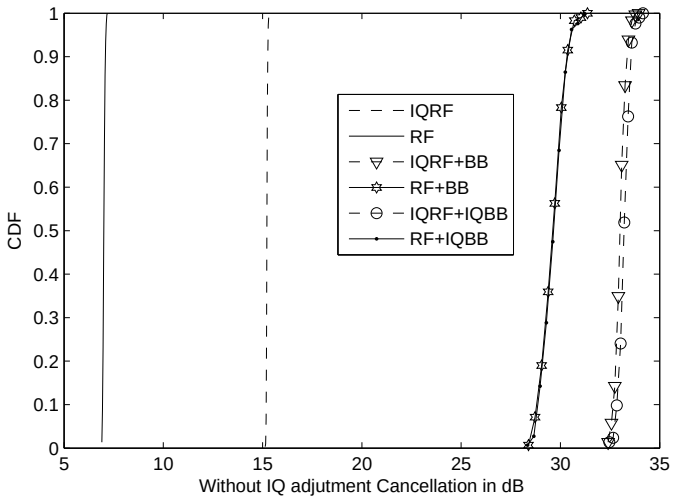

Figure 12.3: Cancellation comparison with IQ adjustment.

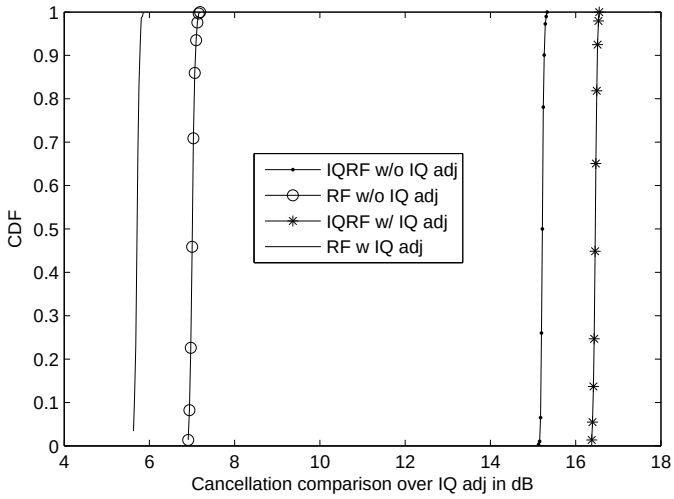

Figure 12.4: Cancellation comparison with IQ adjustment.

Chapter 13

Conclusion

The second part of this dissertation has presented a time domain transmit beamforming method and an adaptive filter method for realizing full-duplex wireless communication. All the technique are supported with numerical analysis and hardware experiment. The transmit beamforming method is verified using Agilent MXA and MXG and a WARP radio platform. 45dB cancellation on a 40MHz signal is achieved using MXA and MXG, with advanced component that is typically used in laboratory. 27dB cancellation on a 20MHz signal is achieved using the Warp platform and off-the-shelf commercial components. The cancellation is limited by the impairment of the transmitter, such as phase noise and non-linear effect. A solution for breaking this limit is the proposed adaptive filter method, which creates a cancellation channel to cancel the self-interference channel. Several architectures of the cancellation channel are presented and compared. A hardware experiment is conducted for a single tap case. Currently we are developing a multi-complex-tap PCB board for further investigation. Other issues such as IQ imbalance are also discussed

and simulated.

To realized full-duplex radio, we have to pay special attention to the impairment of the component. People working on full-duplex radio cannot make many assumptions that are only true for the half-duplex scenario. Self-interference cancellation demands a system that can accurately cancel a waveform up to 100dB or more. A digital domain numerical approach is not enough as shown earlier. Certain modification of hardware is required to achieve a large amount of self-interference cancellation. Our experiment was based on components designed for half-duplex radio. We can expect a more practical and robust solution with advanced components designed for full-duplex radio. This in turn will introduce new topics associated with algorithm development, new architectural designs, and even possibly revolutionary changes in protocols.

When the technique to suppress self-interference becomes mature, full-duplex becomes feasible. Full-duplex radio will not only double the capacity of a two-way communication with the same spectral resource, but also change the current wireless communication structure. Current radio protocols, architectures and regulations are developed based on half-duplex. Self-interference cancellation technology will bring fundamental changes in spectrum management. For example, in WiFi application, co-channel broadband noise and interference can be eliminated and multiple channels can be used to simultaneously boost the speed. With full-duplex radio, future generations of wireless communication will be more efficient in spectral management and more flexible in resource distribution.

Bibliography

[1] Wenyi Zhang, U. Mitra, and Mung Chiang. Optimization of amplify-and-forward multicarrier two-hop transmission. *Communications, IEEE Transactions on*, 59(5):1434 –1445, may 2011.

[2] Y. Ma, A. Liu, and Y. Hua. A dual-phase power allocation scheme for multicarrier relay system with direct link. *Signal Processing, IEEE Transactions on*, 62(1):5–16, Jan 2014.

[3] X. Tang and Y. Hua. Optimal design of non-regenerative MIMO wireless relays. *Wireless Communications, IEEE Transactions on*, 6(4):1398 –1407, april 2007.

[4] Yue Rong. MMSE-based non-regenerative multicarrier MIMO wireless relay communications with direct source-destination link. In *Communications, 2009. ICC '09. IEEE International Conference on*, pages 1 –5, june 2009.

[5] Yue Rong and Feifei Gao. Optimal beamforming for non-regenerative MIMO relays with direct link. *Communications Letters, IEEE*, 13(12):926 –928, december 2009.

[6] Yue Rong. Optimal joint source and relay beamforming for MIMO relays with direct link. *Communications Letters, IEEE*, 14(5):390 –392, may 2010.

[7] Haibin Wan and Wen Chen. Joint source and relay design for multiuser MIMO nonregenerative relay networks with direct links. *Vehicular Technology, IEEE Transactions on*, 61(6):2871 –2876, july 2012.

[8] Haibin Wan, Wen Chen, and Jianbo Ji. Efficient linear transmission strategy for MIMO relaying broadcast channels with direct links. *Wireless Communications Letters, IEEE*, 1(1):14 –17, february 2012.

[9] Xiaoyi Liu, Li Chen, Xin Zhang, and Dacheng Yang. Resource allocation for OFDM-based multi-destination relay networks with direct links. In *Global Telecommunications Conference (GLOBECOM 2011), 2011 IEEE*, pages 1 –6, dec. 2011.

[10] Chan-Byoung Chae, Taiwen Tang, Robert W. Heath, and Sunghyun Cho. MIMO relaying with linear processing for multiuser transmission in fixed relay networks. *Signal Processing, IEEE Transactions on*, 56(2):727 – 738, Feb. 2008.

[11] B. K. Chalise and L. Vandendorpe. MIMO relay design for multipoint-to-multipoint communications with imperfect channel state information. *Signal Processing, IEEE Transactions on*, 57(7):2785 – 2796, July 2009.

[12] Yue Rong, Xiaojun Tang, and Yingbo Hua. A unified framework for optimizing linear nonregenerative multicarrier MIMO relay communication systems. *Signal Processing, IEEE Transactions on*, 57(12):4837 – 4851, Dec 2009.

[13] Yuan Yu and Yingbo Hua. Power allocation for a MIMO relay system with multiple-antenna users. *Signal Processing, IEEE Transactions on*, 58(5):2823 – 2835, May 2010.

[14] Yingbo Hua, Dan Bliss, Saeed Gazor, Yue Rong, and Youngchul Sung, editors. *Special Issue on Theories and Methods for Advanced Wireless Relays*, volume 30. IEEE JSAC, Sept 2012.

[15] S. Boyd and L. Vandenberghe. *Convex optimization*. Cambridge University Press, 2004.

[16] L. Grippo and M. Sciandrone. On the convergence of the block nonlinear gauss-seidel method under convex constraints. *Information Theory, IEEE Transactions on*, 26(3):127–136, 2000.

[17] Ting Kong and Y. Hua. Optimal design of source and relay pilots for MIMO relay channel estimation. *Signal Processing, IEEE Transactions on*, 59(9):4438–4446, 2011.

[18] A. Sabharwal, P. Schniter, D. Guo, D. W. Bliss, S. Rangarajan, and R. Wichman. In-band full-duplex wireless: Challenges and opportunities [arxiv].

[19] Hyungsik Ju, Eunsung Oh, and Daesik Hong. Catching resource-devouring worms in next-generation wireless relay systems: Two-way relay and full-duplex relay. *Communications Magazine, IEEE*, 47(9):58–65, September 2009.

[20] S. Hong, J. Brand, Jung Choi, M. Jain, J. Mehlman, S. Katti, and P. Levis. Applications of self-interference cancellation in 5g and beyond. *Communications Magazine, IEEE*, 52(2):114–121, February 2014.

[21] Jung Il Choi, Mayank Jain, Kannan Srinivasan, Phil Levis, and Sachin Katti. Achieving single channel, full duplex wireless communication. In *Proceedings of the sixteenth annual international conference on Mobile computing and networking*, pages 1–12. ACM, 2010.

[22] Mohammad A. Khojastepour, Karthik Sundaresan, Sampath Rangarajan, Xinyu Zhang, and Sanaz Barghi. The case for antenna cancellation for scalable full-duplex wireless communications. In *Proceedings of the 10th ACM Workshop on Hot Topics in Networks*, HotNets-X, pages 17:1–17:6, New York, NY, USA, 2011. ACM.

[23] In *Proceedings of the 18th Annual International Conference on Mobile Computing and Networking*, Mobicom '12, pages 257–268, New York, NY, USA, 2012. ACM.

[24] Dani Korpi, Sathya Venkatasubramanian, Taneli Riihonen, Lauri Anttila, Strasdosky Otewa, Clemens Icheln, Katsuyuki Haneda, Sergei Tretyakov, Mikko Valkama, and Risto Wichman. Advanced self-interference cancellation and multiantenna techniques for full-duplex radios. *CoRR*, abs/1401.3331, 2014.

[25] Pawinee Meerasri, Peerapong Uthansakul, and Monthippa Uthansakul. Self-interference cancellation-based mutual-coupling model for full-duplex single-channel mimo systems. *International Journal of Antennas and Propagation*, 2014.

[26] E. Everett, M. Duarte, C. Dick, and A. Sabharwal. Empowering full-duplex wireless communication by exploiting directional diversity. In *Signals, Systems and Computers (ASILOMAR), 2011 Conference Record of the Forty Fifth Asilomar Conference on*, pages 2002–2006, Nov 2011.

[27] B. Radunovic, D. Gunawardena, P. Key, A. Proutiere, N. Singh, V. Balan, and G. Dejean. Rethinking indoor wireless mesh design: Low power, low frequency, full-duplex. In *Wireless Mesh Networks (WIMESH 2010), 2010 Fifth IEEE Workshop on*, pages 1–6, June 2010.

[28] Melissa Duarte and Ashutosh Sabharwal. Full-duplex wireless communications using off-the-shelf radios: Feasibility and first results. In *Signals, Systems and Computers (ASILOMAR), 2010 Conference Record of the Forty Fourth Asilomar Conference on*, pages 1558–1562. IEEE, 2010.

[29] Mayank Jain, Jung Il Choi, Taemin Kim, Dinesh Bharadia, Siddharth Seth, Kannan Srinivasan, Philip Levis, Sachin Katti, and Prasun Sinha. Practical, real-time, full duplex wireless. In *Proceedings of the 17th Annual International Conference on Mobile Computing and Networking*, MobiCom '11, pages 301–312, New York, NY, USA, 2011. ACM.

[30] Jong-Ho Lee. Self-interference cancelation using phase rotation in full-duplex wireless. *Vehicular Technology, IEEE Transactions on*, 62(9):4421–4429, Nov 2013.

[31] Yingbo Hua, Ping Liang, Yiming Ma, A.C. Cirik, and Qian Gao. A method for broadband full-duplex mimo radio. *Signal Processing Letters, IEEE*, 19(12):793–796, Dec 2012.

[32] Zhaowu Zhan, Guillaume Villemaud, and Jean-Marie Gorce. Design and evaluation of a wideband full-duplex ofdm system based on aasic. In *Personal Indoor and Mobile Radio Communications (PIMRC), 2013 IEEE 24th International Symposium on*, pages 68–72, Sept 2013.

[33] Joseph G McMichael and Kenneth E Kolodziej. Optimal tuning of analog self-interference cancellers for full-duplex wireless communication. In *Communication, Control, and Computing (Allerton), 2012 50th Annual Allerton Conference on*, pages 246–251. IEEE, 2012.

[34] M. Duarte, C. Dick, and A. Sabharwal. Experiment-driven characterization of full-duplex wireless systems. *Wireless Communications, IEEE Transactions on*, 11(12):4296–4307, December 2012.

[35] Alexios Balatsoukas-Stimming, Pavle Belanovic, Konstantinos Alexandris, and Andreas Burg. On self-interference suppression methods for low-complexity full-duplex mimo. In *Signals, Systems and Computers, 2013 Asilomar Conference on*, pages 992–997, Nov 2013.

[36] Achaleshwar Sahai, Gaurav Patel, and Ashutosh Sabharwal. Pushing the limits of full-duplex: Design and real-time implementation. 2011.

[37] Y Choi and Hooman Shirani-Mehr. Simultaneous transmission and reception: Algorithm, design and system level performance. *IEEE Transactions on Wireless Communications, to appear*.

[38] Shenghong Li and R.D. Murch. Full-duplex wireless communication using transmitter output based echo cancellation. In *Global Telecommunications Conference (GLOBECOM 2011), 2011 IEEE*, pages 1–5, Dec 2011.

[39] M.E. Knox. Single antenna full duplex communications using a common carrier. In *Wireless and Microwave Technology Conference (WAMICON), 2012 IEEE 13th Annual*, pages 1–6, April 2012.

[40] Steven S Hong, Jeffrey Mehlman, and Sachin Katti. Picasso: flexible rf and spectrum slicing. *ACM SIGCOMM Computer Communication Review*, 42(4):37–48, 2012.

[41] D. Bharadia, E.McMilin, and S. Katti. Full duplex radio. In *Proceedings of the ACM SIGCOMM 2013 conference on SIGCOMM*, pages –, 2013.

[42] Jung Il Choi, S. Hong, M. Jain, S. Katti, P. Levis, and J. Mehlman. Beyond full duplex wireless. In *Signals, Systems and Computers (ASILOMAR), 2012 Conference Record of the Forty Sixth Asilomar Conference on*, pages 40–44, Nov 2012.

[43] M. Duarte, A. Sabharwal, V. Aggarwal, R. Jana, K.K. Ramakrishnan, C.W. Rice, and N.K. Shankaranarayanan. Design and characterization of a full-duplex multiantenna system for wifi networks. *Vehicular Technology, IEEE Transactions on*, 63(3):1160–1177, March 2014.

[44] V. Aggarwal and N.K. Shankaranarayanan. Performance of a random-access wireless network with a mix of full- and half-duplex stations. *Communications Letters, IEEE*, 17(11):2200–2203, November 2013.

[45] D. Bharadia and S. Katti. Full-duplex mimo radios. *NSDI 2014*, 2014.

[46] B. Chen, V. Yenamandra, and K. Srinivasan. Flexradio: Fully flexible radios. *NSDI 2014*, 2014.

[47] Brett Kaufman, Jorma Lilleberg, and Behnaam Aazhang. An analog baseband approach for designing full-duplex radios. In *Signals, Systems and Computers, 2013 Asilomar Conference on*, pages 987–991, Nov 2013.

[48] Mohammad A Khojastepour and Sampath Rangarajan. Wideband digital cancellation for full-duplex communications. In *Signals, Systems and Computers (ASILOMAR), 2012 Conference Record of the Forty Sixth Asilomar Conference on*, pages 1300–1304. IEEE, 2012.

[49] John R. Krier and Ian F. Akyildiz. Active self-interference cancellation of passband signals using gradient descent. In *Personal Indoor and Mobile Radio Communications (PIMRC), 2013 IEEE 24th International Symposium on*, pages 1212–1216, Sept 2013.

[50] Na Li, Weihong Zhu, and Haihua Han. Digital interference cancellation in single channel, full duplex wireless communication. In *Wireless Communications, Networking and Mobile Computing (WiCOM), 2012 8th International Conference on*, pages 1–4, Sept 2012.

[51] Junghwan Kim, K. Shamaileh, S. Adusumilli, and V. Rao. Digital interference cancellation for multimedia transmission in full duplex communication link. In *Broadband Multimedia Systems and Broadcasting (BMSB), 2013 IEEE International Symposium on*, pages 1–5, June 2013.

[52] Yingbo Hua, Yiming Ma, Ping Liang, and A. Cirik. Breaking the barrier of transmission noise in full-duplex radio. In *Military Communications Conference, MILCOM 2013 - 2013 IEEE*, pages 1558–1563, Nov 2013.

[53] A. Sahai, G. Patel, c. dick, and A. Sabharwal. On the impact of phase noise on active cancelation in wireless full-duplex. *Vehicular Technology, IEEE Transactions on*, 62(9):4494–4510, Nov 2013.

[54] V. Syrjala, M. Valkama, L. Anttila, T. Riihonen, and D. Korpi. Analysis of oscillator phase-noise effects on self-interference cancellation in full-duplex ofdm radio transceivers, 2014.

[55] Elsayed Ahmed, Ahmed M. Eltawil, and Ashutosh Sabharwal. Self-interference cancellation with nonlinear distortion suppression for full-duplex systems. In *Signals, Systems and Computers, 2013 Asilomar Conference on*, pages 1199–1203, Nov 2013.

[56] T. Riihonen, P. Mathecken, and R. Wichman. Effect of oscillator phase noise and processing delay in full-duplex ofdm repeaters. In *Signals, Systems and Computers (ASILOMAR), 2012 Conference Record of the Forty Sixth Asilomar Conference on*, pages 1947–1951, Nov 2012.

[57] D.W. Bliss, T.M. Hancock, and P. Schniter. Hardware phenomenological effects on cochannel full-duplex mimo relay performance. In *Signals, Systems and Computers (ASILOMAR), 2012 Conference Record of the Forty Sixth Asilomar Conference on*, pages 34–39, Nov 2012.

[58] Elsayed Ahmed, Ahmed M. Eltawil, and Ashutosh Sabharwal. Self-interference cancellation with nonlinear distortion suppression for full-duplex systems. In *Signals, Systems and Computers, 2013 Asilomar Conference on*, pages 1199–1203, Nov 2013.

[59] Lauri Anttila, Dani Korpi, Ville Syrjala, and Mikko Valkama. Cancellation of power amplifier induced nonlinear self-interference in full-duplex transceivers. In *Signals, Systems and Computers, 2013 Asilomar Conference on*, pages 1193–1198, Nov 2013.

[60] D. Korpi, T. Riihonen, V. Syrjala, L. Anttila, M. Valkama, and R. Wichman. Full-duplex transceiver system calculations: Analysis of adc and linearity challenges, 2014.

[61] T. Riihonen and R. Wichman. Analog and digital self-interference cancellation in full-duplex mimo-ofdm transceivers with limited resolution in a/d conversion. In *Signals, Systems and Computers (ASILOMAR), 2012 Conference Record of the Forty Sixth Asilomar Conference on*, pages 45–49, Nov 2012.

[62] Zhaowu Zhan, Guillaume Villemaud, and Jean-Marie Gorce. Analysis and Reduction of the Impact of Thermal Noise on the Full-Duplex OFDM Radio. In *IEEE Radio Wireless Symposium*, Newport Beach, États-Unis, January 2014.

[63] Armen Gholian, Yiming Ma, and Yingbo Hua. A numerical investigation of all-analog radio self-interference cancellation. In *Signal Processing Advances in Wireless Communication, the 14th IEEE international Workshop on*, pages –, June 2014.

[64] Warp project.

Appendix A

Detailed Information of the Component used in the Experiment.

Name	Product Name	Website
Signal Generator	Agilent MXG N5182	www.home.agilent.com
Spectrum Analyzer	Agilent MXA N9020A	www.home.agilent.com
WARP Board	Mango Inc. Warp Project	warpproject.org/trac
Step Attenuator(1)	Mini Circuit ZX76-31R5-SP-S+	www.minicircuits.com
Step Attenuator(2)	Peregrine Semiconductor PE43703	www.psemi.com/index.php
Vector Modulator	Hittite HMC631LP3	www.hittite.com
USB I/O control Box	Mini Circuit USB I/O 16D8R	www.minicircuits.com
Circulator	Mini Circuit CS-2.500	www.minicircuits.com
Power Combiner/Spliter	Mini Circuit ZAPD-4-S+	www.minicircuits.com
90^o Spliter	Mini Circuit ZX10Q2-27-S+	www.minicircuits.com
4 way combiner	Mini Circuit ZB4PD-42-S+	www.minicircuits.com

Table A.1: List of the key component.